

LARGE SAMPLE SPECTRAL ANALYSIS OF GRAPH-BASED MULTI-MANIFOLD CLUSTERING

NICOLÁS GARCÍA TRILLOS, PENGFEI HE, AND CHENGHUI LI

ABSTRACT. In this work we study statistical properties of graph-based algorithms for multi-manifold clustering (MMC). In MMC the goal is to retrieve the multi-manifold structure underlying a given Euclidean data set when this one is assumed to be obtained by sampling a distribution on a union of manifolds $\mathcal{M} = \mathcal{M}_1 \cup \dots \cup \mathcal{M}_N$ that may intersect with each other and that may have different dimensions. We investigate sufficient conditions that similarity graphs on data sets must satisfy in order for their corresponding graph Laplacians to capture the right geometric information to solve the MMC problem. Precisely, we provide high probability error bounds for the spectral approximation of a tensorized Laplacian on \mathcal{M} with a suitable graph Laplacian built from the observations; the recovered tensorized Laplacian contains all geometric information of all the individual underlying manifolds. We provide an example of a family of similarity graphs, which we call annular proximity graphs with angle constraints, satisfying these sufficient conditions. We contrast our family of graphs with other constructions in the literature based on the alignment of tangent planes. Extensive numerical experiments expand the insights that our theory provides on the MMC problem.

1. INTRODUCTION

In this work we study the problem of *multi-manifold clustering* (MMC) from the perspective of spectral geometry. Multi-manifold clustering is the task of identifying the structure of multiple manifolds that underlie an observed data set $X = \{x_1, \dots, x_n\}$, its main challenge being that in general the underlying manifolds may be non-linear, may intersect with each other, and may have different dimensions (see Figures 1-3 and Figures 30-33 for some illustrations). While spectral methods for learning have been analyzed by several authors throughout the past two decades in settings as varied as unsupervised, semi-supervised, and supervised learning, less is known about their theoretical guarantees for the specific multi-manifold clustering problem. We analyze MMC algorithms that are based on the construction of suitable similarity graph representations for the data and in turn on the spectra of their associated graph Laplacians. We provide statistical error guarantees for the identification of the underlying manifolds as well as for the recovery of their individual geometry.

As for most spectral approaches to clustering, we are interested in studying spectral properties of graph Laplacian operators of the form

$$\Delta_n u(x_i) := \sum w_{ij} (u(x_i) - u(x_j)), \quad x_i \in X. \quad (1.1)$$

Acknowledgements: All authors contributed equally to this work. Their names are listed in alphabetic order by lastname. NGT was supported by NSF-DMS grant 2005797. Support for this research was provided by the Office of the Vice Chancellor for Research and Graduate Education at the University of Wisconsin-Madison with funding from the Wisconsin Alumni Research Foundation. The authors would like to thank the IFDS at UW-Madison and NSF through TRIPODS grant 2023239 for their support.

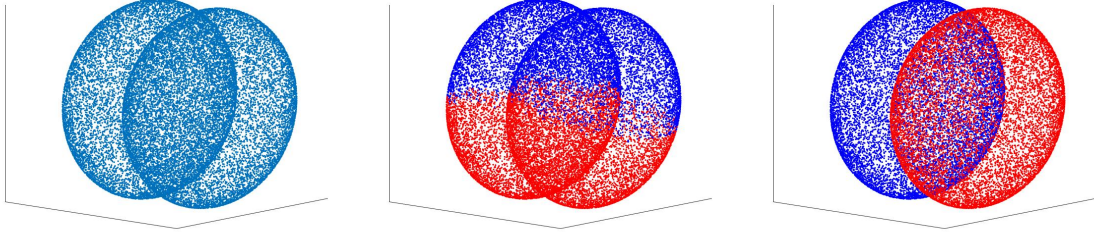


FIGURE
1. Data set
on $\mathcal{M} =$
 $\mathcal{M}_1 \cup \mathcal{M}_2$.

FIGURE
2. Spectral
clustering
with ε -graph.

FIGURE
3. Spectral
clustering
with annular
graph with
angle con-
straints; see
section 3.

For the data set illustrated in Figure 1 a good multi-manifold clustering algorithm must identify the two underlying ellipsoids. Notice that the two manifolds intersect on a lower dimensional manifold.

Here, the ω_{ij} are appropriately defined symmetric weights that in general depend on the proximity of points x_i, x_j , and importantly, on a mechanism that detects when points belong to different manifolds even if lying close to each other. Once the graph Laplacian is constructed we follow the spectral clustering algorithm: the first p eigenvectors of Δ_n (denoted ψ_1, \dots, ψ_N) are used to build an embedding of the data set X into \mathbb{R}^p :

$$x_i \in X \longmapsto \begin{pmatrix} \psi_1(x_i) \\ \vdots \\ \psi_N(x_i) \end{pmatrix} \in \mathbb{R}^p.$$

In turn, with the aid of a simple clustering algorithm such as k -means the embedded data set is clustered. A successful algorithm will produce clusters that are in agreement with the different manifolds underlying the data set.

It is important to highlight that the success of spectral clustering when applied to MMC problems relies strongly on the specific similarity weights ω_{ij} that determine the graph Laplacian, its eigenvectors, and ultimately the partitioning of the data. In the literature, authors have considered different types of mechanisms to discriminate points that lie on different manifolds. Some strategies include the use of local tangent planes from data [3, 23, 29, 51] (whose angles are compared), and the construction of paths between different points (e.g. geodesics) that are considered admissible if they do not exhibit sudden turns (effectively imposing a curvature constraint) [5]. All these methods are inspired by heuristics that are meaningful at the continuum level (i.e. the infinite data setting) and use second order geometric information to detect the different intersecting manifolds; while they provide practical insights, in general these heuristics do not guarantee the success of the employed methodologies for MMC at the finite sample level. Part of the motivation for this work is precisely to establish a more concrete and mathematically precise link between the heuristic motivation at the continuum level and the actual methodologies that are used in practice. It is worth

highlighting that widely known graph constructions such as ε -proximity graphs or k -NN graphs used for standard data clustering tasks (typically aimed at detecting bottle-necks in data sets) are in general not suitable for MMC. To illustrate this, take for example Figure 2. There, we have used a k -NN graph to build a graph Laplacian whose first non-trivial eigenvector has been used to obtain the partition illustrated in the figure; as can be observed, from the geometry induced by the k -NN graph we are unable to distinguish the two underlying ellipsoids.

To start making our results more precise, let us suppose that the data set X is obtained by sampling a distribution μ supported on a set \mathcal{M} of the form

$$\mathcal{M} = \mathcal{M}_1 \cup \dots \cup \mathcal{M}_N, \quad (1.2)$$

where the \mathcal{M}_i are smooth compact connected manifolds with no boundary that for the moment are assumed to have the same dimension m ; the manifolds \mathcal{M}_i may have nonempty pairwise intersections, but these are assumed to have measure zero relative to the volume forms of each of the manifolds involved. The distribution μ is assumed to be a mixture model taking the form

$$d\mu = w_1 \rho_1 d\text{vol}_{\mathcal{M}_1} + \dots + w_N \rho_N d\text{vol}_{\mathcal{M}_N},$$

for smooth density functions $\rho_i : \mathcal{M}_i \rightarrow \mathbb{R}$ and positive weights w_i that add to one; henceforth we use $\text{vol}_{\mathcal{M}_i}$ to denote the Riemannian volume form associated to \mathcal{M}_i . A *tensorized Laplacian* $\Delta_{\mathcal{M}}$ acting on functions f on \mathcal{M} (which will be written as $f = (f_1, \dots, f_N)$, where $f_i : \mathcal{M}_i \rightarrow \mathbb{R}$) can be defined according to

$$\Delta_{\mathcal{M}} f := (w_1 \Delta_{\mathcal{M}_1} f_1, \dots, w_N \Delta_{\mathcal{M}_N} f_N), \quad (1.3)$$

where $\Delta_{\mathcal{M}_l}$ is a Laplacian operator mapping regular enough functions $f_l : \mathcal{M}_l \rightarrow \mathbb{R}$ into functions $\Delta_{\mathcal{M}} f_l : \mathcal{M}_l \rightarrow \mathbb{R}$ according to

$$\Delta_{\mathcal{M}_l} f_l = -\frac{1}{\rho_l} \text{div}_{\mathcal{M}_l} (\rho_l^2 \nabla_{\mathcal{M}_l} f_l).$$

In other words, the operator $\Delta_{\mathcal{M}}$ acts in a coordinatewise fashion effectively treating each manifold \mathcal{M}_i independently. It is then straightforward to show that eigenfunctions of $\Delta_{\mathcal{M}}$ are spanned by functions of the form

$$(0, \dots, f_l, \dots, 0)$$

for some l , where f_l is an eigenfunction of $\Delta_{\mathcal{M}_l}$. This means that the spectrum of $\Delta_{\mathcal{M}}$ splits the geometries of the \mathcal{M}_l , and in particular, the different \mathcal{M}_l can be detected by retrieving the eigenfunctions with zero eigenvalue.

Our first main results (**Theorem 2.5** and **Theorem 2.7**) say that provided that the weights w_{ij} defining the graph Laplacian operator Δ_n in (1.1) satisfy two conditions referred to as *full inner connectivity* and *sparse outer connectivity*, then the eigenvalues (appropriately scaled) and eigenvectors of Δ_n approximate the eigenvalues and eigenfunctions of the tensorized Laplacian $\Delta_{\mathcal{M}}$; we obtain high probability quantitative bounds for the error of this approximation. The bottom line is that our results imply that the spectral methods studied here are guaranteed, at least for large enough n , to recover the underlying multi-manifold structure of the data; see Figure 3 for an illustration. Our work extends the growing literature of works that study the connection between graph Laplacians on data sets and their continuum analogues. This literature, which we review in section 1.1.1, has mostly focused on the smooth setting where multiple intersecting manifolds are not allowed.

In our second main result (**Theorem 2.8**) we present some results for the case when the dimensions of the manifolds \mathcal{M}_i do not agree. In this more general setting, the spectrum of the graph Laplacian Δ_n does not recover the tensorized geometry captured by $\Delta_{\mathcal{M}}$ as introduced earlier, but rather, only the tensorized geometry of the manifolds with the *largest* dimension, effectively

quotienting out the geometric information of manifolds with dimension strictly smaller than the maximum dimension.

Our detailed analysis allows us to provide further insights into the behavior of the graph-based MMC algorithms explored in this paper (the annular proximity graph with angle constraints from section 3). These insights are illustrated and expanded by our numerical experiments in section 4.

1.1. Related work. In this section we provide an overview of some related works that study spectral clustering and its connection with manifold learning, as well as other works that study subspace clustering and multi-manifold clustering.

1.1.1. Spectral clustering and manifold learning. In the past two decades, several authors have attempted to establish precise connections between operators such as graph Laplacians built from random data and analogous differential operators defined at the continuum level. To make this connection mathematically precise, one can assume that the data are sampled from some distribution supported on a certain geometric object \mathcal{M} . In the setting where \mathcal{M} is a smooth compact manifold embedded in \mathbb{R}^d that has no boundary, several authors have studied the connection between ε -graph-based Laplacians and weighted versions of Laplace Beltrami operators on \mathcal{M} . For pointwise consistency results we refer the reader to [6, 28, 30, 31, 40, 43]). Regarding *spectral convergence* of graph Laplacians, a notion of convergence that is relevant for spectral clustering, the regime $n \rightarrow \infty$ and ε constant is studied in [50] and also in [41]. The latter analyzes connection Laplacians which are operators acting on vector fields as opposed to functions. Works that have studied regimes where ε is allowed to decay to zero include [13, 14, 20, 34, 39, 44, 52]. The mathematical theory around graph Laplacians in the smooth manifold setting has developed considerably and even regularity estimates of graph Laplacian eigenvectors are available (see [15]).

In the setting of a smooth compact manifold \mathcal{M} *with* boundary, graph Laplacians are seen to behave differently around the manifold's boundary. This has been observed in works like [42, 45] which study this setting and obtain expansions for graph Laplacians that hold all the way up to the boundary. Earlier works such as [27] use variational methods to provide spectral asymptotic consistency results in this setting but don't obtain convergence rates nor describe the behavior of graph Laplacians close to the boundary. The work [34] provides rates for spectral convergence in the setting of manifolds with boundary and also considers the case where \mathcal{M} is of the form 1.2. However, in contrast to what we do here, the aim in [34] is not to analyze graph constructions that guarantee the recovery of the multi-manifold structure of the data and focuses instead on an intrinsic version of a proximity graph. Our analysis shares aspects and ideas with this and some of the other works previously mentioned, but to fulfill our goals we must introduce new constructions and estimates not currently available. In addition, to the best of our knowledge, we are the first to present an analysis of the spectrum of graph Laplacians when data points are supported on a union of intersecting manifolds that have *different* dimensions.

From a methodological perspective, it is also worth highlighting several other works that have studied the use of metrics different from the Euclidean one to build proximity graphs. The idea in those papers is to use those metrics to improve the performance of spectral clustering when applied to data sets with some special geometric structure. Examples include: [2, 16, 26, 32, 35, 38]. In a sense, the goal in this paper fits the general perspective taken in the previously mentioned papers, only that in our case we have a different geometric structure in mind. i.e. multiple intersecting manifolds.

1.1.2. Multi-manifold clustering. In contrast to the graph constructions which are analyzed in most of the works mentioned in section 1.1.1 (i.e. standard ε -graphs and k -NN graphs), graph constructions for multi-manifold clustering must incorporate a mechanism to discriminate between points that lie on different manifolds. One such mechanism relies on the approximation of tangent planes to

in turn endow pairs of nearby points with high weights whenever their corresponding tangent planes are aligned as has been proposed in [3]. The recovery of tangent planes from data is a problem that has been studied theoretically in papers such as [1] (see also references within). The methodology proposed in [41], which uses a connection Laplacian, can be considered as a MMC algorithm since it also uses tangent plane information to inform the affinity between points. The LLMC algorithm from [29] is also based on locally fitting planes to points and their nearest neighbors. Sparse Manifold Clustering and Embedding(SMCE) [23] implicitly attempts to recover tangent planes too; a sparse representation of points in a neighborhood is sought via a local l^1 optimization problem. Another work that considers affinities based on local tangent planes is [51]. In section 3.2 we will discuss some properties of the tangent plane based graphs and their effect on spectral clustering for MMC.

At a high level, all multi-manifold clustering algorithms use curvature information to detect points that lie on different manifolds. Measuring the difference of tangent planes is one way to capture curvature, but there are alternative ways. For example, works like [17, 18] use the notion of polar curvature between collections of points to define an algorithm known as spectral curvature clustering (SCC). In [17] the authors present some theoretical analysis of SCC in the setting where the data are sampled from multiple flats with the same dimension. Curvature can also be captured by measuring how quickly paths turn as proposed in [5]. Our graph construction from section 3 is inspired by the one proposed in [5], but with some important differences that we will motivate and explain throughout the paper.

1.1.3. Subspace clustering. When the manifolds \mathcal{M}_l are linear subspaces of the ambient space, the multi-manifold clustering problem reduces to subspace clustering (SC), a problem that has received considerable attention in the past decades due to its multiple applications in tasks such as image segmentation, motion segmentation, and image representation (see [46]). Many algorithms in SC rely strongly on the the global linear structure of the data and thus can not be used directly for a general multi-manifold clustering task. We mention some of these algorithms for the sake of context.

The work [7] was one of the first to consider spectral methods for subspace clustering, attempting a SVD decomposition of a feature matrix in an application to motion segmentation. However, while the factorization-based affinity algorithm from [7] can be used to accurately discriminate between points that belong to different subspaces, one can not guarantee that points on the same subspace are correctly matched. LSA [53] and SLBF [55] are approaches based on locality, that is, on the idea that nearby points typically belong to the same subspace (except perhaps when they are close to the origin). An affinity between points is constructed and then used within spectral clustering. These approaches are not substantially different from the methods used for general MMC based on affinity of tangent planes. In [37], two steps, nearest subspace neighbor and greedy subspace recovery, are proposed to recover the underlying subspaces.

Generalized PCA [47, 54] is a method for SC that takes an algebraic perspective and specifically follows a fitting, differentiating, and division of homogeneous polynomials strategy to recover the desired segmentation. At its core, the idea proposed in [47] is based on the fact that the union of multiple subspaces can be represented as the zero set of a collection of homogeneous polynomials.

Other works in the literature take a regression based perspective to the subspace clustering problem. One such example is the sparse subspace clustering algorithm (SSC) from [21] and [22]. A modified regression method called ordered weighted l_1 regression was proposed in [36]. The low rank representation algorithm from [33] is similar in spirit to SSC.

1.2. Contributions and outline. We summarize our contributions as follows:

- We analyze graph Laplacians on families of proximity graphs when the nodes of the graphs are random data points that are supported on a union of unknown *intersecting* manifolds. The manifolds may all have *different* dimensions.
- We introduce two sufficient conditions that similarity graphs must satisfy in order to recover, from a graph Laplacian operator, the geometric information of the individual smooth manifolds underlying the data set. These conditions are referred to as *full inner connectivity* and *sparse outer connectivity*.
- We introduce and analyze *annular* proximity graphs and their effect on multi-manifold clustering. These are simple extensions of ε -proximity graphs that nonetheless can be shown to be, theoretically and numerically, better than the vanilla ε -graphs for multi-manifold clustering.
- We analyze a family of *annular proximity graphs with angle constraints*. This family is shown to satisfy the full inner connectivity and sparse outer connectivity conditions when their parameters are tuned appropriately. We contrast this construction with other constructions such as those based on local PCA which in general do not satisfy the full inner connectivity condition.
- Through numerical examples and some heuristic computations we provide further insights into the use of spectral methods for multi-manifold clustering.

The rest of the paper is organized as follows. Our theoretical framework is presented in section 2 where we formalize the setting for the multi-manifold clustering problem, introduce the definitions of sparsely outer connected and fully inner connected similarity graphs, and state our main theoretical results. In our first results, the ones in section 2.3, we assume that all underlying manifolds have the same dimension, and in section 2.4 we extend to settings where the dimensions of the underlying manifolds can be different. In section 3 we discuss an example of a graph construction which satisfies the full inner connectivity and sparse outer connectivity conditions. In section 4 we present a series of numerical experiments whose goal is to illustrate the theory developed throughout the paper and highlight some drawbacks of the methods for MMC that we discuss. In Appendix A we present the proofs of all the results from sections 2.3 and 2.4.

2. SET UP AND MAIN RESULTS

Let $\{\mathcal{M}_l\}_{l=1}^N$ be a collection of N smooth, compact manifolds without boundary embedded in \mathbb{R}^d . We denote by m_l the dimension of manifold \mathcal{M}_l and $m = \max_{l=1,\dots,N}\{m_l\}$. Let \mathcal{M} be the union:

$$\mathcal{M} := \mathcal{M}_1 \cup \dots \cup \mathcal{M}_N.$$

Let $X = \{x_1, \dots, x_n\}$ be i.i.d. samples from a distribution μ on \mathcal{M} of the form:

$$d\mu = \sum_{l=1}^N w_l \rho_l(x) d\text{vol}_{\mathcal{M}_l}(x), \quad \text{where } w_l > 0, \quad \sum_{l=1}^N w_l = 1. \quad (2.1)$$

In the above, for each l , $\text{vol}_{\mathcal{M}_l}$ is used to denote the Riemannian volume form associated to the manifold \mathcal{M}_l , and the probability density $\rho_l : \mathcal{M}_l \rightarrow \mathbb{R}$ is assumed to be $C^2(\mathcal{M}_l)$ and satisfy

$$\frac{1}{c_\rho} \leq \rho_l(x) \leq c_\rho, \quad \forall l = 1, \dots, N$$

for some positive constant $c_\rho > 1$. We use μ_l to denote the probability measure $\rho_l d\text{vol}_{\mathcal{M}_l}$. Notice that from (2.1) it follows that the number of data points n_l in manifold \mathcal{M}_l is with very high probability within two constants of $w_l n$.

The following assumptions guarantee that the manifolds \mathcal{M}_l , even if intersecting each other, are sufficiently “well separated” in an angular sense.

Assumption 1. For every l, k we assume:

- i) The intersection $\mathcal{M}_{lk} := \mathcal{M}_l \cap \mathcal{M}_k$ is either the empty set or a smooth manifold of dimension m_{lk} satisfying $1 \leq m_{lk} < \min\{m_l, m_k\}$. In particular, \mathcal{M}_{lk} is of measure zero according to $\text{vol}_{\mathcal{M}_l}$ and $\text{vol}_{\mathcal{M}_k}$.
- ii) For every point x in $\mathcal{M}_l \cap \mathcal{M}_k$ we have:

$$\sup_{v \in \mathcal{T}_x \mathcal{M}_{lk}^{\perp l}, \tilde{v} \in \mathcal{T}_x \mathcal{M}_{lk}^{\perp k}} |\angle(v, \tilde{v}) - \frac{\pi}{2}| \leq \beta, \quad (2.2)$$

for some fixed β strictly smaller than $\frac{\pi}{2}$. In the above, $\angle(v, \tilde{v})$ denotes the angle between vectors v, \tilde{v} (recall that all manifolds are embedded in the ambient space \mathbb{R}^d), and $\mathcal{T}_x \mathcal{M}_{lk}^{\perp l}$ denotes the orthogonal complement of $\mathcal{T}_x \mathcal{M}_{lk}$ in $\mathcal{T}_x \mathcal{M}_l$. $\mathcal{T}_x \mathcal{M}_{lk}^{\perp l}$ is defined analogously.

In the above, and in the remainder, we use $\mathcal{T}_x \mathcal{M}_l$ to denote the tangent plane to \mathcal{M}_l at the point $x \in \mathcal{M}_l$; also, we use $\mathcal{T}\mathcal{M}_l$ to denote the tangent bundle associated to \mathcal{M}_l . Notice that the second condition in Assumption 1 states that if two manifolds \mathcal{M}_l and \mathcal{M}_k do intersect, they do so in a non-tangential way.

2.1. Inner fully connected, and outer sparsely connected graphs. We endow the data set X with a weighted graph structure (X, ω) where the weights ω are specified by the data. In this section we present the definitions of fully inner connected and sparsely outer connected graphs. The notion of full inner connectivity is relative to a family of base proximity graphs that we introduce next.

Definition 2.1. Given $0 \leq \varepsilon_- < \varepsilon_+$ and data points x_i, x_j , we define their $\varepsilon_+, \varepsilon_-$ -weight as:

$$\omega_{ij}^{\varepsilon_+, \varepsilon_-} := \begin{cases} 1 & \text{if } \varepsilon_- \leq |x_i - x_j| \leq \varepsilon_+ \\ 0 & \text{otherwise.} \end{cases}$$

We use ω_{ij}^ε as shorthand of $\omega_{ij}^{\varepsilon, 0}$. Notice that with this definition we have the identity:

$$\omega_{yx}^{\varepsilon_+, \varepsilon_-} = \omega_{yx}^{\varepsilon_+} - \omega_{yx}^{\varepsilon_-}.$$

Remark 2.2. We notice that the above definition extends the notion of ε -proximity graph and in principle allows pairs of points that are too close to each other to have zero weight. While in the literature this annular proximity graphs have not been given any attention, we will see later on that this extended notion is convenient from both a qualitative as well as a quantitative point of view for the MMC problem.

Definition 2.3 (Fully inner Connected graphs). Let $X = x_1, \dots, x_n$ be samples from μ as defined in (2.1). A weighted graph (X, ω) is said to be fully inner connected as $n \rightarrow \infty$ if with probability $1 - C_1(n)$, where $C_1(n) \rightarrow 0$ as $n \rightarrow \infty$, for any pair of points x_i, x_j belonging to the same manifold \mathcal{M}_k we have $\omega_{x_i, x_j} = \omega_{x_i, x_j}^{\varepsilon_+, \varepsilon_-}$.

Definition 2.4 (Sparsely Outer Connected graphs). Let $X = x_1, \dots, x_n$ be samples from μ as defined in (2.1), and let (X, ω) be a weighted graph. Let N_{sl} be the number of $x_i \in \mathcal{M}_s$ and $x_j \in \mathcal{M}_l$ such that $\omega_{ij} > 0$, and let

$$N_0 := \max_{l \neq s} \{N_{ls}\}.$$

The graph is said to be sparsely outer connected as $n \rightarrow \infty$ if with probability one, $\frac{N_0}{n^2(\varepsilon_+^{m+2} - \varepsilon_-^{m+2})} \rightarrow 0$ as $n \rightarrow \infty$. We recall that $m = \max_{l=1, \dots, N} m_l$.

The above notions are closely connected to the intuitive desire of giving high weights to pairs of points that are close to each other when they belong to the same manifold (full inner connectivity condition) and to give low weights to pairs of points when they lie on different manifolds (sparse outer connectivity condition). The full inner connectivity condition can be described as saying that with high probability the weights ω_{ij} between points x_i, x_j in the same manifold must coincide with the similarities according to an annular proximity graph, the whole point being that we ignore which points belong to the same manifold. The main graph construction that we discuss in this paper satisfying both the inner and outer conditions is the annular proximity graph with angle constraints introduced in section 3. In that construction, the idea is that for any two points x_i, x_j satisfying $\varepsilon_- < |x_i - x_j| < \varepsilon_+$ for two small values $\varepsilon_-, \varepsilon_+$, a discrete path in X connecting the points with no sharp turns is sought. If such a path is found, high weights are given to the pair of points, otherwise the points are given zero weight. In section 3.2 we discuss other popular choices of affinity matrices based on tangent planes and contrast them with our construction in section 3.

2.2. Basic properties of the spectrum of the operator $\Delta_{\mathcal{M}}$. In order to state our main theoretical results in sections 2.3 and 2.4 we first discuss some basic properties of the spectrum of the operator $\Delta_{\mathcal{M}}$ in (1.3) and its relation to the MMC problem.

Let $L^2(\mu)$ be the space of N tuples (f_1, \dots, f_N) , where each $f_i \in L^2(\mu_i)$. We endow the space $L^2(\mu)$ with the tensorized inner product:

$$\langle f, g \rangle_{L^2(\mu)} := \sum_{i=1}^N w_i \langle f_i, g_i \rangle_{L^2(\mu_i)} = \sum_{i=1}^N w_i \int_{\mathcal{M}_i} f_i(x) g_i(x) d\mu_i(x),$$

where $f = (f_1, \dots, f_N) \in L^2(\mu)$ and $g = (g_1, \dots, g_N) \in L^2(\mu)$. A tensorized Sobolev space $H^1(\mu)$ is defined as the space of $f = (f_1, \dots, f_N) \in L^2(\mu)$ for which $f_i \in H^1(\mathcal{M}_i)$ for each $i = 1, \dots, N$. In particular, for elements $f \in H^1(\mu)$ the quantity

$$\sum_{i=1}^N w_i^2 \int_{\mathcal{M}_i} |\nabla f_i(x)|^2 \rho_i^2(x) dx$$

is finite. We define the weighted Dirichlet energy:

$$D(f) := \begin{cases} \sum_{i=1}^N w_i^2 \int_{\mathcal{M}_i} |\nabla f_i(x)|^2 \rho_i^2(x) d\text{vol}_{\mathcal{M}_i}(x), & \text{if } f \in H^1(\mu), \\ +\infty, & \text{if } f \in L^2(\mu) \setminus H^1(\mu). \end{cases} \quad (2.3)$$

Now, notice that the operator $\Delta_{\mathcal{M}}$ is self-adjoint with respect to the inner product $\langle \cdot, \cdot \rangle_{L^2(\mu)}$ simply because each of the operators $\Delta_{\mathcal{M}_i}$ is self-adjoint w.r.t. $\langle \cdot, \cdot \rangle_{L^2(\mu_i)}$ (e.g. see [27]). Given that each $L^2(\mathcal{M}_i, \rho_i)$ admits an orthonormal basis $\{f_l^k\}_{k \in \mathbb{N}}$ of eigenvectors of $\Delta_{\mathcal{M}_i}$, we can see that the set of $f^k \in L^2(\mu)$ of the form

$$f^k = (0, \dots, \frac{1}{\sqrt{w_l}} f_l^k, \dots, 0) \quad (2.4)$$

for $k \in \mathbb{N}$ and $l = 1, \dots, N$ is an orthonormal basis for $L^2(\mu)$. In addition, for such f^k we have

$$\Delta_{\mathcal{M}} f^k = (0, \dots, \frac{w_l}{\sqrt{w_l}} \Delta_{\mathcal{M}_i} f_l^k, \dots, 0) = w_l \lambda (0, \dots, \frac{1}{\sqrt{w_l}} f_l^k, \dots, 0) = w_l \lambda f^k$$

for some eigenvalue λ of $\Delta_{\mathcal{M}_i}$. In conclusion, we can build an orthonormal basis for $L^2(\mu)$ consisting of eigenfunctions of $\Delta_{\mathcal{M}}$ of the form (2.4). From the above we can also conclude that the set of eigenvalues of $\Delta_{\mathcal{M}}$ is the set of numbers of the form $w_l \lambda$ for some k where λ is an eigenvalue of $\Delta_{\mathcal{M}_i}$.

In terms of the Dirichlet energy defined in (2.3), the eigenvalues of $\Delta_{\mathcal{M}}$, arranged in increasing order according to multiplicity, can be written as

$$\lambda_l = \min_{S \in \mathfrak{S}_l} \max_{f \in S \setminus \{0\}} \frac{D(f)}{\|f\|_{L^2(\mu)}^2}. \quad (2.5)$$

Regarding the zero eigenvalue of $\Delta_{\mathcal{M}}$, notice that since the manifolds \mathcal{M}_l were assumed to be connected, the multiplicity of the zero eigenvalue for the operator $\Delta_{\mathcal{M}}$ is equal to N . Moreover, an orthonormal basis for this eigenspace is the set of functions of the form $(0, \dots, c_l \mathbb{1}_{\mathcal{M}_l}, \dots, 0)$ where c_l is a normalization constant. This observation is the key property that allows us to think of the multi-manifold clustering problem in terms of the spectrum of the operator $\Delta_{\mathcal{M}}$. However, it should be clear that the tensorized Laplacian has much more information than that needed to solve the MMC problem.

For convenience we also introduce Dirichlet energies associated to each manifold \mathcal{M}_l :

$$D_l(f_l) := \begin{cases} \int_{\mathcal{M}_l} |\nabla f_l(x)|^2 \rho_l^2(x) d\text{vol}_{\mathcal{M}_l}(x), & \text{if } f_l \in H^1(\mu_l), \\ +\infty & \text{iff } f_l \in L^2(\mu_l) \setminus H^1(\mu_l). \end{cases} \quad (2.6)$$

2.3. Convergence results in the $m_1 = \dots = m_N$ case. In this section we establish high probability error bounds between the spectrum of a rescaled version of the graph Laplacian Δ_n defined in (1.1) and the spectrum of $\Delta_{\mathcal{M}}$ under the additional assumption that all manifolds \mathcal{M}_k have the same dimension. The results presented in this section apply to generic weighted graphs (X, ω) , but the error estimates are only meaningful when the quantities N_0 , $C_1(n)$ and ε_+ from section 2.1 scale appropriately with the number of data points. In Section 3 we present a specific construction for (X, ω) where we can make our error estimates concrete.

In what follows we make the following assumptions on the parameters $\varepsilon_+, \varepsilon_-, \tilde{\delta}, \theta$. Here $\tilde{\delta}$ and θ are small parameters that we use to tune the probabilities of some random events.

Assumption 2. *We assume that the quantities $\varepsilon_+, \varepsilon_-, \tilde{\delta}, \theta$ satisfy:*

- (1) $\varepsilon_+ \leq \min\{1, \frac{R}{2}, CK^{-1/2}, i_0\}$, where R, K are uniform upper bounds on the reach and on the absolute values of the sectional curvatures for all the manifolds, i_0 is a lower bound on the injectivity radius of all manifolds, and C is a constant no larger than 1.
- (2) $\varepsilon_- \leq (1/4)\varepsilon_+ \ll 1$; the $(1/4)$ here is an arbitrary number smaller than 1.
- (3) $\frac{c}{n^{1/m}} < \tilde{\delta}$
- (4) $C(\tilde{\delta} + \theta) \leq \frac{1}{2c_\rho}$, where $\frac{1}{c_\rho}$ is the lower bound of ρ .

With the above assumptions we can make sure that with the underlying $\varepsilon_+, \varepsilon_-$ -weighted graph we can approximate the operators $\Delta_{\mathcal{M}_k}$ in each of the \mathcal{M}_k ; this part does not rely on the assumption that all manifolds have the same dimension, and only depends on the full inner connectivity property. For the spectrum of the graph Laplacian associated to (X, ω) to successfully recover the spectrum of $\Delta_{\mathcal{M}}$ we need (X, ω) to be fully inner connected and sparsely outer connected as we will make explicit in our first theorem.

Theorem 2.5 (Convergence rate for eigenvalues). *Let μ be a probability measure on \mathcal{M} as in (2.1). Suppose that the \mathcal{M}_k forming the \mathcal{M} satisfy Assumptions 1, and assume also that $m_1 = \dots = m_N$. Let $X = \{x_1, \dots, x_n\}$ be i.i.d. samples from μ . Let (X, ω) be a symmetric weighted graph and let \mathcal{L} be the rescaled graph Laplacian:*

$$\mathcal{L}u(x) := \frac{1}{n^2(\varepsilon_+^{m+2} - \varepsilon_-^{m+2})} \sum_{y \in X} \omega_{xy}(u(x) - u(y)), \quad x_i \in X, u : X \rightarrow \mathbb{R}. \quad (2.7)$$

Suppose that the quantities $\tilde{\delta}, \theta, \varepsilon_+, \varepsilon_-$ satisfy Assumptions 2. Let $\lambda_k^{\varepsilon_+, \varepsilon_-}$ be the k -th eigenvalue of \mathcal{L} and let λ_k be the k -th eigenvalue of $\Delta_{\mathcal{M}}$ where $\Delta_{\mathcal{M}}$ is the tensorized Laplacian from (1.3). Then, there exists a constant C (independent of k), such that with probability at least $1 - \sum_{l=1}^N (nw_l + t) \exp(-C(nw_l - t)\theta^2\tilde{\delta}^m) - 2N \exp\left(\frac{-2t^2}{n}\right) - C_1(n)$, for every $k \in \mathbb{N}$ for which

$$C\tilde{\delta}\sqrt{\lambda_k} + C(\theta + \tilde{\delta}) < \frac{1}{k},$$

we have:

$$|\lambda_k^{\varepsilon_+, \varepsilon_-} - \sigma_{\eta}\lambda_k| \leq e_k + C \left(\varepsilon_+(\sqrt{\lambda_k} + 1) + \theta + \frac{\tilde{\delta}}{\varepsilon_+} \right) \lambda_k.$$

In the above, $e_k = \frac{CN_0}{n^2(\varepsilon_+^{m+2} - \varepsilon_-^{m+2})} \left(1 + C'(\lambda_k^{m/2+1} + \tilde{\delta}\sqrt{\lambda_k} + \theta + \tilde{\delta}) \right)$, and $C_1(n)$ and N_0 are introduced in Definition 2.3 and Definition 2.4 respectively. The constant σ_{η} is given by:

$$\sigma_{\eta} := \int_{B_m(0,1)} |y_1|^2 \eta(|y|) dy, \quad (2.8)$$

where $B_m(0, 1)$ is the unit ball in dimension m .

Remark 2.6. i) In general, we should expect a trade off between the quantities $C_1(n)$ and N_0 . That is, in general, an attempt of making N_0 smaller (i.e. erase connections between different manifolds) will typically result in a smaller probability of having a graph that is well connected within each manifold \mathcal{M}_l .

- ii) The advantages of taking $\varepsilon_- > 0$ for the MMC problem are not explicit in the error bounds from Theorem 2.5. However, we will see later on that by tuning ε_- appropriately, one can substantially eliminate connections between data points in different manifolds when one considers $\varepsilon_- \sim \varepsilon_+$. This means a substantial decrease in N_0 . We explain this in Remark 3.5 for the specific annular graph construction with angle constraints. The fact that we can improve the performance of MMC algorithms by introducing $\varepsilon_+, \varepsilon_-$ -graphs motivates the theoretical analysis that we consider in the Appendix.
- iii) The proof of the estimates in Theorem 2.5 relies on a variational approach that compares Dirichlet energies at discrete and continuum levels. This approach has been used before in [13, 34, 44]. However, the structure of the $\varepsilon_+, \varepsilon_-$ -graph that we consider here forces us to modify the analysis and present new proofs. Even for a single manifold $\mathcal{M} = \mathcal{M}_1$, the analysis of graph Laplacians on $\varepsilon_+, \varepsilon_-$ -graphs is a technical contribution of this work. The actual proof of Theorem 2.5 appears in section A.5 in the Appendix. Several technical preliminary results are established in the preceding sections.
- iv) The scaling factor relating \mathcal{L} and Δ_n in (2.7) is irrelevant for spectral clustering because the eigenvectors of Δ_n are the same as those for \mathcal{L} and the ratio between eigenvalues of Δ_n coincides with the ratio of eigenvalues of \mathcal{L} . In other words in practice we can work directly with Δ_n and we do not have to compute the rescaling factor.
- v) As in the results from [13] and [44] if we choose $1 \gg \varepsilon_+ \gg \left(\frac{\log(n)}{n}\right)^{1/m}$, then high probability, the error of approximation of eigenvalues scales like:

$$\frac{N_0}{n^2(\varepsilon_+^{m+2})} + \frac{\left(\frac{\log(n)}{n}\right)^{1/m}}{\varepsilon_+} + \varepsilon_+.$$

Thus, in order for this error estimates to be meaningful we need the graph to satisfy the sparse outer connectivity condition.

Theorem 2.7 (Convergence rate for eigenvectors). *Under the same setting and assumptions as in Theorem 2.5, for every $k \in \mathbb{N}$ there is a constant $c_k = c_k(\mathcal{M})$ such that if*

$$e_k + C \left(\varepsilon_+ \sqrt{\lambda_k} + \varepsilon_+^2 + \theta + \frac{\tilde{\delta}}{\varepsilon_+} \right) \leq c_k,$$

then with probability at least $1 - \sum_{l=1}^N (nw_l + t) \exp \left(-C(nw_l - t) \theta^2 \tilde{\delta}^m \right) - 2N \exp \left(\frac{-2t^2}{n} \right) - C_1(n)$ for every u_k normalized eigenvector of \mathcal{L} with eigenvalue λ_k , there is a normalized eigenfunction f_k of $\Delta_{\mathcal{M}}$ with eigenvalue λ_k such that

$$\|f_k - v_k\|_{L^2(\mu^n)} \leq \left[Ce_k + C \left(\varepsilon_+ \sqrt{\lambda_k} + \varepsilon_+^2 + \theta + \frac{\tilde{\delta}}{\varepsilon_+} \right) \right]^{1/2} + C_{\mathcal{M}, \lambda} \tilde{\delta}$$

where e_k is the same as in Theorem 2.5.

The proof of this Theorem is presented in section A.6 in the Appendix.

2.4. Mixed dimensions. We generalize our results from section 2.3 to a setting where the manifolds \mathcal{M}_k may have different dimensions. For convenience we introduce some notation first.

Without the loss of generality we can assume that the manifolds \mathcal{M}_k are indexed in decreasing order of dimension, i.e. $m = m_1 \geq m_2 \geq \dots \geq m_N$. We let N_{\max} be the number of manifolds with the maximum dimension m , i.e. $m_1 = \dots = m_{N_{\max}} > m_{N_{\max}+1}$. We set $\mathcal{M}_{\max} := \mathcal{M}_1 \cup \dots \cup \mathcal{M}_{N_{\max}}$ and write $\langle f, g \rangle_{L^2(\mathcal{M}_{\max})}$ to represent:

$$\langle f, g \rangle_{L^2(\mathcal{M}_{\max})} = \sum_{i=1}^N w_i \langle f_i, g_i \rangle_{L^2(\mu_i)} = \sum_{i=1}^N w_i \int_{\mathcal{M}_i} f_i(x) g_i(x) d\mu_i(x).$$

We also use $\|f\|_{L^2(\mathcal{M}_{\max})}^2 = \langle f, f \rangle_{L^2(\mathcal{M}_{\max})}$.

Notice that with the above inner product we can identify (isometrically) elements in $L^2(\mathcal{M}_{\max})$ with elements in $L^2(\mu)$ that are zero outside of \mathcal{M}_{\max} ; throughout section A.7 in the Appendix we may use this identification without any further explanation. Finally, we use $\Delta_{\mathcal{M}_{\max}}$ to denote the tensorized Laplacian (1.3) for \mathcal{M}_{\max} (i.e. just as in (1.3) but with only the first N_{\max} coordinates); we use D_{\max} to denote the corresponding Dirichlet energy defined for $L^2(\mathcal{M}_{\max})$ functions.

Theorem 2.8. *Let μ be a probability measure on \mathcal{M} as in (2.1). Suppose that the \mathcal{M}_k forming \mathcal{M} satisfy Assumptions 1, and let $N_{\max}, \mathcal{M}_{\max}, \Delta_{\mathcal{M}_{\max}}$ be defined as before. Set $\lambda_1, \dots, \lambda_N = 0$ and let $\lambda_{N+1} \leq \lambda_{N+2} \leq \dots$ be the list of non-zero eigenvalues of $\Delta_{N_{\max}}$ repeated according to multiplicity.*

Let $X = \{x_1, \dots, x_n\}$ be i.i.d. samples from μ , let (X, ω) be a symmetric weighted graph and let \mathcal{L} be the rescaled graph Laplacian from (2.7). Finally, suppose that the quantities $\tilde{\delta}, \theta, \varepsilon_+, \varepsilon_-$ satisfy Assumptions 2.

Then, for some constant $C = C(\mathcal{M}, \mu)$, with probability at least

$$1 - \sum_{l=1}^N (nw_l + t) \exp \left(-C(nw_l - t) \theta^2 \tilde{\delta}^m \right) - 2N \exp \left(\frac{-2t^2}{n} \right) - C_1(n),$$

for every $k \in \mathbb{N}$ for which

$$C \tilde{\delta} \sqrt{\lambda_k} + C(\theta + \tilde{\delta}) < \frac{1}{k},$$

we have:

$$|\lambda_k^{\varepsilon_+, \varepsilon_-} - \sigma_{\eta} \lambda_k| \leq e_k + C \left(\varepsilon_+ (\sqrt{\lambda_k} + 1) + \theta + \frac{\tilde{\delta}}{\varepsilon_+} \right) \lambda_k.$$

In the above, $e_k = \frac{CN_0}{n^2(\varepsilon_+^{m+2} - \varepsilon_-^{m+2})} \left(1 + C'(\lambda_k^{m/2+1} + \tilde{\delta}\sqrt{\lambda_k} + \theta + \tilde{\delta})\right)$, and $C_1(n)$ and N_0 are introduced in Definition 2.3 and Definition 2.4 respectively.

In addition, there is a constant $c_k = c_k(\mathcal{M})$ such that if

$$e_k + C \left(\varepsilon_+ \sqrt{\lambda_k} + \varepsilon_+^2 + \theta + \frac{\tilde{\delta}}{\varepsilon_+} \right) \leq c_k,$$

then with probability at least $1 - \sum_{l=1}^N (nw_l + t) \exp\left(-C(nw_l - t)\theta^2\tilde{\delta}^m\right) - 2N \exp\left(\frac{-2t^2}{n}\right) - C_1(n)$ for every u_k normalized eigenvector of \mathcal{L} with eigenvalue λ_k , there is a normalized eigenfunction f_k of $\Delta_{\mathcal{M}_{max}}$ with eigenvalue λ_k such that

$$\|f_k - v_k\|_{L^2(\mu^n)} \leq \left[Ce_k + C \left(\varepsilon_+ \sqrt{\lambda_k} + \varepsilon_+^2 + \theta + \frac{\tilde{\delta}}{\varepsilon_+} \right) \right]^{1/2} + C_{\mathcal{M}, \lambda} \tilde{\delta}.$$

We interpret the functions f_1, \dots, f_k as another orthonormal basis for $\text{Span}\{\mathbb{1}_{\mathcal{M}_1}, \dots, \mathbb{1}_{\mathcal{M}_N}\}$.

Remark 2.9. i) The proof of this theorem appears in section A.7 in the Appendix. Assuming that we have already established Theorems 2.5 and 2.7 (and some associated preliminary results) we can proceed to the proof of Theorem 2.8 almost directly.

ii) When manifolds have different dimensions, making sure that the full inner connectivity condition is satisfied is more difficult because in general N_{kl} is much larger when the dimensions of the manifolds \mathcal{M}_k and \mathcal{M}_l are small than when the dimensions are large. In particular, Theorem 2.8 does not answer the question of what happens when $\frac{N_{kl}}{n^2(\varepsilon_+^{m+2} - \varepsilon_-^{m+2})} \not\rightarrow 0$ for some manifolds \mathcal{M}_k and \mathcal{M}_l that have dimension strictly smaller than m . Part of our analysis allows us to speculate that under some additional mild assumptions it may still be possible recover the spectrum of the tensorized Laplacian on \mathcal{M}_{max} , but with a different structure for the zero eigenvalue than the one in Theorem 2.8. In particular, we can expect that if manifolds \mathcal{M}_k and \mathcal{M}_l can not be separated, then asymptotically they get merged together. In such situation one may consider a peeling strategy where we remove higher dimensional manifolds first, before repeating the algorithm with a smaller data set until all manifolds have been separated. Making this type of mathematical statement precise, and describing this peeling strategy in detail, are tasks left for future work.

3. ANNULAR PROXIMITY GRAPHS WITH ANGLE CONSTRAINTS

In this section we introduce a graph construction that is both inner fully connected and outer sparsely connected. We start with a definition.

Definition 3.1. Let $\alpha \in (0, \pi/2)$ and $r > 0$. We call an ordered sequence of data points

$$(x_{i_1}, x_{i_2}, \dots, x_{i_m})$$

an (α, r) -constrained path between x_{i_1} and x_{i_m} if the following two conditions hold:

- i) $\angle(x_{i_m} - x_{i_1}, x_{i_{j+1}} - x_{i_j}) < \alpha, \forall j = 1, 2, \dots, m-1$.
- ii) $|x_{i_j} - x_{i_{j+1}}| < r, \forall j = 1, 2, \dots, m-1$.

In words, the first condition requires that the angle between any step in the path and the segment between the first and last points in the path must be small. The second condition requires consecutive points in the path to be close enough.

We consider the following similarity weights. If x_i, x_j are two data points such that $|x_i - x_j| \leq \varepsilon_-$ or $|x_i - x_j| \geq \varepsilon_+$, then we set $\omega_{ij} = 0$. If $\varepsilon_- < |x_i - x_j| < \varepsilon_+$ and there is an (α, r) -constrained path between x_i and x_j , then we set $\omega_{ij} = 1$, otherwise we set $\omega_{ij} = 0$. We refer to this type of graph as an *annular proximity graph with angle constraints*. We show that with the right choice of parameters these graphs satisfy the full inner connectivity and sparse outer connectivity conditions. The precise statements are contained in Theorem 3.2 and Theorem 3.3 below. In Theorem 3.3 we also quantify the advantages of annular graphs with $\varepsilon_- \sim \varepsilon_+$ for MMC. In section 4.2.1 we revisit again the effect of annular graphs on MMC, this time from a numerical perspective. Finally, it is worth saying that the weights ω can be constructed following a simple modification of the constrained Dijkstra's algorithm from [5].

Theorem 3.2. *Let n_k be the number of data points in $X \cap \mathcal{M}_k$, let $\alpha \in [0, \pi/4)$ and let $r \leq C\varepsilon_+$. Then, with probability at least*

$$1 - \frac{C_k n^2 \varepsilon_+}{r} \exp(-C_k n_k r^{m_k} (\tan \alpha)^{m_k-1}),$$

for any two points $x_i, x_j \in \mathcal{M}_l$ such that $|x_i - x_j| < \varepsilon_+$, there exists an (α, r) -constrained path between x_i and x_j . In the above, C_k is a constant that depends on \mathcal{M}_k and ρ_k .

Theorem 3.3. *Suppose that Assumptions 1 hold and suppose that $\mathcal{M}_{kl} = \mathcal{M}_k \cap \mathcal{M}_l \neq \emptyset$.*

(1) *If $\varepsilon_- \leq (1/4)\varepsilon_+$, $\alpha < \arcsin(\frac{Cr}{\varepsilon_+})$, and $r \leq c\varepsilon_+$, then, with probability no less than*

$$1 - C_{k,l} n \exp(-C_{k,l} n \min\{r^{m_k-m_{kl}}, r^{m_l-m_{kl}}, \varepsilon_+^{m_k}, \varepsilon_+^{m_l}\}),$$

N_{kl} , the number of connections between points in $X \cap \mathcal{M}_k$ and $X \cap \mathcal{M}_l$, satisfies

$$N_{kl} \leq C_{k,l} n^2 \max\{r^{m_k-m_{kl}} \varepsilon_+^{m_l}, r^{m_l-m_{kl}} \varepsilon_+^{m_k}\}.$$

(2) *If in (1) we further assume the lower bound $\varepsilon_- \geq c\varepsilon_+$, then with probability no less than*

$$1 - C_{k,l} n \exp(-C_{k,l} n \min\{(r^2/\varepsilon_+)^{m_k-m_{kl}}, (r^2/\varepsilon_+)^{m_l-m_{kl}}, \varepsilon_+^{m_k}, \varepsilon_+^{m_l}\}),$$

we have

$$N_{kl} \leq C_{k,l} n^2 \max\{(r^2/\varepsilon_+)^{m_k-m_{kl}} \varepsilon_+^{m_l}, (r^2/\varepsilon_+)^{m_l-m_{kl}} \varepsilon_+^{m_k}\}.$$

Remark 3.4. *To illustrate our results and obtain concrete error estimates in Theorem 2.5, for example, consider the case where all manifolds have the same dimension m . Going back to the last point in Remark 2.6 we need to tune the parameters r and α so that $N_0 \ll n^2 \varepsilon_+^{m+2}$ and also, following Theorem 3.2, we should have $nr^m \tan(\alpha)^{m-1} \gg 1$. Now, from Theorem 3.3 it follows that we need $r \ll \varepsilon_+^{3/2}$ (assuming the worst case scenario where the dimension $m_{kl} = m-1$, and assuming we impose the lower bound on ε_- , i.e. we treat $\varepsilon_- \sim \varepsilon_+$). On the other hand, if we set $\sin(\alpha) = C \frac{r}{\varepsilon_+}$ we see from Theorem 3.3 that we need $r^{2m-1}/\varepsilon_+^{m-1} \gg \frac{1}{n}$ (omitting logarithmic terms). Thus, if we take $r \sim \varepsilon_+^2$ and we set $\varepsilon_+ = C \left(\frac{1}{n}\right)^{\frac{1}{3m-1}}$ for large enough constants C we can satisfy all constraints and get the rate (omitting logarithmic terms):*

$$O\left(\frac{1}{n^{1/(3m-1)}}\right)$$

for the convergence of the eigenvalues of the graph Laplacian on an annular path with angle constraints towards the eigenvalues of the tensorized Laplacian on \mathcal{M} . For comparison, recall that the convergence rate obtained in [44] for the spectral convergence of graph Laplacians was $O\left(\frac{1}{n^{1/(2m)}}\right)$ and the convergence rate in [14] is $O\left(\frac{1}{n^{1/(m+4)}}\right)$. Of course, the distinction between our work and those previously mentioned is that here we are concerned with a multi-manifold clustering problem.

Remark 3.5. From Theorem 3.3 we can see the quantitative effect of considering a non-zero ε_- . Indeed, when r is taken to be considerably smaller than ε_+ , the number of wrong connections in the $\varepsilon_- \sim \varepsilon_+$ setting is much smaller than when $\varepsilon_- = 0$ because $\frac{r}{\varepsilon_+}$ is a small quantity. Intuitively, removing points should always reduce the number of wrong connections, but what Theorem 3.3 says is that the ratio of wrong connections erased by simply removing an inner ball with volume comparable to that of the outer ball is actually quite significant. This result motivates the theoretical analysis that we present in the Appendix. In our numerical experiments we illustrate further the superior performance of our MMC algorithm when we set $\varepsilon_- \sim \varepsilon_+$.

Remark 3.6. It is not difficult to show that in general one can not relax the requirement that $\sin(\alpha) \ll 1$ in order to get sparse outer connected graphs. Indeed, take for example two flats \mathcal{M}_k and \mathcal{M}_l with dimension 2 that meet perpendicularly at a straight line. If $\alpha \geq c > 0$ for all n , it is straightforward to see that there is a small enough constant c_1 (depending on the lower bound for α) such that for all pairs of points $x \in \mathcal{M}_k$ and $y \in \mathcal{M}_l$ for which $\text{dist}(x, \mathcal{M}_{kl}) \leq c\varepsilon_+$, $\text{dist}(y, \mathcal{M}_{kl}) \leq c\varepsilon_+$, and $|x - y| < \varepsilon_+$, there is an (α, r) constrained path between x and y . In turn, from this one can see that the number of connections that a point $x \in \mathcal{M}_k$ with $\text{dist}(x, \mathcal{M}_{kl}) \leq c_1\varepsilon_+$ has with points in \mathcal{M}_l is $O(n\varepsilon_+^2)$ (i.e. the same order as with points in \mathcal{M}_k). In that case, $N_0 \sim n^2\varepsilon_+^{2+1}$ and thus $N_0/(n^2\varepsilon_+^{2+2}) \rightarrow \infty$.

3.1. Proofs of Theorems 3.2 and 3.3.

Proof of Theorem 3.2. Given that the manifold \mathcal{M}_k is smooth and compact, and given that we only consider connecting two points $x, y \in X \cap \mathcal{M}_k$ when they are within a small distance ε_+ from each other, we can (and will) assume for simplicity that \mathcal{M}_k is a flat of dimension m_k . As will become clear from our argument, the reduction to the flat case is sufficient as all curvature effects only introduce lower order corrections to our estimates.

Consider then the line segment connecting the points x and y and consider also the cylinder in \mathcal{M}_k with axis given by the segment $y - x$ and circular base of radius h_1 centered at x and orthogonal to the segment xy ; see Figure 4. We split this bigger cylinder into l parallel smaller cylinders with height h_2 . The smaller cylinders are labeled as $\mathcal{C}_1, \dots, \mathcal{C}_l$. By taking $h_2 = cr$ for small enough constant $(1/4) > c > 0$, $h_1 = \frac{c}{2} \tan(\alpha)r$, and assuming that $|x - y| > 4cr$, we can guarantee that

- i) l is an odd number.
- ii) $4h_1^2 + 9h_2^2 \leq r^2$.
- iii) $\frac{2h_1}{h_2} \leq \tan(\alpha)$.

With this construction it is clear that if $X \cap \mathcal{C}_s \neq \emptyset$ for every even s , then we can construct an (α, r) -constrained path between x and y ; see Figure 4. Notice that if on the other hand $|x - y| \leq 4cr \leq r$, then x and y can be connected directly.

In the more interesting case $\varepsilon_+ \geq |x - y| > 4cr$, the probability that there is at least one sample from the n_k samples in \mathcal{M}_k in all the cylinders \mathcal{C}_s is no smaller than

$$1 - \frac{C\varepsilon_+}{r} (1 - C_k r^{m_k} (\tan \alpha)^{m_k-1})^{n_k} = 1 - \frac{C_k \varepsilon_+}{r} \exp(-C_k n_k r^{m_k} (\tan \alpha)^{m_k-1}).$$

By the discussion above, we conclude that the probability that there exists an (α, r) -constrained path between x and y is no smaller than the above quantity.

To bound from below the probability that *all* pairs of points $x, y \in X \cap \mathcal{M}_k$ that are within distance ε_+ are connected by (α, r) -constrained paths it is sufficient to take a union bound using the above estimates. \square

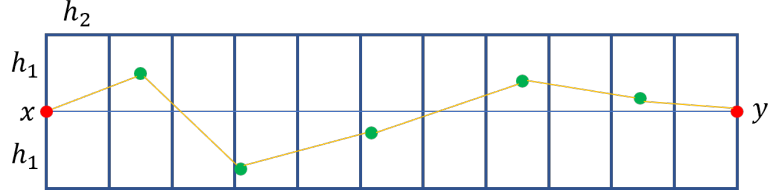


FIGURE 4. This is a valid path between x and y on the flat.

Next we discuss the outer sparsity for the annular proximity graph with angle constraints. We start with a result that applies for all choices of $\varepsilon_- \in [0, (1/4)\varepsilon_+]$ and then refine the estimates when we take $\varepsilon_- = c\varepsilon_+$.

Lemma 3.7. *Suppose that $\mathcal{M}_l \cap \mathcal{M}_k \neq \emptyset$ and let $x \in \mathcal{M}_l$ and $y \in \mathcal{M}_k$ be such that $|x - y| < \varepsilon_+$. Assume that $\text{dist}(x, \mathcal{M}_{kl}) > r$. If y is such that*

$$\cos(\beta) \frac{\text{dist}(y, \mathcal{M}_{kl})}{|y - x|} > C_{k,l} \sin(\alpha),$$

then there is no (α, r) -path between x and y . In the above, the constant $C_{k,l}$ depends on the manifolds \mathcal{M}_k and \mathcal{M}_l through their curvature and that of \mathcal{M}_{kl} . In particular, if we set α to be such that $\sin(\alpha) \leq \frac{r \cos(\beta)}{\varepsilon_+ C_{k,l}}$, then there is no (α, r) -constrained path between points x and y if

$$\text{dist}(y, \mathcal{M}_{kl}) \geq r.$$

On the other hand suppose that $x \in \mathcal{M}_k$ is such that $\text{dist}(x, \mathcal{M}_{lk}) < r$, $\sin(\alpha) \leq \frac{r \cos(\beta)}{\varepsilon_+ C_{kl}}$ and $y \in \mathcal{M}_k$ is such that $|x - y| \leq \varepsilon_+$. Then, the first point of any (α, r) -constrained path connecting x and y starting from x must belong to \mathcal{M}_k .

Proof. Given that the manifolds \mathcal{M}_k , \mathcal{M}_l , and \mathcal{M}_{kl} are smooth and compact, and given that we only consider connecting two points x, y when they are within a small distance ε_+ from each other, we can (and will) assume for simplicity that \mathcal{M}_k and \mathcal{M}_l are flats of dimension m_k and m_l respectively. Indeed, notice that all curvature effects introduce at most second order corrections to the estimates we present in the flat case.

Without the loss of generality we can assume that both \mathcal{M}_k and \mathcal{M}_l are subspaces (i.e. cross the origin) as we can always recenter the flats at one of the points in their intersection. In fact, we will center the coordinate system at the closest point in \mathcal{M}_{kl} to y . In this new coordinate system the point y can be written as

$$y = y_l v_l + y_{kl} v_{kl},$$

for unit vectors $v_l \in \mathcal{M}_k^\perp$ and $v_{kl} \in \mathcal{M}_{kl}^{\perp k}$ (where we use $\mathcal{M}_{kl}^{\perp k}$ to denote the orthogonal complement of \mathcal{M}_{kl} in \mathcal{M}_k); y_l and y_{kl} are non-negative scalars. Indeed, notice that y has no \mathcal{M}_{kl} component because the origin has been chosen to be the closest point to y in \mathcal{M}_{kl} . From basic trigonometry we have

$$y_l = |y| \sin(\vartheta),$$

where ϑ is the angle between v_{kl} and y . Recall that $\vartheta \in [\pi/2 - \beta, \pi/2 + \beta]$ according to Assumption 1.

Now, if there exists an α -constrained path connecting $x \in \mathcal{M}_k$ and $y \in \mathcal{M}_l$ for points x, y for which $\text{dist}(x, \mathcal{M}_{kl}) > r$, then there will be at least one segment x' in the path (here interpreted as the difference between two consecutive points in the path) that belongs to \mathcal{M}_k . Thus, we must have

$$\frac{\langle y_{kl} v_{kl} - x, x' \rangle}{|y - x| \cdot |x'|} = \frac{\langle y - x, x' \rangle}{|y - x| \cdot |x'|} > \cos(\alpha).$$

Using the Cauchy Schwartz inequality we obtain:

$$\frac{|y_{kl}v_{kl} - x|^2}{|y - x|^2} > \cos^2(\alpha).$$

On the other hand, by the Pythagorean theorem we have $|y_{kl}v_{kl} - x|^2 + |y_lv_l|^2 = |x - y|^2$. Thus,

$$1 - \frac{\sin^2(\vartheta)|y|^2}{|y - x|^2} > \cos^2(\alpha).$$

In particular,

$$\sin^2(\alpha) \geq \cos^2(\beta) \frac{\text{dist}(y, \mathcal{M}_{kl})^2}{|y - x|^2}.$$

In other words, if the above relationship is not satisfied there can not exist an (α, r) -path between x and y .

For the second part we assume for the sake of contradiction that there is an (α, r) -constrained path between x and y such that the first step (starting from x) in the path belongs to \mathcal{M}_l ; we call this first step x_1 . We can then repeat the same argument as above with $x' = x_1 - x$ to conclude that if $\sin^2(\alpha) \leq \cos^2(\beta) \frac{r^2}{\varepsilon_+^2}$, then we would reach a contradiction. \square

The next lemma helps us justify why, for the multi-manifold clustering problem, choosing ε_- of the same order as ε_+ is better than choosing $\varepsilon_- = 0$ (or in general ε_- much smaller than ε_+).

Lemma 3.8. *Suppose that $\mathcal{M}_l \cap \mathcal{M}_k \neq \emptyset$ and let $x \in \mathcal{M}_l$ and $y \in \mathcal{M}_k$ be such that $\varepsilon_- < |x - y| < \varepsilon_+$, where $\varepsilon_- = c\varepsilon_+$. Let $\alpha > 0$ be such that*

$$\sin(\alpha) < C_{k,l} \cos(\beta) \frac{r}{\varepsilon_+}.$$

If $\text{dist}(x, \mathcal{M}_{kl}) > r$ and $\text{dist}(y, \mathcal{M}_{kl}) > C \frac{r^2}{\varepsilon_+^2}$, then there can not exist an (α, r) constrained path between x and y .

Proof. As in Lemma 3.7 we assume for simplicity that \mathcal{M}_k and \mathcal{M}_l are flats of dimension m_k and m_l respectively.

Let $x \in \mathcal{M}_l$ be such that $\text{dist}(x, \mathcal{M}_{kl}) > r$ and let $y \in \mathcal{M}_k$ be such that $\text{dist}(x, \mathcal{M}_{kl}) > C \frac{r^2}{\varepsilon_+^2}$. If $\text{dist}(y, \mathcal{M}_{kl}) > r$, then by Lemma 3.7 there can not exist an (α, r) -constrained path between x, y . Thus, without the loss of generality we can assume that $\text{dist}(y, \mathcal{M}_{kl}) \leq r$. We now show that if the constant C above is large enough, then there can not exist an (α, r) -constrained path between x and y .

Assume for the sake of contradiction that there is an (α, r) -constrained path between x and y as above. Let z be the projection of y onto \mathcal{M}_l , let $t := |y - z|$, and finally let $d := |y - x| > \varepsilon_-$. Notice that by the Pythagorean theorem we must have $t \leq \text{dist}(y, \mathcal{M}_{kl}) \leq r$. In addition, by the second part of Lemma 3.7 we know that the first step in the path (starting from y) must lie in \mathcal{M}_l ; we denote by y_1 this first step. From a simple geometric observation (just consider the triangles $\triangle xyz$ and $\triangle y_1yz$) we can see that the angle between the vectors $x - y$ and $y_1 - y$, let's call it ϑ , satisfies

$$\alpha > \vartheta \geq \arccos \frac{t}{d} - \arccos \frac{t}{|y - y_1|} \geq \arccos \frac{t}{d} - \arccos \frac{t}{r} =: f(d, t).$$

The function $f(d, t)$ is strictly increasing in both coordinates because $\partial_d f(d, t) = \frac{t}{d^2} \cdot \frac{1}{\sqrt{1 - \frac{t^2}{d^2}}} > 0$ and $\partial_t f(d, t) = \frac{1}{\sqrt{r^2 - t^2}} - \frac{1}{\sqrt{d^2 - t^2}} > 0$. In particular, $f(d, t) \geq f(\varepsilon_-, t)$. We also see that if $t > t_0$

where

$$t_0 := \frac{r\varepsilon_- \sin(\alpha)}{\sqrt{\varepsilon_-^2 - 2r\varepsilon_- \cos(\alpha + r^2)}},$$

then

$$\alpha \geq f(d, t) \geq f(\varepsilon_-, t) > f(\varepsilon_-, t_0) = \alpha$$

and thus we reach a contradiction. From the fact that

$$t_0 = \frac{r\varepsilon_- \sin \alpha}{\sqrt{\varepsilon_-^2 - 2\varepsilon_- r \cos \alpha + r^2}} < \frac{r\varepsilon_- \sin \alpha}{\varepsilon_- \cos \alpha - r} < \frac{Cr^2}{\varepsilon_+}$$

we conclude that if $t > C \frac{r^2}{\varepsilon_+}$, then there can not be an (α, r) -constrained path between y and x . \square

With Proposition 3.2, Lemma 3.7 and 3.8, we can show the main result in this Section.

Proof of Theorem 3.3. i) For arbitrary $\varepsilon_- \leq (1/4)\varepsilon_+$ we can use Lemma 3.7 and a standard concentration bound to see that with probability no less than

$$1 - C_{k,l} n \exp(-C_{k,l} n \min\{r^{m_k - m_{kl}}, r^{m_l - m_{kl}}, \varepsilon_+^{m_k}, \varepsilon_+^{m_l}\}),$$

N_{kl} , the number of connections between points in $X \cap \mathcal{M}_k$ and $X \cap \mathcal{M}_l$, satisfies

$$N_{kl} \leq C_{k,l} n^2 \max\{r^{m_k - m_{kl}} \varepsilon_+^{m_l}, r^{m_l - m_{kl}} \varepsilon_+^{m_k}\}.$$

ii) When we have the lower bound $\varepsilon_- \geq c\varepsilon_+$ we can proceed as above but now using Lemma 3.8. \square

3.2. A local PCA approach to MMC. An alternative spectral approach to the multimaniifold clustering problem that is popular in the literature (e.g. see [3]) is based on building weights ω_{ij} that depend on the level of alignment of local tangent planes around nearby data points. To be precise, as in the path-construction from section 3 we only consider giving an edge to a pair of data points x_i, x_j if $\varepsilon_- < |x_i - x_j| < \varepsilon_+$. If this condition is satisfied, we then set $\omega_{x_i x_j} = 1$ provided that the angle between \hat{T}_{x_i} (a local tangent plane around x_i) and \hat{T}_{x_j} is smaller than a certain threshold, and otherwise we set $\omega_{x_i x_j} = 0$. These local “tangent” planes can be constructed from the observed data using local PCA. Namely, the idea is to run PCA with the data set $X \cap B(x_i, r)$ for some small enough r in order to obtain a collection of principal directions which are then used as generators for the plane $\hat{T}(x_i)$; see [3] for more details.

Using the estimates from [3] (and some additional computations) it is possible to show that the local PCA graph construction satisfies the sparse outer connectivity condition (with very high probability) provided that the parameter r is tuned appropriately. However, from a theoretical perspective, one should not expect that the full inner connectivity holds with high probability. This is an observation already made in [3] (even if not with the exact same words). Indeed, let x_i be a point in the manifold \mathcal{M}_l that is close to the intersection of \mathcal{M}_l and \mathcal{M}_k (closer than r). For points $x_j \in \mathcal{M}_l$ within distance ε_+ from x_i and away enough from the intersection $\mathcal{M}_k \cap \mathcal{M}_l$ we expect their PCA-based tangent planes to resemble those of the actual manifold \mathcal{M}_l at those same points (if r has been chosen so that there is consistency in the approximation of tangent planes). However, x_i ’s empirical tangent plane will be influenced by the presence of the points in \mathcal{M}_k that belong to the ball $B(x_i, r)$ and thus one should not expect this plane to be aligned with the planes of all the other points $x_j \in \mathcal{M}_l$ lying nearby. In contrast, the full inner connectivity for the path-based graph construction from section 3 just depends on the points on each single manifold: having

additional points can only help with the full inner connectivity (more points means more possible paths) but never tamper with it.

One of the implications of the above discussion is that the local PCA approach to MMC may in principle produce more clusters than desirable and for example groups of points that lie close to the intersection of two manifolds may form their own clusters; see the discussion in section 3 in [3]. It is thus possible that some of the manifolds get split into different components and in particular one may not be able to recover the multi-manifold structure underlying the data without information on the actual location of the manifolds' intersections.

4. NUMERICAL EXPERIMENTS

The purpose of this section is twofold. On the one hand, we want to explore the limitations and difficulties that may arise when using the MMC methodologies based on spectral clustering that we have discussed thus far. On the other hand, we want to provide further insights into the theoretical results that we discussed in the previous sections. We present a series of numerical experiments aimed at achieving these two goals.

4.1. Bottlenecks and multiple manifolds. Our theoretical results imply that the spectra of suitable graphs resemble the spectrum of a tensorized Laplacian on the union of the smooth manifolds underlying the data set. In particular, when using spectral clustering on finite data sets with a multi-manifold structure, it is possible to obtain a partition of the data into multiple smooth manifolds and/or into regions that are separated by thin bottlenecks. In this section we explore numerically the “confounding” role that bottlenecks may play in MMC.

First, let us consider the bottle and plane example illustrated in Figures 5, 6, and 7. There, the data set X is obtained by sampling uniformly from the set $\mathcal{M} = \mathcal{M}_1 \cup \mathcal{M}_2$, where \mathcal{M}_1 is a plane and \mathcal{M}_2 is a 2-dimensional dumbbell with a bottleneck at its center. A graph (X, ω) has been constructed as in section 3 for appropriate values of $\varepsilon_-, \varepsilon_+, r, \alpha$. Intuitively, this graph should help identify the two manifolds given that they meet perpendicularly (i.e. β is zero in (2.2)). On the other hand, the same graph captures the internal geometry of \mathcal{M}_2 and thus should also detect the bottleneck in \mathcal{M}_2 . Figure 5 shows the sign of the first non-trivial eigenvector of the graph Laplacian which, as we can observe from the picture, is able to detect the bottleneck. Figure 6 shows the sign of the second non-trivial eigenvector (orthogonal to the first non-trivial eigenvector). It is worth mentioning that in our experiments our graph Laplacian's first two non-zero eigenvalues are close to zero and their relative difference is quite small compared to the relative difference between the second and third non-zero eigenvalues. The partition illustrated in Figure 6 is not directly interpretable. However, when considering a suitable linear combination of the first and second non-trivial eigenvectors we recover the partition illustrated in Figure 7 which correctly separates the two manifolds. This linear combination was obtained by minimizing the *Ratio cut* functional (see [48] for a definition) among the partitions induced by norm one linear combinations of the first two non-trivial eigenvectors (in this case a simple one dimensional search).

This example illustrates that bottlenecks are indeed confounders for MMC when using spectral methods. Still, even in the presence of competitor bottlenecks, we see that the spectrum of the graph Laplacian does possess the information needed to recover the desired partition of the data, and the combination of spectral clustering with Ratio cut minimization is shown to help in the detection of the desired partition. Warm start initialization for balanced cut minimization using spectral clustering has been considered in the literature before (e.g. [8–12]).

Another example where multiple manifolds and bottlenecks are present is the one illustrated in Figures 8 and 9 which we will refer to as the *dollar sign* example. We again build the graph Laplacian as in section 3. Figure 8 shows the sign of the first non-trivial eigenvector which, as

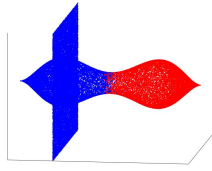


FIGURE
5. Ratio cut:
0.1286

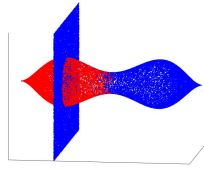


FIGURE
6. Ratio cut:
0.3385

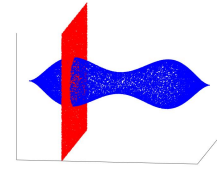


FIGURE
7. Ratio cut:
0.0834

we can observe, is able to detect the ‘‘bottleneck’’ at the center of the dollar sign shape. Figure 9 shows the sign of the second non-trivial eigenvector. Notice that the multi-manifold structure is identified correctly using this eigenvector. In this example it is also true that the partition induced by the second non-trivial eigenvector is a minimizer of the Ratio cut functional among partitions induced by linear combinations of the first two non-trivial eigenvectors. For comparison, in Figures 10 and 11 we illustrate the partitions induced by the first and second non-trivial eigenvectors of a graph Laplacian on a standard ε -graph. The first eigenvector behaves similarly to that output by spectral clustering with the annular graph, but the second eigenvector is quite different. The bottom line is that spectral clustering with a standard ε -graph fails to detect the two underlying manifolds.

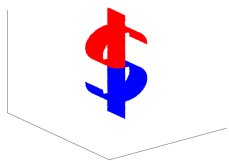


FIGURE
8

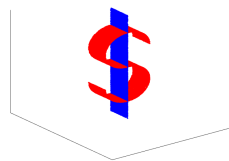


FIGURE
9

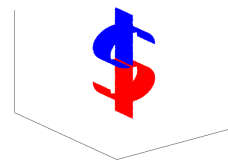


FIGURE
10

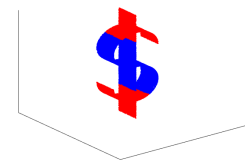


FIGURE
11

In Figures 8 and 9 2nd and 3th eigenvectors from annular graph with angle constraints. In Figures 10 and 11 2nd 3th eigenvectors from standard ε -proximity graph.

Remark 4.1. *When using ratio cut for MMC the important energy to consider is the cut functional/total variation functional:*

$$TV_n(u) \sim \frac{1}{n^2 \varepsilon_+^{m+1}} \sum_{i,j} \omega_{ij} |u(x_i) - u(x_j)|.$$

Notice that the correct scaling factor $\frac{1}{n^2 \varepsilon_+^{m+1}}$ for TV_n is different from the one for the graph Dirichlet energy which scales like $\frac{1}{n^2 \varepsilon_+^{m+2}}$ (see (A.2) in the Appendix). In general, this discrepancy in scaling factors explains the superior performance of Ratio cut over spectral clustering on MMC problems. To see this, we return to the discussion in Remark 3.6, and notice that in order to create a very cheap balanced cut that captures the multi-manifold structure underlying the data it is sufficient to choose the angle α to be small enough without making it arbitrarily small.

While in general ratio cut minimization is expected to be superior to spectral clustering from a theoretical perspective, it is at the algorithmic level that ratio cut is less appealing. In general, using spectral clustering as a warm start for ratio cut minimization is a reasonable strategy to consider as we have illustrated in the dumbbell-and-plane and dollar-sign examples.

4.2. Comparison of different proximity graphs. The approach to build graphs for multi-manifold clustering that we have discussed in this paper can be interpreted as a two step process where in the first step one builds an $\varepsilon_+, \varepsilon_-$ -graph, and in the second step one enforces a curvature constraint to eliminate some of the connections built initially. It is possible to imagine a similar construction using a k -nearest neighbor approach in the first step, this being motivated by the fact that k -nearest neighbors graphs tend to have better properties than their ε -graph counterparts. In this section we illustrate some of the disadvantages of using a k -nearest neighbor approach for multi-manifold clustering.

First, we consider the setting illustrated in Figures 12 and 13 where we have generated 6500 points on the horizontal line and 2000 points on the vertical line, i.e. an uneven setting. We can see that when we add angle constraints to a k_+, k_- -NN base graph (defined in the obvious way) we do not recover the two lines as we do when we use the $\varepsilon_+, \varepsilon_-$ -graph setting. The outcomes illustrated here are markedly different with the ones in the even case where the k -NN approach actually provides more stable results. The reason for the poor performance of k -NN in the uneven setting has to do with the fact that around the intersection of the two lines a k -NN neighborhood of a point in the vertical line mostly picks points in the horizontal line (since there is higher density of points there) resulting in very few connection with other points on the vertical line.

In general, we expect the k -NN setting to struggle in settings where the densities of points are different around the intersections of the manifolds as illustrated by the “inclusion problem” in the setting from Figures 14 and 15. In Figure 14 we illustrate the clusters output by spectral clustering in the path constrained k -NN setting. We see that the part of the plane contained inside the cone has been merged with the cone despite the fact that a strong angle constraint was used. The points in the inner part of the plane around the boundary have many more nearest neighbors in the cone than in the external portion of the plane, thus effectively discarding connections that would otherwise keep the plane better connected (as it is the case with the $\varepsilon_+, \varepsilon_-$ construction as shown in Figure 15).

We remark that the effect of density in clustering can be reduced by considering suitable normalized versions of proximity graphs as in [19], where in particular one can take the random walk Laplacian associated to a new set of weights ω_{ij}^α of the form:

$$\omega_{ij}^\alpha = \frac{\omega_{ij}}{d_i^\alpha d_j^\alpha},$$

for some $\alpha \in (0, 1]$, where d_i and d_j are the degrees of x_i and x_j relative to the original weight matrix ω . It is possible to show that with the choice $\alpha = 1$ one can effectively remove the effect of density in clustering. We notice that in the multi-manifold clustering setting, when manifolds have different dimensions, the role of density is more severe than when manifolds have the same dimension. This is because we are assuming that the number of points in each manifold is roughly the same, and so, densities on smaller dimensional objects tend to be considerably larger than densities on larger dimensional objects. The use of appropriate normalized Laplacians may thus help considerably with multi-manifold clustering problems.

4.2.1. Role of ε_- in annular graphs. Here we illustrate the effect of ε_- in the performance of spectral clustering. We focus on two possible choices: $\varepsilon_- = 0$ Vs $\varepsilon_- \sim \varepsilon_+$. We consider points uniformly sampled from two intersecting 2 dimensional spheres with radius 1 and distance between

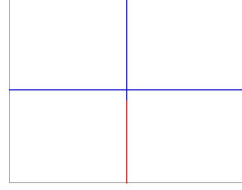


FIGURE 12. KNN setting

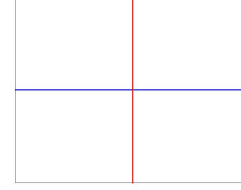


FIGURE 13. $\varepsilon_+, \varepsilon_-$ setting

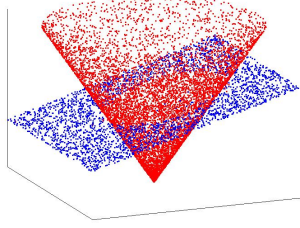


FIGURE 14. k -NN setting

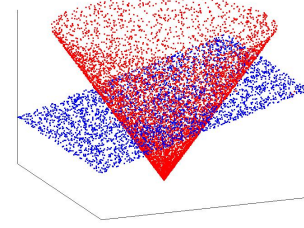


FIGURE 15. $\varepsilon_+, \varepsilon_-$ setting

their centers equal to 0.6 as illustrated in Figures 17 and 16. We can observe the discrepancy between the clusters obtained in both settings and how when we set $\varepsilon_- \sim \varepsilon_+$ the two manifolds are correctly identified. ε_+ is the same in both cases.

Notice that our theory predicts that in principle any choice of ε_- (not too close to ε_+) provides a correct identification of the manifolds as long as the number of samples is large enough. Yet, our theory also suggests that by considering a non-zero ε_- we can reduce the error of approximation (see Remark 3.5) as intuitively we can remove more wrong connections between pairs of points that are too close to the intersection of two distinct manifolds. Our numerical experiments complement our theoretical findings.

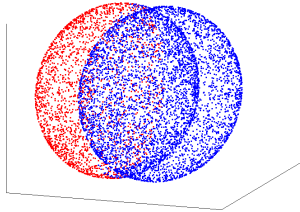


FIGURE 16. Path Algorithm with $\varepsilon_- = 0$

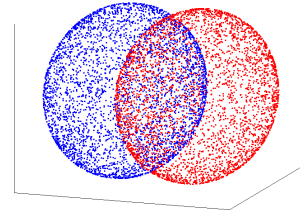


FIGURE 17. Path Algorithm with $\varepsilon_- = \frac{2\varepsilon_+}{3}$

4.2.2. *Path constraint graphs Vs other proximity graphs: self-intersections.* In general, the use of inner fully connected and outer sparsely connected graphs on data sets imposes a specific geometric structure on the set \mathcal{M} that is not necessarily the one inherited from the ambient space \mathbb{R}^d . This

is true in the multi-manifold setting or even in the case of a single self-intersecting manifold (a setting not considered in our theoretical results). Take for example the self-intersecting manifold illustrated in Figures 18-20. We can see that when running spectral clustering with the annular graph with angle constraints we get a partition of the data that corresponds to the one we would have obtained when clustering a one dimensional curve with no self intersections (i.e. as if there wasn't any self-intersections). This is illustrated in Figure 18. Figures 19 and 20, on the other hand, show the clusters obtained when running spectral clustering based on a standard k -NN graph and a standard ε -proximity graph respectively. As can be observed, these partitions are markedly different from the one in Figure 18. Notice that in this example the MMC method is able to detect the self-intersection point of the manifold.

Figures 18-20 illustrate the effect of different graphs on the output clusters. Likewise, when using higher eigenmodes to summarize more geometric content (*a* geometric content) of the self intersecting manifold, different graphs capture the underlying manifold differently. Diffusion maps is a popular approach that uses the spectrum of a graph Laplacian operator to obtain a geometric summary of a data set (see [19]).

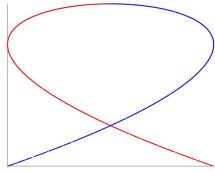


FIGURE
18. path al-
gorithm with
 $\varepsilon_+, \varepsilon_-$ -setting

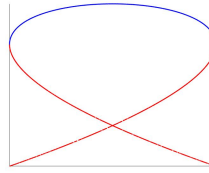


FIGURE
19. simple
KNN

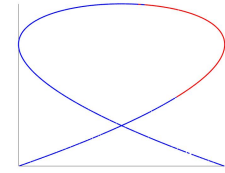


FIGURE
20. simple
 ε -neighbor

4.2.3. Other path algorithms. The path based similarity weights that we study in this paper are inspired by an algorithm proposed in [5]. There, in order to construct a proximity graph on the data set, a less stringent notion of “smooth” discrete path is considered. In our construction, we force discrete paths to satisfy that every line segment in the path must be aligned with the segment connecting the first and last point in the path (i.e. essentially requiring a straight path). In contrast, in [5] the constraint is that any two consecutive segments in the path must be aligned (i.e. a path that does not turn too quickly). It is straightforward to see that when two manifolds with dimension larger than two intersect, it is possible to construct paths connecting points in the two manifolds that meet the criterion in [5] but not our criterion. In summary, the more stringent constraint that we impose helps remove more connections (wrong and right). The removal of wrong connections seems to be more significant, and overall, our path algorithm outperforms the one in [5].

Another sensible path algorithm is to directly find geodesic paths along the graph using Dijkstra's algorithm and then check whether they satisfy the angle constraints or not. The theoretical analysis for this approach is more involved since one needs to check that geodesics do satisfy the angle constraint in the cases where one expects them to (i.e. when connecting two points on the same manifold). Still, in practice this graph construction behaves comparably to the path algorithm that we analyze. Our path construction and the geodesic based one are two extremes of a more general procedure where one seeks a path that connects a pair of points satisfying the angle constraints *and* whose length is no larger than a constant parameter times the geodesic distance along the path between the two points. This construction can be analyzed by combining ideas similar to the

ones we have presented in section 3 with some analysis for the geodesic distance along a proximity graph.

4.3. Sensitivity of theoretical assumptions.

4.3.1. *Angles.* We test the performance of spectral clustering on an annular graph with angle constraints when trying to separate manifolds as their angles of intersection decrease (i.e. β in (2.2) grows). In our experiment we consider the simple setting of two intersecting planes. We see

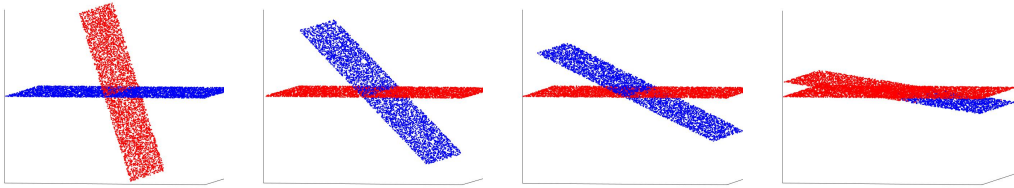


FIGURE
21. 75°

FIGURE
22. 50°

FIGURE
23. 30°

FIGURE
24. 10°

that in Figures 21-23 we recover the two planes perfectly, while in Figure 24 we do not. The results here are reasonable because when the angle of intersection is too small a much smaller threshold value for the angle constraint is needed to discriminate different manifolds, this at the expense of removing connections between points that should have been connected otherwise.

4.3.2. *Orthogonal noise.* In our theoretical results we assumed data points to lie exactly on top of a set of the form $\mathcal{M} = \mathcal{M}_1 \cup \dots \cup \mathcal{M}_K$. However, a natural question is whether spectral clustering with the similarity graph constructed with the path algorithm continues to perform well when orthogonal noise is added to the data. In Figures 25 and 26 we show two examples of data sets that have been contaminated by orthogonal noise. In both cases the multi-manifold structure is readily apparent: three intersecting lines at a single point. However, in the setting depicted in Figure 26, where the noise level is larger, we see that the path algorithm does not recover the multi-manifold structure correctly. This suggests that the path algorithm is quite sensitive to noise.

We can use the number of connection to see how the noise affects the algorithm. In Figure 26, where we exhibit the clean data, the total number of connections between data points is 579208, while the number of wrong connections is 1126. When noise is added, the number of total connections is 193426, while the number of wrong connections is 5414. That is, in general we expect noise to worsen both inner and outer connectivities.

A potential remedy for this is to pre-process the data set by running a denoiser. However, some naive denoising methods including the centering method or projected PCA do not seem to make the MMC problem significantly better. In Figure 27 we illustrate the outcome of spectral clustering on an annular proximity graph with angle constraints on the denoised data set. Specifically, using the centering method, the total number of connections was 215260, and the number of wrong connections was 5418. For the projected PCA method, the total number of connections was 271498, and the number of wrong connections 6956. Roughly speaking, these methods can improve the inner connectivity while worsening the outer connectivity. How to implement a good denoising strategy in the MMC setting is an interesting direction to explore.

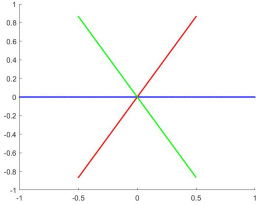


FIGURE
25. Small
Perturbation

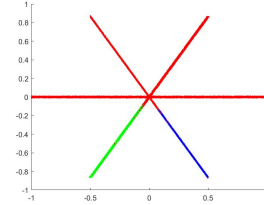


FIGURE
26. Large
Perturbation

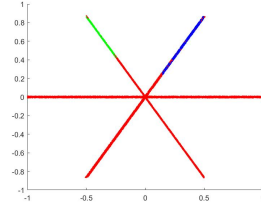


FIGURE
27. After
denoising

4.3.3. *Small Vs large number of data points.* In this section we consider data sets supported on the union of three intersecting planes as illustrated in Figures 28 and 29. In both figures the underlying planes are the same, and the only thing that changes from one figure to the other is the sample size. As can be observed, in the small sample size regime from Figure 28, the three planes are not

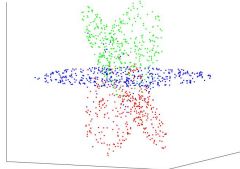


FIGURE 28. n
data points

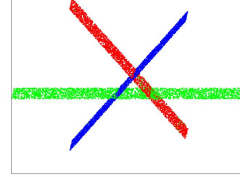


FIGURE
29. $2n$ data
points

identified properly. In contrast, when we duplicate the amount of data as in Figure 29 the three planes are identified perfectly.

This simple example illustrates some important drawbacks of the MMC methods based on spectral clustering that we have discussed throughout the paper. Part of the problem is the fact that in order to correctly construct local paths (or local tangent planes) to in turn detect the underlying manifolds, one actually needs to consider a large enough neighborhood around every point containing enough samples for the variance of the estimation to be small at the expense of increasing considerably the bias. Building MMC methods that can operate at smaller sample sizes is an interesting direction to explore in future research. We would like to remark that in the *subspace clustering problem* (where more structure is present) there are methods in the literature that seem to perform quite well for relatively small data sets (e.g. [36]).

4.4. Different dimensions. In section 2.4 we presented a series of theoretical results for multi-manifold clustering when \mathcal{M} is the union of smooth manifolds with different dimensions. We now illustrate these results with a few simple numerical examples.

4.4.1. Planes and lines. We consider a data set uniformly sampled from the union of two planes and two lines that meet orthogonally as illustrated in Figures 30-33. We run spectral clustering with $K = 2, 3, 4, 5$ to understand how the geometry of the manifolds gets captured.

In Figure 30, i.e. when we consider $K = 2$, the whole data set splits into 2 parts: lines and planes, indicating that manifolds with different dimensions are separated and manifolds with the

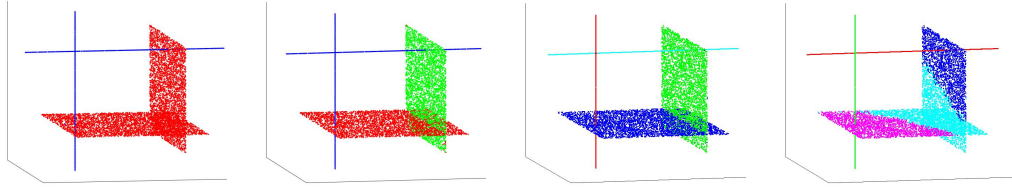


FIGURE
30. 2
Clus-
ters

FIGURE
31. 3
Clus-
ters

FIGURE
32. 4
Clus-
ters

FIGURE
33. 5
Clus-
ters

same dimension are put into the same cluster. In Figure 31, when we try $K = 3$ clusters, the two planes get separated perfectly while the lines are clustered as one; this is supported by our theory which indeed suggests that the geometry of the higher dimensional objects is detected first. When we set $K = 4$, lines get separated as shown in Figure 32. The case $K = 5$ illustrates the theory developed in this paper quite well as it shows how the internal geometry of the higher dimensional manifolds (in this case the planes) is detected while the internal geometry of each individual line seems to be more expensive to detect.

Another illustration of the behavior of spectral clustering with constrained annular proximity graphs is presented in Figures 34- 36. Here the data set is supported in the union of a 2-dimensional sphere and three lines that connect at one point. The same observations we made in the planes and lines example apply to this setting as well.

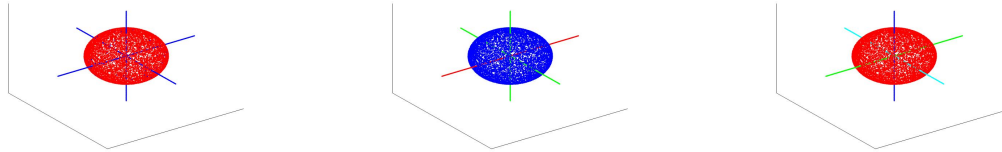


FIGURE 34. 2
clusters

FIGURE 35. 3
clusters

FIGURE 36. 4
clusters

REFERENCES

- [1] E. AAMARI AND C. LEVRARD, *Stability and minimax optimality of tangential delaunay complexes for manifold reconstruction*, 2018.
- [2] M. AHMED, B. T. FASY, K. S. HICKMANN, AND C. WENK, *A path-based distance for street map comparison*, ACM Trans. Spatial Algorithms Syst., 1 (2015).
- [3] E. ARIAS-CASTRO, G. LERMAN, AND T. ZHANG, *Spectral clustering based on local pca*, The Journal of Machine Learning Research, 18 (2017), pp. 253–309.
- [4] T. AUBIN, *Some Nonlinear Problems in Riemannian Geometry*, Springer Monographs in Mathematics, Springer Berlin Heidelberg, 1998.
- [5] A. BABAIEAN, M. BABAEE, A. BAYESTEHTASHK, AND M. BANDARABADI, *Nonlinear subspace clustering using curvature constrained distances*, Pattern Recognition Letters, 68 (2015), pp. 118 – 125.
- [6] M. BELKIN AND P. NIYOGI, *Towards a theoretical foundation for Laplacian-based manifold methods*, in International Conference on Computational Learning Theory, Springer, 2005, pp. 486–500.
- [7] T. E. BOULT AND L. G. BROWN, *Factorization-based segmentation of motions*, in Proceedings of the IEEE workshop on visual motion, IEEE, 1991, pp. 179–186.

[8] X. BRESSON AND T. LAURENT, *Asymmetric Cheeger cut and application to multi-class unsupervised clustering*, CAM report, 2012.

[9] X. BRESSON, T. LAURENT, D. UMINSKY, AND J. VON BRECHT, *Multiclass total variation clustering*, in Advances in Neural Information Processing Systems, 2013, pp. 1421–1429.

[10] X. BRESSON, T. LAURENT, D. UMINSKY, AND J. H. VON BRECHT, *Convergence and energy landscape for Cheeger cut clustering*, in Advances in Neural Information Processing Systems (NIPS), 2012, pp. 1394–1402.

[11] X. BRESSON, T. LAURENT, D. UMINSKY, AND J. H. VON BRECHT, *An adaptive total variation algorithm for computing the balanced cut of a graph*, preprint arXiv:1302.2717, (2013).

[12] X. BRESSON, X.-C. TAI, T. F. CHAN, AND A. SZLAM, *Multi-class transductive learning based on l_1 relaxations of Cheeger cut and mumford-shah-potts model*, UCLA CAM Report, (2012), pp. 12–03.

[13] D. BURAGO, S. IVANOV, AND Y. KURYLEV, *A graph discretization of the Laplace-Beltrami operator*, J. Spectr. Theory, 4 (2014), pp. 675–714.

[14] J. CALDER AND N. GARCÍA TRILLOS, *Improved spectral convergence rates for graph laplacians on epsilon-graphs and k -nn graphs*, arXiv preprint arXiv:1910.13476, (2019).

[15] J. CALDER, N. G. TRILLOS, AND M. LEWICKA, *Lipschitz regularity of graph laplacians on random data clouds*, 2020.

[16] H. CHANG AND D.-Y. YEUNG, *Robust path-based spectral clustering*, Pattern Recogn., 41 (2008), p. 191–203.

[17] G. CHEN AND G. LERMAN, *Foundations of a multi-way spectral clustering framework for hybrid linear modeling*, Foundations of Computational Mathematics, 9 (2009), pp. 517–558.

[18] ———, *Spectral curvature clustering (scc)*, International Journal of Computer Vision, 81 (2009), pp. 317–330.

[19] R. R. COIFMAN AND S. LAFON, *Diffusion maps*, Applied and computational harmonic analysis, 21 (2006), pp. 5–30.

[20] D. B. DUNSON, H.-T. WU, AND N. WU, *Spectral convergence of graph laplacian and heat kernel reconstruction in l^∞ from random samples*, 2019.

[21] E. ELHAMIFAR AND R. VIDAL, *Sparse subspace clustering*, in 2009 IEEE Conference on Computer Vision and Pattern Recognition, IEEE, 2009, pp. 2790–2797.

[22] ———, *Clustering disjoint subspaces via sparse representation*, in 2010 IEEE International Conference on Acoustics, Speech and Signal Processing, IEEE, 2010, pp. 1926–1929.

[23] ———, *Sparse manifold clustering and embedding*, in Advances in neural information processing systems, 2011, pp. 55–63.

[24] L. C. EVANS, *Partial differential equations*, vol. 19 of Graduate Studies in Mathematics, American Mathematical Society, Providence, RI, second ed., 2010.

[25] H. FEDERER, *Curvature measures*, Trans. Amer. Math. Soc., (1959), p. 418–491.

[26] B. FISCHER, T. ZÖLLER, AND J. M. BUHMANN, *Path based pairwise data clustering with application to texture segmentation*, (2001), p. 235–250.

[27] N. GARCÍA TRILLOS AND D. SLEPČEV, *A variational approach to the consistency of spectral clustering*, Applied and Computational Harmonic Analysis, 45 (2018), pp. 239–281.

[28] E. GINÉ AND V. KOLTCHINSKII, *Empirical graph Laplacian approximation of Laplace-Beltrami operators: large sample results*, in High dimensional probability, vol. 51 of IMS Lecture Notes Monogr. Ser., Inst. Math. Statist., Beachwood, OH, 2006, pp. 238–259.

[29] A. GOH AND R. VIDAL, *Segmenting motions of different types by unsupervised manifold clustering*, in 2007 IEEE Conference on Computer Vision and Pattern Recognition, IEEE, 2007, pp. 1–6.

[30] M. HEIN, J.-Y. AUDIBERT, AND U. V. LUXBURG, *Graph laplacians and their convergence on random neighborhood graphs*, Journal of Machine Learning Research, 8 (2007), pp. 1325–1368.

[31] M. HEIN, J.-Y. AUDIBERT, AND U. VON LUXBURG, *From graphs to manifolds–weak and strong pointwise consistency of graph laplacians*, in International Conference on Computational Learning Theory, Springer, 2005, pp. 470–485.

[32] A. LITTLE, M. MAGGIONI, AND J. M. MURPHY, *Path-based spectral clustering: Guarantees, robustness to outliers, and fast algorithms*, arXiv preprint arXiv:1712.06206, (2017).

[33] G. LIU, Z. LIN, AND Y. YU, *Robust subspace segmentation by low-rank representation*, in Proceedings of the 27th International Conference on International Conference on Machine Learning, ICML’10, Madison, WI, USA, 2010, Omnipress, p. 663–670.

[34] J. LU, *Graph approximations to the laplacian spectra*, arXiv: Differential Geometry, (2019).

[35] N. NORMAND, R. STRAND, P. EVENOU, AND A. ARLICOT, *Path-based distance with varying weights and neighborhood sequences*, in Discrete Geometry for Computer Imagery, I. Debled-Rennesson, E. Domenjoud, B. Ker-autret, and P. Even, eds., Berlin, Heidelberg, 2011, Springer Berlin Heidelberg, pp. 199–210.

[36] U. OSWAL AND R. NOWAK, *Scalable sparse subspace clustering via ordered weighted l_1 regression*, in 2018 56th Annual Allerton Conference on Communication, Control, and Computing (Allerton), IEEE, 2018, pp. 305–312.

- [37] D. PARK, C. CARAMANIS, AND S. SANGHAVI, *Greedy subspace clustering*, in Advances in neural information processing systems, 2014, pp. 2753–2761.
- [38] A. ROSENFELD AND J. L. PFALTZ, *Sequential operations in digital picture processing*, J. ACM, 13 (1966), p. 471–494.
- [39] Z. SHI, *Convergence of Laplacian spectra from random samples*, arXiv preprint arXiv:1507.00151, 2015.
- [40] A. SINGER, *From graph to manifold laplacian: The convergence rate*, Applied and Computational Harmonic Analysis, 21 (2006), pp. 128–134.
- [41] A. SINGER AND H.-T. WU, *Spectral convergence of the connection Laplacian from random samples*, Information and Inference: A Journal of the IMA, 6 (2017), pp. 58–123.
- [42] H. TIENG WU AND N. WU, *When locally linear embedding hits boundary*, 2018.
- [43] D. TING, L. HUANG, AND M. JORDAN, *An analysis of the convergence of graph laplacians*, arXiv preprint arXiv:1101.5435, (2011).
- [44] N. G. TRILLOS, M. GERLACH, M. HEIN, AND D. SLEPČEV, *Error estimates for spectral convergence of the graph laplacian on random geometric graphs toward the laplace–beltrami operator*, Foundations of Computational Mathematics, (2019), pp. 1–61.
- [45] R. VAUGHN, T. BERRY, AND H. ANTIL, *Diffusion maps for embedded manifolds with boundary with applications to pdes*, 2019.
- [46] R. VIDAL, *A tutorial on subspace clustering*, (2010).
- [47] R. VIDAL, Y. MA, AND S. SASTRY, *Generalized principal component analysis (GPCA)*, CoRR, abs/1202.4002 (2012).
- [48] U. VON LUXBURG, *A tutorial on spectral clustering*, CoRR, abs/0711.0189 (2007).
- [49] ———, *A tutorial on spectral clustering*, 2007.
- [50] U. VON LUXBURG, M. BELKIN, AND O. BOUSQUET, *Consistency of spectral clustering*, Ann. Statist., 36 (2008), pp. 555–586.
- [51] Y. WANG, Y. JIANG, Y. WU, AND Z.-H. ZHOU, *Spectral clustering on multiple manifolds*, IEEE Transactions on Neural Networks, 22 (2011), pp. 1149–1161.
- [52] C. L. WORMELL AND S. REICH, *Spectral convergence of diffusion maps: improved error bounds and an alternative normalisation*, 2020.
- [53] J. YAN AND M. POLLEFEYS, *A general framework for motion segmentation: Independent, articulated, rigid, non-rigid, degenerate and non-degenerate*, in Computer Vision – ECCV 2006, A. Leonardis, H. Bischof, and A. Pinz, eds., Berlin, Heidelberg, 2006, Springer Berlin Heidelberg, pp. 94–106.
- [54] YING WU, ZHENGYOU ZHANG, T. S. HUANG, AND J. Y. LIN, *Multibody grouping via orthogonal subspace decomposition*, in Proceedings of the 2001 IEEE Computer Society Conference on Computer Vision and Pattern Recognition. CVPR 2001, vol. 2, 2001, pp. II–II.
- [55] T. ZHANG, A. SZLAM, Y. WANG, AND G. LERMAN, *Hybrid linear modeling via local best-fit flats*, CoRR, abs/1010.3460 (2010).

APPENDIX A. PROOFS OF MAIN RESULTS

A.1. Discrete Dirichlet energies. It is well known that an operator like $\mathcal{L}^{\varepsilon_+, \varepsilon_-}$ (defined in (2.7)) is positive semi-definite with respect to $\langle \cdot, \cdot \rangle_{L^2(\mu^n)}$ (e.g. [49]); here and in the remainder we use μ^n to denote the mepirical measure of X . Notice that $\mathcal{L}^{\varepsilon_+, \varepsilon_-}$ ’s eigenvalues, labeled in ascending order as

$$0 = \lambda_1^{\varepsilon_+, \varepsilon_-} \leq \lambda_2^{\varepsilon_+, \varepsilon_-} \leq \lambda_3^{\varepsilon_+, \varepsilon_-} \leq \dots \leq \lambda_n^{\varepsilon_+, \varepsilon_-},$$

can be characterized variationally according to the Courant-Fisher minmax principle:

$$\lambda_l^{\varepsilon_+, \varepsilon_-} = \min_{S \in \mathcal{G}_l} \max_{u \in S \setminus \{0\}} \frac{b^{\varepsilon_+, \varepsilon_-}(u)}{\|u\|_{L^2(\mu^n)}^2}, \quad (\text{A.1})$$

where \mathcal{G}_l denotes the set of all linear subspaces of $L^2(\mu^n)$ of dimension l . Here, $b^{\varepsilon_+, \varepsilon_-}$ is the Dirichlet energy:

$$b^{\varepsilon_+, \varepsilon_-}(u) := \frac{1}{n^2(\varepsilon_+^{m+2} - \varepsilon_-^{m+2})} \sum_{x_i, x_j \in \mathcal{X}_n} \omega_{x_i x_j} (u(x_i) - u(x_j))^2 = \frac{1}{2} \langle \mathcal{L}^{\varepsilon_+, \varepsilon_-} u, u \rangle_{L^2(\mu^n)}, \quad u \in L^2(\mu^n). \quad (\text{A.2})$$

We introduce *inner* and *outer* weights associated to the ω defined as $\omega_{x_i x_j}^I = \omega_{x_i x_j}$ and $\omega_{x_i x_j}^O = 0$ when x_i, x_j belong to the same manifold, and $\omega_{x_i x_j}^I = 0$ and $\omega_{x_i x_j}^O = \omega_{x_i x_j}$ otherwise. With this notation in place, we can introduce outer and inner Dirichlet energies associated to $\mathcal{L}^{\varepsilon+, \varepsilon-}$ according to:

$$\begin{aligned} b_O^{\varepsilon+, \varepsilon-}(u) &:= \frac{1}{n^2(\varepsilon_+^{m+2} - \varepsilon_-^{m+2})} \sum_{x_i, x_j \in \mathcal{X}_n} \omega_{x_i x_j}^O (u(x_i) - u(x_j))^2, \\ b_I^{\varepsilon+, \varepsilon-}(u) &:= \frac{1}{n^2(\varepsilon_+^{m+2} - \varepsilon_-^{m+2})} \sum_{x_i, x_j \in \mathcal{X}_n} \omega_{x_i x_j}^I (u(x_i) - u(x_j))^2. \end{aligned} \quad (\text{A.3})$$

Clearly $b^{\varepsilon+, \varepsilon-} = b_O^{\varepsilon+, \varepsilon-} + b_I^{\varepsilon+, \varepsilon-}$.

It will be convenient for our analysis to decompose $b_I^{\varepsilon+, \varepsilon-}$ further and write it as the sum of Dirichlet energies associated to each of the manifolds \mathcal{M}_k . For that purpose we split the data set X into disjoint sets $X = \bigcup_{k=1}^N X_k$, where each of the X_k can be taken to be, without the loss of generality, equal to $X_k = X \cap \mathcal{M}_k$ (this is due to the first condition in Assumption 1 which implies that with probability one no x_i belongs to two or more of the \mathcal{M}_k). It is worth highlighting that the previous partitioning of the data makes sense mathematically even if it is not meaningful in practice (because we do not know the manifolds \mathcal{M}_k). In what follows and whenever needed we list the points in X_k as $\{x_{1k}, x_{2k}, \dots, x_{nk}\}$ and use μ_k^n to denote their associated empirical probability measure. The number of data points in \mathcal{M}_k , i.e. n_k , is easily seen to satisfy $\mathbb{E} n_l = n w_l$. Moreover, the following concentration estimate holds.

Proposition A.1. *With probability no less than $1 - 2 \exp\left(\frac{-2t^2}{n}\right)$, we can have*

$$n w_i - t < n_i < n w_i + t. \quad (\text{A.4})$$

The graph Dirichlet energy associated to an individual manifold is defined by

$$b_l^{\varepsilon+, \varepsilon-}(u_l) := \frac{1}{n_l^2(\varepsilon_+^{m+2} - \varepsilon_-^{m+2})} \sum_{x_i, x_j \in \mathcal{X}_n^l} \omega_{x_i x_j} (u_l(x_i) - u_l(x_j))^2, \quad u_l \in L^2(\mu_l^n). \quad (\text{A.5})$$

It follows that

$$b_I^{\varepsilon+, \varepsilon-}(u) = \sum_{l=1}^N \left(\frac{n_l^2}{n^2} \right) b_l^{\varepsilon+, \varepsilon-}(u_l), \quad u \in L^2(\mu^n),$$

where in the above and in the remainder we identify a function $u : X \rightarrow \mathbb{R}$ with a tuple (u_1, \dots, u_N) where each of the u_k is a function from X_k into \mathbb{R} .

Remark A.2. *The local discrete Dirichlet energies $b_k^{\varepsilon+, \varepsilon-}$ are similar to discrete Dirichlet energies that have been studied in the literature under the smooth manifold assumption. There is however an important difference. Indeed, although the weight matrix ω is assumed to satisfy the full inner connectivity condition, i.e. with high probability the weights $\omega_{x_i x_j}$ can be thought of as those coming from a proximity graph, the type of proximity graph that we consider here is not standard since it is built with a kernel that has annular geometric structure. This type of kernel has not been considered nor analyzed before. As observed intuitively, as well as in our experiments, the idea of removing connections between points that are too close to each other significantly helps in reducing the number of connections between points in different manifolds, a feature that is useful for the multi-manifold clustering problem.*

A.2. Discretization and interpolation maps. Our first goal is to find a quantitative relationship between the Dirichlet energies D and $b^{\varepsilon+, \varepsilon-}$ via two conveniently chosen maps $P : L^2(\mu) \rightarrow L^2(\mu^n)$ and $\mathcal{I} : L^2(\mu_n) \rightarrow L^2(\mu)$. We look forward to obtaining inequalities of the form:

$$\sigma_\eta D(Iu) \leq (1 + e_1) b^{\varepsilon+, \varepsilon-}(u); \quad b^{\varepsilon+, \varepsilon-}(Pf) \leq (1 + e_2) \sigma_\eta D(f) + e_3 \quad (\text{A.6})$$

where e_1, e_2, e_3 are small error terms depending on the problem's parameters, and σ_η is the constant in (2.8).

We start by combining Proposition 2.11 in [14] with Proposition (A.1) to obtain the probabilistic estimates that we use in the remainder to connect graph-based energies with their continuum counterparts.

Corollary A.3. *With probability at least $1 - \sum_{l=1}^N (nw_l + t) \exp(-C(nw_l - t)\theta^2 \tilde{\delta}^{m_l}) - 2N \exp\left(\frac{-2t^2}{n}\right)$, there exist:*

- i) probability density functions $\tilde{\rho}_l^n : \mathcal{M}_l \rightarrow \mathbb{R}$ satisfying:

$$\|\rho_l - \tilde{\rho}_l^n\|_{L^\infty(\mathcal{M}_k)} \leq C(\theta + \tilde{\delta})$$

for each $l = 1, \dots, N$, and also

- ii) maps $\tilde{T}_1, \dots, \tilde{T}_N$ such that for each l , $\tilde{T}_l : \mathcal{M}_l \rightarrow X_l$ is the ∞ -OT map between $\tilde{\rho}_l^n d\text{vol}_{\mathcal{M}_l}$ and μ_l^n , and

$$\sup_{x \in \mathcal{M}_l} d_{\mathcal{M}_l}(x, \tilde{T}_l(x)) \leq \tilde{\delta}.$$

Each of the maps \tilde{T}_k in the above corollary induces a partition $\tilde{U}_{1l}, \dots, \tilde{U}_{nl}$ of \mathcal{M}_l , where:

$$\tilde{U}_{il} := \tilde{T}_l^{-1}(\{x_{il}\}).$$

For each $l = 1, \dots, N$, a (local) *discretization* map $\tilde{P}_l : L^2(\mu_l) \rightarrow L^2(\mu_l^n)$ is defined as

$$(\tilde{P}_l f_l)(x_{il}) := n_l \cdot \int_{\tilde{U}_{il}} f(x) \tilde{\rho}_l^n(x) d\text{vol}_{\mathcal{M}_l}(x), \quad f_l \in L^2(\mu_l), \quad (\text{A.7})$$

and an associated (local) *extension* map $\tilde{P}_l^* : L^2(\mu_l^n) \rightarrow L^2(\tilde{\mu}_l^n)$ defined as

$$\tilde{P}_l^* u = u \circ \tilde{T}_l.$$

The (global) discretization map $P : L^2(\mu) \rightarrow L^2(\mu_n)$ can now be defined according to

$$Pf := (P_1 f_1, \dots, P_N f_N)$$

where $f = (f_1, \dots, f_N) \in L^2(\mu)$. In other words, P acts on f according to the coordinatewise action of the P_l on the f_l . Likewise, we may define $\tilde{P}^* : L^2(\mu_n) \rightarrow L^2(\mu)$ according to:

$$P^* u = (P_1^* u_1, \dots, P_N^* u_N).$$

We now introduce the interpolation map $\mathcal{I} : L^2(\mu^n) \rightarrow L^2(\mu)$. This map takes the form $\mathcal{I} = \Lambda \tilde{P}^*$, i.e. it is the composition of the extension map \tilde{P}^* and a smoothening operator that acts coordinatewise. The smoothening operator is chosen conveniently so as to make the error in the first inequality in (A.6) as small as possible; the first work to our knowledge that attempted to do something similar when analyzing graph Laplacians is [13]. To conduct the analysis in our setting we must introduce new constructions and prove new results given the annular geometry of the kernel used to build the data graph.

Let $\eta : [0, \infty) \rightarrow \mathbb{R}$ and $\psi : [0, \infty) \rightarrow [0, \infty)$ be the functions given by

$$\eta(t) := \begin{cases} 1 & 0 \leq t \leq 1 \\ 0 & t > 1, \end{cases} \quad \psi(t) := \frac{1}{\sigma_\eta} \int_t^\infty \eta(s) s ds, \quad (\text{A.8})$$

where recall σ_η was defined in (2.8).

For every r_1, r_2 such that $r_1 > r_2$ we define the function:

$$\mathcal{K}_{r_1, r_2}^l(x, y) := \left(\frac{r_1^2}{r_1^{m+2} - r_2^{m+2}} \psi \left(\frac{d_{\mathcal{M}_l}(x, y)}{r_1} \right) - \frac{r_2^2}{r_1^{m+2} - r_2^{m+2}} \psi \left(\frac{d_{\mathcal{M}_l}(x, y)}{r_2} \right) \right), \quad x, y \in \mathcal{M}_l,$$

which serves as “kernel” and induces the convolution operator:

$$\Lambda_{r_1, r_2}^l f(x) := \frac{1}{\tau_l(x)} \int_{\mathcal{M}_l} \mathcal{K}_{r_1, r_2}^l(x, y) f_l(y) d\text{vol}_{\mathcal{M}_l}(y),$$

which acts on functions $f_l : \mathcal{M}_l \rightarrow \mathbb{R}$. In the above, $\tau_l(x)$ is a normalization factor given by

$$\tau_l(x) := \int_{\mathcal{M}_l} \mathcal{K}_{r_1, r_2}^l(x, y) d\text{vol}_{\mathcal{M}_l}(y);$$

notice that \mathcal{K}_{r_1, r_2}^l is non-negative.

We can put together the action of each convolution operator on each of the manifolds and define:

$$\Lambda_{r_1, r_2} f := (\Lambda_{r_1, r_2}^1 f_1, \dots, \Lambda_{r_1, r_2}^N f_N), \quad f = (f_1, \dots, f_N) \in L^2(\mu).$$

Our global *interpolation operator* takes the form:

$$\mathcal{I}u := \Lambda \tilde{P}^* u, \quad u \in L^2(\mu^n);$$

In the remainder it will be convenient to write the above in coordinates as:

$$\mathcal{I}u = (\mathcal{I}_1 u_1, \dots, \mathcal{I}_N u_N).$$

Having defined the maps P and \mathcal{I} we are now ready to state precisely the connection between the Dirichlet energies D and b .

Proposition A.4 (Inequality for Dirichlet energies). *Let $\varepsilon_+, \varepsilon_-, \delta$, and θ be fixed but small enough numbers satisfying Assumptions 2. Let b be the Dirichlet energy associated to the weighted graph (X, ω) defined in (A.2) and D the Dirichlet energy defined in (2.3).*

Then, with probability greater than $1 - \sum_{l=1}^N (nw_l + t) \exp(-C(nw_l - t)\theta^2 \tilde{\delta}^m) - 2N \exp\left(\frac{-2t^2}{n}\right) - C_1(n)$, we have:

(1) *For any $f \in L^2(\mu)$,*

$$D(\tilde{\mathcal{I}}u) \leq (1 + C(\varepsilon_+ + \frac{\tilde{\delta}}{\varepsilon_+} + \theta + \tilde{\delta})) b^{\varepsilon_+, \varepsilon_-}(u)$$

(2) *For any $f \in L^2(\mu_n)$,*

$$b_I^{\varepsilon_+, \varepsilon_-}(\tilde{P}f) \leq \left(1 + C(\varepsilon_+ + \frac{\tilde{\delta}}{\varepsilon_+} + \theta + \tilde{\delta})\right) D(f)$$

In addition, if f is in the span of $\Delta_{\mathcal{M}}$ ’s eigenfunctions with corresponding eigenvalue less than λ , then:

$$b_O^{\varepsilon_+, \varepsilon_-}(\tilde{P}f) \leq \frac{CNN_0}{w_{\min}^3 n^2 (\varepsilon_+^{m+2} - \varepsilon_-^{m+2})} \left(1 + \lambda^{m/2+2}\right) \|f\|_{L^2(\mathcal{M})}^2$$

We recall that the quantity N_0 was introduced in Section 2.1 in Definition 2.4 and it represents the largest number of connections in the graph (X, ω) between two distinct manifolds. The following estimates complement Proposition A.4 and essentially state that the maps \mathcal{I} and P are almost isometries.

Proposition A.5 (Discretization and interpolation maps are almost isometries). *Let $\varepsilon_+, \varepsilon_-, \tilde{\delta}$, and θ be fixed but small enough numbers satisfying Assumptions 2. Then, with probability at least $1 - \sum_{l=1}^N (nw_l + t) \exp(-C(nw_l - t)w_l^2 \tilde{\delta}^m) - 2N \exp\left(\frac{-2t^2}{n}\right) - C_1(n)$, we have:*

(1) *For every $f \in L^2(\mu)$*

$$\left| \|f\|_{L^2(\mu)}^2 - \|Pf\|_{L^2(\mu_n)}^2 \right| \leq C\tilde{\delta}\|f\|_{L^2(\mu)}\sqrt{D(f)} + C(\theta + \tilde{\delta})\|f\|_{L^2(\mu)}^2$$

(2) *For every $u \in L^2(\mu_n)$*

$$\left| \|u\|_{L^2(\mu_n)}^2 - \|\mathcal{I}u\|_{L^2(\mu)}^2 \right| \leq C\varepsilon_+\|u\|_{L^2(\mu_n)}\sqrt{b^{\varepsilon_+, \varepsilon_-}(u)} + C(\theta + \tilde{\delta})\|u\|_{L^2(\mu_n)}^2$$

A.3. Preliminary local energy estimates. In order to prove the above results we first establish a sequence of preliminary estimates on each of the individual manifolds \mathcal{M}_l . The results presented in this subsection are independent of the fact that all manifolds forming our model 1.2 have the same dimension or not.

Lemma A.6. *Suppose $0 < r_2 < \frac{1}{4}r_1$ are small enough, in particular smaller than half the injectivity radius of the manifold \mathcal{M}_l . Then, there exists an absolute constant $C > 0$ such that*

$$(1 + Cm_lK_l r_1^2)^{-1} \leq \tau_l(x) \leq 1 + Cm_lK_l r_1^2, \quad \text{and} \quad |\nabla \tau_l(x)| \leq \frac{Cm_lK_l r_1}{\sigma_\eta},$$

for all $x \in \mathcal{M}_l$. Here K_l is a uniform bound on the absolute value of sectional curvatures.

Proof. First, notice that:

$$\begin{aligned} \tau_l(x) &= \frac{r_1^2}{r_1^{m_l+2} - r_2^{m_l+2}} \int_{\mathcal{M}_l} \psi\left(\frac{d_{\mathcal{M}_l}(x, y)}{r_1}\right) d\text{vol}_{\mathcal{M}_l}(y) - \frac{r_2^2}{r_1^{m_l+2} - r_2^{m_l+2}} \int_{\mathcal{M}_l} \psi\left(\frac{d_{\mathcal{M}_l}(x, y)}{r_2}\right) d\text{vol}_{\mathcal{M}_l}(y) \\ &= \frac{r_1^2}{r_1^{m_l+2} - r_2^{m_l+2}} \int_{B_{m_l}(0, r_1)} \psi\left(\frac{|v|}{r_1}\right) J_x(v) dv - \frac{r_2^2}{r_1^{m_l+2} - r_2^{m_l+2}} \int_{B_{m_l}(0, r_2)} \psi\left(\frac{|v|}{r_2}\right) J_x(v) dv, \end{aligned}$$

where in the above J_x denotes the Jacobian of the exponential map $\exp_x : B_{m_l}(0, \iota_l) \rightarrow B_{\mathcal{M}_l}(x, \iota_l)$. Using a standard estimate for the Jacobian, namely

$$(1 + Cm_lK_l|v|^2)^{-1} \leq J_x(v) \leq 1 + Cm_lK_l|v|^2, \quad \forall v \in B_{m_l}(0, \iota_l/2), \quad (\text{A.9})$$

we can see that $\tau_l(x)$ satisfies $(1 + Cm_lK_l r_1^2)^{-1}C_\alpha \leq \tau_l(x) \leq (1 + Cm_lK_l r_1^2)C_\alpha$ for some constant C , and for

$$C_\alpha := \frac{r_1^2}{r_1^{m_l+2} - r_2^{m_l+2}} \int_{B_{m_l}(0, r_1)} \psi\left(\frac{|v|}{r_1}\right) dv - \frac{r_2^2}{r_1^{m_l+2} - r_2^{m_l+2}} \int_{B_{m_l}(0, r_2)} \psi\left(\frac{|v|}{r_2}\right) dv.$$

A direct computation using polar coordinates and integration by parts reveals that C_α is actually equal to one. This establishes the first assertion

To obtain the estimate for the gradient of $\tau_l(x)$, we notice that from the the definition of ψ in (A.8), the chain rule, and the fact that $\nabla d_{\mathcal{M}_l}(\cdot, y)(x) = -\frac{1}{d_{\mathcal{M}_l}(x, y)} \exp_x^{-1}(y)$, it follows:

$$\begin{aligned}
|\nabla \tau_l(x)| &= \frac{1}{\sigma_\eta(r_1^{m_l+2} - r_2^{m_l+2})} \left| \int_{B_{\mathcal{M}_l}(x, r_1)} \left(\eta\left(\frac{d_{\mathcal{M}_l}(x, y)}{r_1}\right) - \eta\left(\frac{d_{\mathcal{M}_l}(x, y)}{r_2}\right) \right) \exp_x^{-1}(y) d\text{vol}_{\mathcal{M}_l}(y) \right| \\
&= \frac{1}{\sigma_\eta(r_1^{m_l+2} - r_2^{m_l+2})} \left| \int_{B_{m_l}(r_1)} \eta\left(\frac{|v|}{r_1}\right) v J_x(v) dv - \int_{B_{m_l}(r_2)} \eta\left(\frac{|v|}{r_2}\right) v J_x(v) dv \right| \\
&\leq \frac{C m_l K_l r_1^2}{\sigma_\eta(r_1^{m_l+2} - r_2^{m_l+2})} \left(\int_{B_{m_l}(r_1)} \eta\left(\frac{|v|}{r_1}\right) |v| dv + \int_{B_{m_l}(r_2)} \eta\left(\frac{|v|}{r_2}\right) |v| dv \right) \\
&\leq \frac{C m_l K_l r_1^2 (r_1^{m_l+1} + r_2^{m_l+1})}{\sigma_\eta(r_1^{m_l+2} - r_2^{m_l+2})} \leq \frac{C m_l K_l r_1}{\sigma_\eta}.
\end{aligned}$$

Notice that in the first inequality we have used (A.9) and the radial symmetry of the integrands (which induces a cancellation). In the last step we used $0 < r_2 \leq \frac{1}{4}r_1$. \square

The next definitions is used in the subsequent lemmas. For every $l = 1, \dots, N$ we define

$$\begin{aligned}
\tilde{D}_{NL,l}^{\varepsilon_+, \varepsilon_-}(f_l) &:= \frac{1}{\varepsilon_+^{m+2} - \varepsilon_-^{m+2}} \int_{\mathcal{M}_l} \int_{\mathcal{M}_l} \left[\eta\left(\frac{d_{\mathcal{M}_l}(x, y)}{\varepsilon_+}\right) - \eta\left(\frac{d_{\mathcal{M}_l}(x, y)}{\varepsilon_-}\right) \right] (f_l(x) - f_l(y))^2 \\
&\quad \tilde{\rho}_l^n(x) \tilde{\rho}_l^n(y) d\text{vol}_{\mathcal{M}_l}(x) d\text{vol}_{\mathcal{M}_l}(y),
\end{aligned} \tag{A.10}$$

where we recall that the densities $\tilde{\rho}_l^n$ are defined in Corollary (A.3). We also consider:

$$E_l^r(f_l) := \int_{\mathcal{M}_l} \int_{\mathcal{M}_l} \eta\left(\frac{d_{\mathcal{M}_l}(x, y)}{r}\right) (f_l(x) - f_l(y))^2 \tilde{\rho}_l^n(x) \tilde{\rho}_l^n(y) d\text{vol}_{\mathcal{M}_l}(x) d\text{vol}_{\mathcal{M}_l}(y), \quad f_l \in L^2(\mu_l). \tag{A.11}$$

Notice that for every $r_1 > r_2 > 0$ we have:

$$(r_1^{m+2} - r_2^{m+2}) D_{NL,l}^{r_1, r_2}(f_l) = E_l^{r_1}(f_l) - E_l^{r_2}(f_l), \quad f_l \in L^2(\mu_l). \tag{A.12}$$

Lemma A.7. *Suppose $\varepsilon_+, \varepsilon_-$ satisfy Assumptions 2. Then, there exists a universal constant $C > 0$ such that for every $0 < \varepsilon_- < \frac{1}{4}\varepsilon_+$ and every $f_l \in L^2(\mu_l)$*

$$\frac{1}{\varepsilon_+^{m+2} - \varepsilon_-^{m+2}} E_l^{\varepsilon_+}(f_l) \leq C (1 + c_\rho L_{\rho_l}) D_{NL,l}^{\varepsilon_+, \varepsilon_-}(f_l),$$

where L_{ρ_l} is a constant depending on ρ_l .

Proof. The proof is very similar to the one in Lemma 4 in [44]. In that Lemma the idea is to cover a larger ball with smaller balls and use the triangle inequality. Here the only difference is that we want to cover a larger ball with a collection of annuli. \square

Lemma A.8. *Suppose that $\varepsilon_+, \varepsilon_-$ satisfy Assumptions 2. Then, there exists a universal constant $C > 0$ such that*

$$D_l(\Lambda_{\varepsilon_+, \varepsilon_-}^l f_l) \leq (1 + c_\rho L_{\rho_l} \varepsilon_+) \left[1 + C m_l K_l \varepsilon_+^2 \left(1 + \frac{\sqrt{1 + c_\rho L_p}}{\sigma_\eta} \right) \right] \frac{1}{\sigma_\eta} D_{NL,l}^{\varepsilon_+, \varepsilon_-}(f_l), \quad \forall f_l \in L^2(\mathcal{M}_l, \rho_l).$$

We recall that D_l was defined in (2.6) and $D_{NL,l}^{\varepsilon_+, \varepsilon_-}$ in (A.10).

Proof. We can write $\nabla(\Lambda_{\varepsilon_+, \varepsilon_-}^l f_l)$ as

$$\nabla(\Lambda_{\varepsilon_+, \varepsilon_-}^l f_l) = \frac{1}{\tau_l(x)} A_1(x) + A_2(x),$$

where

$$A_1(x) := \int_{R_{\mathcal{M}_l}(x, \varepsilon_+, \varepsilon_-)} \nabla \mathcal{K}_{\varepsilon_+, \varepsilon_-}^l(\cdot, y)(x) (f_l(y) - f_l(x)) d\text{vol}_{\mathcal{M}_l}(y)$$

and

$$A_2(x) = \nabla\left(\frac{1}{\tau_l(x)}\right) \int_{R_{\mathcal{M}_l}(x, \varepsilon_+, \varepsilon_-)} \mathcal{K}_{\varepsilon_+, \varepsilon_-}^l(x, y) (f_l(y) - f_l(x)) d\text{vol}_{\mathcal{M}_l}(y);$$

here $R_{\mathcal{M}_l}(x, \varepsilon_+, \varepsilon_-) := \{\tilde{x} \in \mathcal{M}_l : \varepsilon_- < d_{\mathcal{M}_l}(x, \tilde{x}) < \varepsilon_+\}$.

We find a bound for $|A_1(x)|^2$; notice that $\frac{1}{\tau_l(x)} \leq 1 + Cm_l K_l \varepsilon_+^2$ by (A.6). First, notice that:

$$\begin{aligned} \nabla \mathcal{K}_{\varepsilon_+, \varepsilon_-}^l(\cdot, y)(x) &= \nabla \left[\frac{\varepsilon_+^2}{\varepsilon_+^{m+2} - \varepsilon_-^{m+2}} \psi\left(\frac{d_{\mathcal{M}_l}(x, y)}{\varepsilon_+}\right) - \frac{\varepsilon_-^2}{\varepsilon_+^{m+2} - \varepsilon_-^{m+2}} \psi\left(\frac{d_{\mathcal{M}_l}(x, y)}{\varepsilon_-}\right) \right] \\ &= -\frac{1}{\varepsilon_+^{m+2} - \varepsilon_-^{m+2}} \left(\varepsilon_+ \psi'\left(\frac{d_{\mathcal{M}_l}(x, y)}{\varepsilon_+}\right) - \varepsilon_- \psi'\left(\frac{d_{\mathcal{M}_l}(x, y)}{\varepsilon_-}\right) \right) \frac{\exp_x^{-1}(y)}{d_{\mathcal{M}_l}(x, y)} \\ &= \frac{\exp_x^{-1}(y)}{\sigma_\eta(\varepsilon_+^{m+2} - \varepsilon_-^{m+2})} \left[\eta\left(\frac{d_{\mathcal{M}_l}(x, y)}{\varepsilon_+}\right) - \eta\left(\frac{d_{\mathcal{M}_l}(x, y)}{\varepsilon_-}\right) \right]. \end{aligned}$$

Since for $A_1(x)$ we have $|A_1(x)| = \langle A_1(x), w \rangle$ for some unit vector $w \in T_x \mathcal{M}_l$, we can combine with the inequality above to obtain:

$$\begin{aligned} |A_1(x)| &= \langle A_1(x), w \rangle \\ &= \frac{1}{\sigma_\eta(\varepsilon_+^{m+2} - \varepsilon_-^{m+2})} \int_{R_{\mathcal{M}_l}(x, \varepsilon_+, \varepsilon_-)} \left[\eta\left(\frac{d(x, y)}{\varepsilon_+}\right) - \eta\left(\frac{d(x, y)}{\varepsilon_-}\right) \right] \\ &\quad \cdot (f_l(y) - f_l(x)) \langle \exp_x^{-1}(y), w \rangle d\text{vol}_{\mathcal{M}_l}(y) \\ &= \frac{1}{\sigma_\eta(\varepsilon_+^{m+2} - \varepsilon_-^{m+2})} \int_{R(\varepsilon_+, \varepsilon_-)} \left[\eta\left(\frac{|u|}{\varepsilon_+}\right) - \eta\left(\frac{|u|}{\varepsilon_-}\right) \right] \phi(u) \langle u, w \rangle J_x(u) du, \end{aligned}$$

where $\phi(u) = f_l(\exp_x(u)) - f_l(x)$ and $R(\varepsilon_+, \varepsilon_-) := \{u \in \mathbb{R}^{m_l} : \varepsilon_- < |u| < \varepsilon_+\}$. By the Cauchy-Schwartz inequality,

$$\begin{aligned} |A_1(x)|^2 &\leq \frac{1}{\sigma_\eta^2(\varepsilon_+^{m+2} - \varepsilon_-^{m+2})^2} \int_{R(\varepsilon_+, \varepsilon_-)} |\phi(u)|^2 J_x(u)^2 \left[\eta\left(\frac{|u|}{\varepsilon_+}\right) - \eta\left(\frac{|u|}{\varepsilon_-}\right) \right] du \\ &\quad \cdot \int_{R(\varepsilon_+, \varepsilon_-)} \langle u, w \rangle^2 \left[\eta\left(\frac{|u|}{\varepsilon_+}\right) - \eta\left(\frac{|u|}{\varepsilon_-}\right) \right] du \\ &= \frac{1}{\sigma_\eta(\varepsilon_+^{m+2} - \varepsilon_-^{m+2})} \int_{R(\varepsilon_+, \varepsilon_-)} |\phi(u)|^2 J_x(u)^2 \left[\eta\left(\frac{|u|}{\varepsilon_+}\right) - \eta\left(\frac{|u|}{\varepsilon_-}\right) \right] du \\ &\leq \frac{1 + Cm_l K_l \varepsilon_+^2}{\sigma_\eta(\varepsilon_+^{m+2} - \varepsilon_-^{m+2})} \int_{\mathcal{M}_l} \left[\eta\left(\frac{d_{\mathcal{M}_l}(x, y)}{\varepsilon_+}\right) - \eta\left(\frac{d_{\mathcal{M}_l}(x, y)}{\varepsilon_-}\right) \right] (f_l(y) - f_l(x))^2 d\text{vol}_{\mathcal{M}_l}(y), \end{aligned} \tag{A.13}$$

where the equality comes from

$$\int_{R(\varepsilon_+, \varepsilon_-)} \langle u, w \rangle^2 \left[\eta\left(\frac{|u|}{\varepsilon_+}\right) - \eta\left(\frac{|u|}{\varepsilon_-}\right) \right] du = \int_{B_m(\varepsilon_+)} \langle u, w \rangle^2 du - \int_{B_m(\varepsilon_-)} \langle u, w \rangle^2 du = \sigma_\eta(\varepsilon_+^{m+2} - \varepsilon_-^{m+2}),$$

and the last inequality from the bound (A.9). Integrating (A.13) against $\rho_l^2 d\text{vol}_{\mathcal{M}_l}$ and using the Lipschitz continuity of ρ_l we deduce

$$\begin{aligned} \left\| \frac{A_1}{\tau_l} \right\|_{L^2(\mathcal{M}_l, \rho_l^2 \text{vol}_{\mathcal{M}_l})}^2 &\leq \frac{(1 + Cm_l K_l \varepsilon_+^2)(1 + c_\rho L_{\rho_l} \varepsilon_+)}{\sigma_\eta(\varepsilon_+^{m+2} - \varepsilon_-^{m+2})} \\ &\quad \cdot \int_{\mathcal{M}_l} \int_{B_{\mathcal{M}_l}(x, \varepsilon_+, \varepsilon_-)} \left[\eta \left(\frac{d_{\mathcal{M}_l}(x, y)}{\varepsilon_+} \right) - \eta \left(\frac{d_{\mathcal{M}_l}(x, y)}{\varepsilon_-} \right) \right] |f_l(y) - f_l(x)|^2 d\mu_l(x) d\mu_l(y) \\ &\leq \frac{(1 + Cm_l K_l \varepsilon_+^2)(1 + c_\rho L_{\rho_l} \varepsilon_+)}{\sigma_\eta} D_{NL, l}^{\varepsilon_+, \varepsilon_-}(f_l). \end{aligned}$$

Now we analyze the term $A_2(x)$. First, recall that $|\nabla(\tau_l^{-1})| \leq \frac{Cm_l K_l \varepsilon_+}{\sigma_\eta}$ and $\tau_l \leq 1 + Cm_l K_l \varepsilon_+^2$ by Lemma A.6. Using the mean value theorem, it is straightforward to show that

$$\mathcal{K}_{\varepsilon_+, \varepsilon_-}^l(x, y) \leq \frac{\varepsilon_+^2}{\varepsilon_+^{m+2} - \varepsilon_-^{m+2}} \psi \left(\frac{d_{\mathcal{M}_l}(x, y)}{\varepsilon_+} \right) \leq \frac{\varepsilon_+^2 \eta \left(\frac{d_{\mathcal{M}_l}(x, y)}{\varepsilon_+} \right)}{\sigma_\eta(\varepsilon_+^{m+2} - \varepsilon_-^{m+2})}. \quad (\text{A.14})$$

Thus, by the Cauchy-Schwartz inequality and (A.14), we have

$$\begin{aligned} |A_2(x)|^2 &\leq |\nabla(\frac{1}{\tau_l(x)})|^2 \int_{\mathcal{M}_l} \mathcal{K}_{\varepsilon_+, \varepsilon_-}^l(x, y) d\mu_l(y) \int_{\mathcal{M}_l} |f_l(x) - f_l(y)|^2 \mathcal{K}_{\varepsilon_+, \varepsilon_-}^l(x, y) d\mu_l(y) \\ &\leq \frac{C^2 m^2 K_l^2 \varepsilon_+^2}{\sigma_\eta^3(\varepsilon_+^{m+2} - \varepsilon_-^{m+2})} \int_{\mathcal{M}_l} \varepsilon_+^2 \eta \left(\frac{d_{\mathcal{M}_l}(x, y)}{\varepsilon_+} \right) |f_l(x) - f_l(y)|^2 d\mu_l(y). \end{aligned}$$

Integrating both sides of the above inequality with respect to $\rho_l^2 d\text{vol}_{\mathcal{M}_l}$, using the Lipschitz continuity of ρ_l , and using Lemma A.7, we conclude that

$$\|A_2\|_{L^2(\mathcal{M}_l, \rho_l^2 \text{vol}_{\mathcal{M}_l})} \leq \frac{Cm_l K_l \varepsilon_+^2 (1 + c_\rho L_{\rho_l} \varepsilon_+) \sqrt{1 + c_\rho L_{\rho_l}}}{\sigma_\eta} \sqrt{\frac{1}{\sigma_\eta} D_{NL, l}^{\varepsilon_+, \varepsilon_-}(f_l)},$$

for some universal constant C . Combining the estimates for $\left\| \frac{A_1}{\tau_l} \right\|_{L^2(\mathcal{M}_l, \rho_l^2 \text{vol}_{\mathcal{M}_l})}^2$ and $\|A_2\|_{L^2(\mathcal{M}_l, \rho_l^2 \text{vol}_{\mathcal{M}_l})}$ we finally obtain:

$$(D_l(\Lambda_{\varepsilon_+, \varepsilon_-} f_l))^{1/2} \leq (1 + c_\rho L_{\rho_l} \varepsilon_+) \left[1 + Cm_l K_l \varepsilon_+^2 \left(1 + \frac{\sqrt{1 + c_\rho L_{\rho_l}}}{\sigma_\eta} \right) \right] \sqrt{\frac{1}{\sigma_\eta} D_{NL, l}^{\varepsilon_+, \varepsilon_-}(f_l)}.$$

□

Lemma A.9. *Suppose $\varepsilon_+, \varepsilon_-$ satisfy Assumptions 2. Then, there exists a universal constant $C > 0$ such that*

$$D_{\varepsilon_+, \varepsilon_-}^{NL, l}(f_l) \leq (1 + c_\rho L_{\rho_l} \varepsilon_+) (1 + Cm_l K_l \varepsilon_+^2) \sigma_\eta D_l(f_l), \quad \forall f_l \in L(\mu_l).$$

Proof. By a density argument we may assume without the loss of generality that f_l is smooth. Now, for every $x \in \mathcal{M}_l$,

$$\int_{R_{\mathcal{M}_l}(x, \varepsilon_+, \varepsilon_-)} |f_l(x) - f_l(y)|^2 d\mu_l(y) = \int_{R(\varepsilon_+, \varepsilon_-)} |f_l(\exp_x(v)) - f_l(x)|^2 \rho_l(\exp_x(v)) J_x(v) dv,$$

where $R_{\mathcal{M}_l}(x, \varepsilon_+, \varepsilon_-)$ and $R(\varepsilon_+, \varepsilon_-)$ are as defined in the proof of Lemma A.8, and J_x is the Jacobian of the exponential map at x . From the Fundamental Theorem of Calculus it follows that

$$|f_l(\exp_x(v)) - f_l(x)|^2 \leq \int_0^1 \left| \frac{d}{dt} f_l(\exp_x(tv)) \right|^2 dt = \int_0^1 |df_l(\Phi_t(x, v)_2)|^2 dt,$$

where Φ_t denotes the time t geodesic flow on \mathcal{M}_l 's tangent bundle $\mathcal{T}\mathcal{M}_l$: that is, $\Phi_t(x, v) = (\varphi_{x,v}(t), \varphi'_{x,v}(t)) \in \mathcal{T}\mathcal{M}_l$, where $\varphi_{x,v}(t) := \exp_x(tv)$ and $\varphi'_{x,v}(t)$ is obtained by parallel transporting the vector $v \in \mathcal{T}_x\mathcal{M}_l$ along the geodesic connecting x and $\exp_x(tv)$; $\Phi_t(x, v)_2$ denotes the second coordinate of $\Phi_t(x, v)$. We can then obtain:

$$\begin{aligned} & \int_{\mathcal{M}_l} \int_{R(\varepsilon_+, \varepsilon_-)} |f_l(\exp_x(v)) - f_l(x)|^2 \rho_l(\exp_x(v)) dv \rho_l(x) d\text{vol}_{\mathcal{M}_l}(x) \\ & \leq \int_0^1 \int_{\mathcal{M}} \int_{R(\varepsilon_+, \varepsilon_-)} |df_l(\Phi_t(x, v))|^2 \rho_l(\Phi_1(x, v)_1) \rho_l(\Phi_0(x, v)_1) dv d\text{vol}_{\mathcal{M}_l}(x) dt, \end{aligned}$$

where we use $\Phi_0(x, v)_1$ and $\Phi_1(x, v)_1$ to denote the first coordinates of $\Phi_0(x, v)$ and $\Phi_1(x, v)$ respectively. From the Lipschitz continuity of ρ_l it follows $\rho_l(x) \leq (1 + c_\rho L_{\rho_l} \varepsilon_+) \rho_l(y)$ for all $x, y \in \mathcal{M}_l$ satisfying $d(x, y) \leq \varepsilon_+$. Combining the fact that Φ_t preserves the canonical volume form $\text{vol}_{T\mathcal{M}_l}$ on $T\mathcal{M}_l$ and that

$$\mathcal{R}(\varepsilon_+, \varepsilon_-) := \{\xi = (x, v) \in T\mathcal{M} : \varepsilon_- \leq |v| \leq \varepsilon_+\}; \quad \mathcal{B}_r := \{\xi = (x, v) \in T\mathcal{M} : |v| \leq r\}$$

are invariant under Φ_t , we obtain

$$\begin{aligned} & \int_{\mathcal{M}} \int_{R(\varepsilon_+, \varepsilon_-)} |f_l(\exp_x(v)) - f_l(x)|^2 \rho_l(\exp_x(v)) dv \rho_l(x) d\text{vol}_{\mathcal{M}_l}(x) \\ & \leq (1 + c_\rho L_{\rho_l} \varepsilon_+) \int_0^1 \int_{\mathcal{R}(\varepsilon_+, \varepsilon_-)} |df_l(\Phi_t(\xi)_2)|^2 \rho_l^2(\Phi_t(\xi_1)) d\text{vol}_{T\mathcal{M}_l}(\xi) dt \\ & = (1 + c_\rho L_{\rho_l} \varepsilon_+) \left[\int_{\mathcal{B}_{\varepsilon_+}} |df_l(\xi_2)|^2 \rho_l^2(\xi_1) d\text{vol}_{T\mathcal{M}_l}(\xi) - \int_{\mathcal{B}_{\varepsilon_-}} |df_l(\xi_2)|^2 \rho_l^2(\xi_1) d\text{vol}_{T\mathcal{M}_l}(\xi) \right] \\ & = (1 + c_\rho L_{\rho_l} \varepsilon_+) \sigma_\eta(\varepsilon_+^{m+2} - \varepsilon_-^{m+2}) \int_{\mathcal{M}} |\nabla f_l|^2 \rho_l^2(x) d\text{vol}_{\mathcal{M}_l}(x). \end{aligned}$$

Therefore,

$$\begin{aligned} D_{NL,l}^{\varepsilon_+, \varepsilon_-}(f_l) & \leq (1 + Cm_l K_l \varepsilon_+^2) \cdot \\ & \cdot \frac{1}{\varepsilon_+^{m+2} - \varepsilon_-^{m+2}} \int_{\mathcal{M}_l} \int_{R(\varepsilon_+, \varepsilon_-)} |f_l(\exp_x(v)) - f_l(x)|^2 \rho_l(\exp_x(v)) dv \rho_l(x) d\text{vol}_{\mathcal{M}_l}(x) \\ & \leq (1 + Cm_l K_l \varepsilon_+^2) \cdot (1 + c_\rho L_{\rho_l} \varepsilon_+) \sigma_\eta D_l(f_l). \end{aligned}$$

□

The following is an adaptation of Lemma 14 in [44] to the kernel with annular geometry that we consider in this paper.

Lemma A.10. *Suppose $\tilde{\delta}, \varepsilon_+, \varepsilon_-$ satisfy Assumptions 2. Then, with probability at least $1 - \sum_{l=1}^N (nw_l + t) \exp\left(-C(nw_l - t)\theta^2 \tilde{\delta}^m\right) - 2N \exp\left(\frac{-2t^2}{n}\right)$ and for a universal constant $C > 0$, the following statements hold:*

(1) *For every $u_l : \mathcal{X}_n^l \rightarrow \mathbb{R}$ we have*

$$\frac{1}{\sigma_\eta} D_{NL,l}^{\varepsilon'_+, \varepsilon'_-}(P_l^* u_l) \leq \left(1 + C(\theta + \tilde{\delta})\right) \left(1 + C\tilde{\delta}\left(\frac{1}{\varepsilon_+} + \varepsilon_-^2\right)\right) b_l^{\varepsilon_+, \varepsilon_-}(u_l),$$

where $\varepsilon'_+ := \varepsilon_+ - 2\tilde{\delta}$ and $\varepsilon'_- := \varepsilon_- + 2\tilde{\delta} + \frac{8\varepsilon'^3}{R^2}$. Applying Assumption 2, $C \frac{\tilde{\delta}\varepsilon_+^{m+1} + \varepsilon_-^{m+4}}{\varepsilon_+^{m+2} - \varepsilon_-^{m+2}}$ can be simplified to $C_1 \frac{\tilde{\delta}}{\varepsilon_+} + C_2 \tilde{\delta} \varepsilon_-^2$, where $C_1 \leq \frac{16C}{15}$, $C_2 \leq \frac{C}{15}$; or just $C\tilde{\delta}\left(\frac{1}{\varepsilon_+} + \varepsilon_-^2\right)$

(2) For every $f_l \in H^1(\mathcal{M}_l)$

$$b_l^{\varepsilon_+, \varepsilon_-}(P_l f_l) \leq \left(1 + C(\theta + \tilde{\delta})\right) \left(1 + C\tilde{\delta}\left(\frac{1}{\varepsilon_+} + \varepsilon_-^2\right)\right) \frac{1}{\sigma_\eta} D_{NL,l}^{\varepsilon_+'' \varepsilon_-''}(f_l), \quad (\text{A.15})$$

where $\varepsilon_+'' := \varepsilon_+ + \frac{8\varepsilon_+''^3}{R^2} + 2\tilde{\delta}$ and $\varepsilon_-'' := \varepsilon_- - 2\tilde{\delta}$. We recall that b^l was introduced in (A.3).

Proof. We first recall a well known relation between the geodesic distance in \mathcal{M}_l and the Euclidean distance in the ambient space \mathbb{R}^d . Namely,

$$|x - y| \leq d_{\mathcal{M}_l}(x, y) \leq |x - y| + \frac{8}{R_l^2} |x - y|^3, \quad x, y \in \mathcal{M}_l, \quad (\text{A.16})$$

where R_l is the reach of the manifold \mathcal{M}_l (see [25] for a definition of reach).

To show (1), notice that if $|x - y| < \varepsilon_-$, then from (A.16) we get

$$|x - y| \leq d_{\mathcal{M}_l}(x, y) \leq |x - y| + \frac{8\varepsilon_-^3}{R_l^2}. \quad (\text{A.17})$$

We now use the map \tilde{T}_l , the density $\tilde{\rho}_l^n$ from Corollary A.3, and the induced partition $\{U_{1l}, \dots, U_{nl}\}$ on \mathcal{M}_l of the form $U_{il} = \tilde{T}_l^{-1}(x_{il})$, where $x_{il} \in X_l$, to write

$$\begin{aligned} & n_l^2 (\varepsilon_+^{m+2} - \varepsilon_-^{m+2}) b_l^{\varepsilon_+, \varepsilon_-}(u_l) \\ &= \sum_{i,j} \int_{U_{il}} \int_{U_{jl}} \left[\eta \left(\frac{|\tilde{T}_l(x) - \tilde{T}_l(y)|}{\varepsilon_+} \right) - \eta \left(\frac{|\tilde{T}_l(x) - \tilde{T}_l(y)|}{\varepsilon_-} \right) \right] \\ & \quad \cdot |(P^* u_l)(x) - (P^* u_l)(y)|^2 \tilde{\rho}_l^n(x) \tilde{\rho}_l^n(y) d\text{vol}_{\mathcal{M}_l}(y) d\text{vol}_{\mathcal{M}_l}(x) \\ & \geq \left(1 - C(\theta + \tilde{\delta})\right) \int_{\mathcal{M}_l} \int_{\mathcal{M}_l} \left[\eta \left(\frac{d(\tilde{T}_l(x), \tilde{T}_l(y))}{\varepsilon_+} \right) - \eta \left(\frac{\left[d(\tilde{T}_l(x), \tilde{T}_l(y)) - \frac{8\varepsilon_-^3}{R^2} \right]_+}{\varepsilon_-} \right) \right] \\ & \quad \cdot |(P^* u_l)(x) - (P^* u_l)(y)|^2 d\mu_l(y) d\mu_l(x) \\ & \geq \left(1 - C(\theta + \tilde{\delta})\right) \int_{\mathcal{M}_l} \int_{\mathcal{M}_l} \left[\eta \left(\frac{d(x, y) + 2\tilde{\delta}}{\varepsilon_+} \right) - \eta \left(\frac{\left[d(x, y) - \frac{8\varepsilon_-^3}{R^2} - 2\tilde{\delta} \right]_+}{\varepsilon_-} \right) \right] \\ & \quad \cdot |(P^* u_l)(x) - (P^* u_l)(y)|^2 d\mu_l(y) d\mu_l(x) \\ &= \left(1 - C(\theta + \tilde{\delta})\right) (\varepsilon_+'^{m+2} - \varepsilon_-'^{m+2}) \frac{1}{\sigma_\eta} D_{NL,l}^{\varepsilon_+' \varepsilon_-'}(P_l^* u_l), \end{aligned}$$

where in the first inequality we use i) in Corollary A.3 and (A.17), and in the second inequality we use ii) in Corollary (A.3). Combining the above inequality with Assumptions 2 we conclude that

$$\left(1 + C(\theta + \tilde{\delta})\right) \left(1 + C \frac{\tilde{\delta} \varepsilon_+^{m+1} + \varepsilon_-^{m+4}}{\varepsilon_+^{m+2} - \varepsilon_-^{m+2}}\right) b_l^{\varepsilon_+, \varepsilon_-}(u_l) \geq \frac{1}{\sigma_\eta} D_{NL,l}^{\varepsilon_+' \varepsilon_-'}(P_l^* u_l).$$

For (2), we proceed similarly as in the proof of (1) to deduce

$$\begin{aligned}
b_l^{\varepsilon+, \varepsilon-}(Pf_l) &\leq \frac{1 + C(\theta + \tilde{\delta})}{\sigma_\eta(\varepsilon_+^{m+2} - \varepsilon_-^{m+2})} \sum_i \sum_j \int_{U_{il}} \int_{U_{jl}} \left[\eta \left(\frac{|\tilde{T}(x) - \tilde{T}(y)|}{\varepsilon_+} \right) - \eta \left(\frac{|\tilde{T}(x) - \tilde{T}(y)|}{\varepsilon_-} \right) \right] \\
&\quad \cdot |f_l(y) - f_l(x)|^2 d\mu_l(y) d\mu_l(x) \\
&\leq \frac{1 + C(\theta + \tilde{\delta})}{\sigma_\eta(\varepsilon_+^{m+2} - \varepsilon_-^{m+2})} \int_{\mathcal{M}_l} \int_{\mathcal{M}_l} \left[\eta \left(\frac{[d(x, y) - \frac{8\varepsilon_+^3}{R^2} - 2\tilde{\delta}]_+}{\varepsilon_+} \right) - \eta \left(\frac{d(x, y) + 2\tilde{\delta}}{\varepsilon_-} \right) \right] \\
&\quad \cdot |f_l(y) - f_l(x)|^2 d\mu_l(y) d\mu_l(x) \\
&\leq \frac{1 + C(\theta + \tilde{\delta})}{\sigma_\eta(\varepsilon_+^{m+2} - \varepsilon_-^{m+2})} \left[E_l^{\varepsilon''_+}(f_l) - E_l^{\varepsilon''_-}(f_l) \right] \\
&\leq (1 + C(\theta + \tilde{\delta})) \left(1 + C \frac{\varepsilon_-^{m+4} + \varepsilon_+^{m+1}\tilde{\delta}}{\varepsilon_+^{m+2} - \varepsilon_-^{m+2}} \right) D_{NL, l}^{\varepsilon''_+, \varepsilon''_-}(f_l),
\end{aligned}$$

where in the last line we have used (A.11) and Assumptions 2. \square

We are ready to prove Proposition A.4.

A.4. Proofs of Propositions A.4 and A.5.

Proof of Proposition A.4. (1): Let $u \in L^2(\mu^n)$. We write u in coordinates as $u = (u_1, \dots, u_N)$. We combine Lemmas A.8 and A.10 to obtain for every $l = 1, \dots, N$:

$$D_l(\mathcal{I}_l u_l) \leq (1 + C(\theta + \tilde{\delta})) (1 + C \frac{\tilde{\delta}}{\varepsilon_+}) (1 + c_\rho L_\rho \varepsilon_+) \left[1 + C m_l K_l \varepsilon_+^2 \left(1 + \frac{\sqrt{1 + c_\rho L_\rho}}{\sigma_\eta} \right) \right] b_l^{\varepsilon+, \varepsilon-}(u_l).$$

From the above we deduce that $D(\mathcal{I}u) = \sum_{l=1}^N w_l^2 D_l(\mathcal{I}_l u_l)$ is smaller than:

$$(1 + C(\theta + \tilde{\delta})) (1 + C \frac{\tilde{\delta}}{\varepsilon_+}) (1 + c_\rho L_\rho \varepsilon_+) \left[1 + C m K \varepsilon_+^2 \left(1 + \frac{\sqrt{1 + c_\rho L_\rho}}{\sigma_\eta} \right) \right] \sum_{l=1}^N w_l^2 b_l^{\varepsilon+, \varepsilon-}(u_l).$$

In turn, Proposition A.1 implies that with probability at least $1 - 2N \exp\left(\frac{-2t^2}{n}\right)$ we have

$$\sum_{l=1}^N w_l^2 b_l^{\varepsilon+, \varepsilon-}(u_l) \leq (1 + t) \sum_{l=1}^N \left(\frac{n_l}{n} \right)^2 b_l^{\varepsilon+, \varepsilon-}(u_l) = (1 + t) b_I^{\varepsilon+, \varepsilon-}(u) \leq (1 + t) b^{\varepsilon+, \varepsilon-}(u).$$

Putting together the above inequalities we obtain the desired estimate. Here it is worth highlighting that the last inequality in the above expression comes from the fact that the discrete Dirichlet energy $b^{\varepsilon+, \varepsilon-}$ is the sum of $b_I^{\varepsilon+, \varepsilon-}$ and $b_O^{\varepsilon+, \varepsilon-}$. As we will see below, in order to obtain a reverse inequality between $b^{\varepsilon+, \varepsilon-}$ and D one needs to control $b_O^{\varepsilon+, \varepsilon-}(Pf)$ using regularity estimates of f in each of the \mathcal{M}_l . We will be able to obtain this control when f is in the span of the eigenfunctions of $\Delta_{\mathcal{M}}$ smaller than a certain value (which is all we need in the remainder).

(2): Similarly to (1), we may combine Lemma A.9 and Lemma A.10, to deduce:

$$\begin{aligned}
b_I^{\varepsilon+, \varepsilon-}(Pf) &\leq (1 + c_\rho L_\rho \varepsilon_+''_+) (1 + C m_l K_l \varepsilon_+''^2) \left(1 + C \left(\frac{\varepsilon_+^{m+4} + \varepsilon_+^{m+1}\tilde{\delta}}{\varepsilon_+^{m+2} - \varepsilon_-^{m+2}} + \theta + \tilde{\delta} \right) \right) \frac{1}{\sigma_\eta} D(f) \\
&\leq \left(1 + C(\varepsilon_+'' + \frac{\tilde{\delta}}{\varepsilon_+} + \theta + \tilde{\delta}) + t \right) D(f).
\end{aligned} \tag{A.18}$$

where the last step we used Assumption 2.

Let $f \in L^2(\mathcal{M})$ belong to the span of $\Delta_{\mathcal{M}}$'s eigenfunctions with corresponding eigenvalue less than λ . Then, f can be written as $f = \sum_{l=1}^N f^l$ where each f^l has support on \mathcal{M}_l , and where, abusing notation slightly, each f^l has the form $f^l = \sum_q b_{ql} f_q^l$ for an orthonormal basis of eigenfunctions of $\Delta_{\mathcal{M}_l}$, $\{f_q^l\}$, with corresponding eigenvalues smaller than λ . It is straightforward to see that:

$$\begin{aligned}
b_O^{\varepsilon_+, \varepsilon_-}(\tilde{P}f) &= \frac{1}{n^2(\varepsilon_+^{m+2} - \varepsilon_-^{m+2})} \sum_{x_i, x_j \in \mathcal{X}_n} \omega_{x_i x_j}^O (\tilde{P}f(x_i) - \tilde{P}f(x_j))^2 \\
&\leq \frac{2}{\varepsilon_+^{m+2} - \varepsilon_-^{m+2}} \sum_{x_i \in \mathcal{X}_n} \sum_{x_j \in \mathcal{X}_n} \omega_{x_i x_j}^O (\tilde{P}f(x_i))^2 \\
&= \frac{2}{\varepsilon_+^{m+2} - \varepsilon_-^{m+2}} \sum_{l=1}^N \sum_{s: s \neq l} \sum_{x_i \in \mathcal{M}_l} \sum_{x_j \in \mathcal{M}_s} \omega_{x_i x_j}^O \left| \int_{U_{il}} f^l(x) \tilde{p}_l^n(x) d\text{vol}_{\mathcal{M}_l}(x) \right|^2 \\
&= \frac{2}{\varepsilon_+^{m+2} - \varepsilon_-^{m+2}} \sum_{l=1}^N \frac{\|f^l\|_{L^\infty(\mathcal{M}_l)}^2}{n_l^2} \sum_{s: s \neq l} \sum_{x_i \in \mathcal{M}_l} \sum_{x_j \in \mathcal{M}_s} \omega_{x_i x_j}^O \\
&= \frac{2N \cdot N_0}{\varepsilon_+^{m+2} - \varepsilon_-^{m+2}} \sum_{l=1}^N \frac{\|f^l\|_{L^\infty(\mathcal{M}_l)}^2}{n_l^2} \\
&\leq \frac{2N \cdot N_0(1+t)}{w_{\min}^2 n^2 (\varepsilon_+^{m+2} - \varepsilon_-^{m+2})} \sum_{l=1}^N \|f^l\|_{L^\infty(\mathcal{M}_l)}^2.
\end{aligned} \tag{A.19}$$

In the above, the last inequality follows with high probability according to Proposition (A.1). To complete the proof we find estimates for each of the terms $\|f^l\|_{L^\infty(\mathcal{M}_l)}^2$ and to do this we adapt the argument in Lemma 3.3 of [34]. From standard higher order elliptic regularity results (e.g. Theorem 2 in [24]) it follows that for every $s \in \mathbb{N}$

$$\|f^l\|_{H^{2s}(\mathcal{M}_l)}^2 \leq C(\mathcal{M}_l, \rho_l, s) \left(\left\| \Delta_{\mathcal{M}_l}^s f^l \right\|_{L^2(\mathcal{M}_l)}^2 + \|f^l\|_{L^2(\mathcal{M}_l)}^2 \right) ,$$

where in the above $H^{2s}(\mathcal{M}_l)$ is the Sobolev space of functions on \mathcal{M}_l with square-integrable derivatives of order up to $2s$; it is at this stage that we use the smoothness of the manifold \mathcal{M}_l and the density ρ_l . Moreover, by the Sobolev embedding theorem on compact manifolds (e.g. Theorem 2.20 in [4]), we have $H^{2s}(\mathcal{M}_l) \subset C^1(\mathcal{M}_l)$ as long as $2s > m/2 + 1$. Choosing $2s = m/2 + 2$ we obtain:

$$\|f^l\|_{L^\infty(\mathcal{M}_l)} \leq \|f^l\|_{C^1(\mathcal{M}_l)} \leq C(\mathcal{M}_l, \rho_l) \|f^l\|_{H^{m/2+2}(\mathcal{M}_l)} \leq C(\mathcal{M}_l, \rho_l) (\lambda^{m/4+1} + 1) \|f^l\|_{L^2(\mathcal{M}_l)}. \tag{A.20}$$

Recalling that f^l has the form $\sum_q b_{ql} f_q^l$, where the f_q^l are orthonormal in $L^2(\mathcal{M}_l, \rho_l)$ and are eigenfunctions of $\Delta_{\mathcal{M}_l}$ with eigenvalues λ_q^l smaller than λ , we can see that

$$\begin{aligned}
\left\| \Delta_{\mathcal{M}_l}^s f^l \right\|_{L^2(\mathcal{M}_l, \rho_l)}^2 &= \left\| \sum_q b_{ql} (\lambda_q^l)^s f_q^l \right\|_{L^2(\mathcal{M}_l, \rho_l)}^2 \\
&= \sum_q b_{ql}^2 (\lambda_q^l)^{2s} \|f_q^l\|_{L^2(\mathcal{M}_l, \rho_l)}^2 \leq \lambda^{2s} \|f^l\|_{L^2(\mathcal{M}_l)}^2.
\end{aligned}$$

Putting the above estimates together and combining with (A.19) gives us the desired result. \square

Before proving Proposition A.5 we need one last preliminary estimate.

Lemma A.11. *Suppose $\varepsilon_+, \varepsilon_-$ satisfy Assumptions 2. Then, there exists a universal constant $C > 0$ such that*

$$\|\Lambda_{\varepsilon_+, \varepsilon_-} f\|_{L^2(\mathcal{M}, \rho)}^2 \leq (1 + Cc_\rho L_\rho \varepsilon_+) (1 + CmK\varepsilon_+^2) \|f\|_{L^2(\mathcal{M}, \rho)}^2,$$

and

$$\|\Lambda_{\varepsilon_+, \varepsilon_-} f - f\|_{L^2(\mathcal{M}, \rho)}^2 \leq \frac{Cc_\rho^2 \varepsilon_+^2}{\sigma_\eta} \sum_{l=1}^N w_l D_{NL, l}^{\varepsilon_+, \varepsilon_-}(f_l) \leq \frac{Cc_\rho^2 \varepsilon_+^2}{\sigma_\eta w_{\min}} D(f).$$

for all $f \in L^2(\mathcal{M}, \rho)$. In the above, $w_{\min} := \min_{l=1, \dots, N} w_l$.

Proof. Since $\Lambda_{\varepsilon_+, \varepsilon_-}$ acts on f coordinatewise, we get

$$\begin{aligned} \int_{\mathcal{M}} (\Lambda_{\varepsilon_+, \varepsilon_-} f(x))^2 d\mu(x) &= \sum_{l=1}^N w_l \int_{\mathcal{M}_l} (\Lambda_{\varepsilon_+, \varepsilon_-}^l f_l(x))^2 \rho_l(x) d\text{vol}_{\mathcal{M}_l}(x) \\ &\leq \sum_{l=1}^N w_l \int_{\mathcal{M}_l} \int_{\mathcal{M}_l} \frac{\mathcal{K}_{\varepsilon_+, \varepsilon_-}^l(x, y)}{\tau_l(x)} (f_l(y))^2 \rho_l(x) d\text{vol}_{\mathcal{M}_l}(y) d\text{vol}_{\mathcal{M}_l}(x) \\ &\leq (1 + Cc_\rho L_\rho \varepsilon_+) (1 + CmK\varepsilon_+^2) \sum_{l=1}^N w_l \int_{\mathcal{M}_l} (f_l(y))^2 \rho_l(y) d\text{vol}_{\mathcal{M}_l}(y) \\ &= (1 + Cc_\rho L_\rho \varepsilon_+) (1 + CmK\varepsilon_+^2) \int_{\mathcal{M}} (f(x))^2 d\mu(x), \end{aligned}$$

where the first inequality follows from Jensen's inequality, and the second inequality follows from Lemma A.6 and the properties of the density functions ρ_l .

For the second inequality, we first calculate the difference between $\Lambda_{\varepsilon_+, \varepsilon_-}^l f_l(x)$ and $f_l(x)$:

$$\begin{aligned} |\Lambda_{\varepsilon_+, \varepsilon_-}^l f_l(x) - f_l(x)|^2 &= \left(\frac{1}{\tau_l(x)} \int_{\mathcal{M}_l} \mathcal{K}_{\varepsilon_+, \varepsilon_-}^l(x, y) (f_l(y) - f_l(x)) d\mu_l(y) \right)^2 \\ &\leq \frac{1}{\tau_l(x)^2} \int_{\mathcal{M}_l} \mathcal{K}_{\varepsilon_+, \varepsilon_-}^l(x, y) d\mu_l(y) \int_{\mathcal{M}_l} \mathcal{K}_{\varepsilon_+, \varepsilon_-}^l(x, y) (f_l(x) - f_l(y))^2 d\mu_l(y) \\ &= \frac{1}{\tau_l(x)} \int_{\mathcal{M}_l} \mathcal{K}_{\varepsilon_+, \varepsilon_-}^l(x, y) (f_l(x) - f_l(y))^2 d\mu_l(y). \end{aligned}$$

Then we integrate with respect to $\rho_l(x) d\text{vol}_{\mathcal{M}_l}(x)$ to get:

$$\begin{aligned} \|\Lambda_l^{\varepsilon_+, \varepsilon_-} f_l - f_l\|_{L^2(\mathcal{M}_l, \rho_l)}^2 &\leq (1 + Cm_l K_l \varepsilon_+^2) \int_{\mathcal{M}_l} \int_{\mathcal{M}_l} \mathcal{K}_{\varepsilon_+, \varepsilon_-}^l(x, y) (f_l(x) - f_l(y))^2 d\mu_l(y) d\mu_l(x) \\ &\leq \frac{(1 + Cm_l K_l \varepsilon_+^2) \varepsilon_+^2}{\sigma_\eta (\varepsilon_+^{m+2} - \varepsilon_-^{m+2})} \int_{\mathcal{M}_l} \int_{\mathcal{M}_l} \eta \left(\frac{d(x, y)}{\varepsilon_+} \right) (f_l(x) - f_l(y))^2 d\mu_l(y) d\mu_l(x) \\ &\leq \frac{Cc_\rho^2 \varepsilon_+^2}{\sigma_\eta} D_{NL, l}^{\varepsilon_+, \varepsilon_-}(f_l), \end{aligned}$$

where the second inequality follows from the fact that $\eta \leq \frac{1}{\sigma_\eta} \psi$ (recall (A.8)), and the third inequality follows from Lemma A.7. Multiplying the above by w_l , adding over l , and using Lemma A.9 we get the desired result. \square

Proof of Proposition A.5. (1): For each $l = 1, \dots, N$, we use estimates proved in [14] (appearing in Pages 24-25 in the proof of Proposition 4.2) to conclude that there is a constant C for which

$$\begin{aligned} \left| \|f_l\|_{L^2(\tilde{\mu}_l^n)}^2 - \|f_l\|_{L^2(\mu_l)}^2 \right| &\leq C(\theta + \tilde{\delta}) \|f_l\|_{L^2(\mu_l)}^2 \\ \left| \|\tilde{P}_l f_l\|_{L^2(\mu_l^n)}^2 - \|f_l\|_{L^2(\mu_l)}^2 \right| &\leq C \|f_l\|_{L^2(\mu_l)} \|\tilde{P}_l^* \tilde{P}_l f_l - f_l\|_{L^2(\tilde{\mu}_l^n)} + C(\theta + \tilde{\delta}) \|f_l\|_{L^2(\mu_l)}^2 \\ \|\tilde{P}_l^* \tilde{P}_l f_l - f_l\|_{L^2(\tilde{\mu}_l^n)}^2 &\leq C \tilde{\delta}^2 D_l(f_l), \end{aligned}$$

for every $f_l \in L^2(\mu_l)$; in the above we use $\tilde{\mu}_l^n$ to denote the measure $\tilde{\rho}_l^n d\text{vol}_{\mathcal{M}_l}(x)$. Combining the previous inequalities, we deduce that:

$$\begin{aligned} \left| \|\tilde{P}f\|_{L^2(\mu)}^2 - \|f\|_{L^2(\mu)}^2 \right| &\leq \sum_{l=1}^N w_l \left| \|\tilde{P}_l f_l\|_{L^2(\mu_l^n)}^2 - \|f_l\|_{L^2(\mu_l)}^2 \right| \\ &\leq C \sum_{l=1}^N w_l \|f_l\|_{L^2(\mu_l)} \|\tilde{P}_l^* \tilde{P}_l f_l - f_l\|_{L^2(\tilde{\mu}_l^n)} + C(\theta + \tilde{\delta}) \|f\|_{L^2(\mu)}^2. \end{aligned}$$

Now, the first term in the last inequality above is controlled by $C\tilde{\delta} \|f\|_{L^2(\mu)} \sqrt{D(f)}$. Indeed, this follows from Cauchy-Schwartz inequality:

$$\begin{aligned} \left(\sum_{l=1}^N w_l \|f_l\|_{L^2(\mu_l)} \|\tilde{P}_l^* \tilde{P}_l f_l - f_l\|_{L^2(\tilde{\mu}_l^n)} \right)^2 &\leq \left(\sum_{l=1}^N w_l \|f_l\|_{L^2(\mu_l)}^2 \right) \left(\sum_{l=1}^N w_l \|\tilde{P}_l^* \tilde{P}_l f_l - f_l\|_{L^2(\tilde{\mu}_l^n)}^2 \right) \\ &\leq C \frac{\tilde{\delta}^2}{w_{\min}} \|f\|_{L^2(\mu)}^2 D(f). \end{aligned}$$

Putting things together we finally deduce

$$\left| \|\tilde{P}f\|_{L^2(\mu^n)}^2 - \|f\|_{L^2(\mu)}^2 \right| \leq C \frac{\tilde{\delta}}{\sqrt{w_{\min}}} \|f\|_{L^2(\mu)} \sqrt{D(f)} + C(\theta + \tilde{\delta}) \|f\|_{L^2(\mu)}^2.$$

(2): From the identity $\|u_l\|_{L^2(\mu_l^n)} = \|\tilde{P}_l^* u_l\|_{L^2(\tilde{\mu}_l^n)}$ (which follows automatically from the fact that the map \tilde{T}_l is a transport map between $\tilde{\mu}_l^n$ and μ_l^n) and the triangle inequality we get

$$\begin{aligned} \left| \|\mathcal{I}_l u_l\|_{L^2(\tilde{\mu}_l^n)} - \|u_l\|_{L^2(\mu_l^n)} \right| &\leq \|\Lambda_l^{\varepsilon_+, \varepsilon_-} \tilde{P}_l^* u_l - \tilde{P}_l^* u_l\|_{L^2(\tilde{\mu}_l^n)} \\ &\leq (1 + c_\rho \|\rho_l - \tilde{\rho}_l^n\|_{L^\infty(\mathcal{M}_l)}) \cdot \|\Lambda_l^{\varepsilon_+, \varepsilon_-} \tilde{P}_l^* u_l - \tilde{P}_l^* u_l\|_{L^2(\mu_l)} \\ &\leq (1 + c_\rho \|\rho_l - \tilde{\rho}_l^n\|_{L^\infty(\mathcal{M}_l)}) \cdot C \varepsilon_+ \sqrt{D_{NL,l}^{\varepsilon_+, \varepsilon_-}(\tilde{P}_l^* u_l)} \\ &\leq C \varepsilon_+ \sqrt{b_l^{\varepsilon_+, \varepsilon_-}(u_l)}, \end{aligned}$$

where the third inequality comes from Lemma A.11 and the last one follows from Lemma A.10. Also, notice that

$$\|\mathcal{I}_l u_l\|_{L^2(\tilde{\mu}_l^n)} = \|\Lambda_l^{\varepsilon_+, \varepsilon_-} \tilde{P}_l^* u_l\|_{L^2(\tilde{\mu}_l^n)} \leq C \|\tilde{P}_l^* u_l\|_{L^2(\tilde{\mu}_l^n)} = C \|u_l\|_{L^2(\mu_l^n)}.$$

This inequality is also a consequence of Lemma A.11. So far we have proved that

$$\left| \|\mathcal{I}_l u_l\|_{L^2(\tilde{\mu}_l^n)}^2 - \|u_l\|_{L^2(\mu_l^n)}^2 \right| \leq C \varepsilon_+ \sqrt{b_l^{\varepsilon_+, \varepsilon_-}(u)} \|u_l\|_{L^2(\mu_l^n)}.$$

Next, we compare $\|\mathcal{I}_l u_l\|_{L^2(\tilde{\mu}_l^n)}$ and $\|\mathcal{I}_l u_l\|_{L^2(\mu_l)}$, bounding their difference with

$$\left| \|\tilde{I}_l u_l\|_{L^2(\tilde{\mu}_l^n)}^2 - \|\mathcal{I}_l u_l\|_{L^2(\mu_l)}^2 \right| \leq C(\theta + \tilde{\delta}) \|\tilde{I}_l u_l\|_{L^2(\tilde{\mu}_l^n)}^2 \leq C c_\rho (\theta + \tilde{\delta}) \|u_l\|_{L^2(\mu_l^n)}^2,$$

as it follows from the fact that the difference between ρ_l and $\tilde{\rho}_l^n$ is uniformly controlled with very high probability, i.e. i) in Corollary A.3.

Finally, we obtain

$$\begin{aligned} \left\| \|u_l\|_{L^2(\mu_l^n)}^2 - \|\tilde{\mathcal{I}}_l u_l\|_{L^2(\mu_l)}^2 \right\| &\leq \left\| \|\tilde{\mathcal{I}}_l u_l\|_{L^2(\tilde{\mu}_l^n)}^2 - \|u_l\|_{L^2(\mu_l^n)}^2 \right\| + \left\| \|\tilde{\mathcal{I}}_l u_l\|_{L^2(\tilde{\mu}_l^n)}^2 - \|\tilde{\mathcal{I}}_l u_l\|_{L^2(\mu_l)}^2 \right\| \\ &\leq C\varepsilon_+ \sqrt{b_l^{\varepsilon_+, \varepsilon_-}(u_l)} \|u_l\|_{L^2(\mu_l^n)} + Cc_\rho(\theta + \tilde{\delta}) \|u_l\|_{L^2(\mu_l^n)}^2. \end{aligned}$$

Adding over all $l = 1, \dots, N$ and using Cauchy-Schwarz inequality we obtain the desired estimate:

$$\begin{aligned} \left\| \|u\|_{L^2(\mu^n)}^2 - \|\tilde{\mathcal{I}}_l u\|_{L^2(\mu)}^2 \right\| &= \left\| \sum_{l=1}^N \|u_l\|_{L^2(\mu_l^n)}^2 - \sum_{l=1}^N w_l \|\tilde{\mathcal{I}}_l u_l\|_{L^2(\mu_l)}^2 \right\| \\ &\leq C\varepsilon_+ \sum_{l=1}^N w_l \sqrt{b_l^{\varepsilon_+, \varepsilon_-}(u)} \|u_l\|_{L^2(\mu_l^n)} + Cc_\rho(\theta + \tilde{\delta}) \sum_{l=1}^N w_l \|u_l\|_{L^2(\mu_l^n)}^2 \\ &\leq C\varepsilon_+ \|u\|_{L^2(\mu^n)} \sqrt{b^{\varepsilon_+, \varepsilon_-}(u)} + Cc_\rho(\theta + \tilde{\delta}) \|u\|_{L^2(\mu^n)}^2. \end{aligned}$$

□

A.5. Proof of Theorem 2.5.

Proof of Theorem 2.5. With the aid of Propositions A.4 and A.5 we can now compare $\lambda_k^{\varepsilon_+, \varepsilon_-}$ and λ_k , the k -th eigenvalues of \mathcal{L} and $\Delta_{\mathcal{M}}$ (listed according to multiplicity) respectively.

First, to find an upper bound for $\lambda_k^{\varepsilon_+, \varepsilon_-}$ in terms of λ_k , let f^1, \dots, f^k be an orthonormal set (w.r.t. $L^2(\mu)$) consisting of eigenfunctions of $\Delta_{\mathcal{M}}$ corresponding to its first k eigenvalues (and let us label them $\lambda_1 \leq \dots \leq \lambda_k$). Let

$$v_i := \tilde{P} f_i, \forall i = 1, \dots, k.$$

Applying Proposition A.5 to every f of the form

$$f := f_i - f_j,$$

we deduce that

$$|\langle f_i, f_j \rangle_{L^2(\mu)} - \langle v_i, v_j \rangle_{L^2(\mu^n)}| \leq C\tilde{\delta} \sqrt{\lambda_k} + C(\theta + \tilde{\delta}) < \frac{1}{k}.$$

We can then conclude that v_1, \dots, v_k are linearly independent and that the subspace $S := \text{Span}\{v_1, \dots, v_k\}$ has dimension k . From (A.1) we deduce that

$$\lambda_k^{\varepsilon_+, \varepsilon_-} \leq \max_{v \in S, \|v\|_{L^2(\mu^n)}=1} b^{\varepsilon_+, \varepsilon_-}(v).$$

For $v \in S$, written as $v = \sum_{i=1}^k a_i v_i = \sum_{i=1}^k a_i \tilde{P} f_i$, we can write $v := \tilde{P} f$ where $f = \sum_{i=1}^k a_i f_i$. This f satisfies:

$$D(f) = \langle \Delta_{\mathcal{M}} f, f \rangle_{L^2(\mu)} \leq \lambda_k \|f\|_{L^2(\mu)}^2$$

according to the spectral decomposition of $\Delta_{\mathcal{M}}$. Applying part (2) of Proposition (A.4) we obtain:

$$\begin{aligned} b^{\varepsilon_+, \varepsilon_-}(v) &\leq \frac{C N N_0}{w_{\min}^3 n^2 (\varepsilon_+^{m+2} - \varepsilon_-^{m+2})} \left(1 + \lambda_k^{m/2+2}\right) \|f\|_{L^2(\mathcal{M})}^2 + \left(1 + C(\varepsilon_+'' + \frac{\tilde{\delta}}{\varepsilon_+})\right) D(f) \\ &\leq \frac{C N N_0}{w_{\min}^3 n^2 (\varepsilon_+^{m+2} - \varepsilon_-^{m+2})} \left(1 + \lambda_k^{m/2+2}\right) \|f\|_{L^2(\mathcal{M})}^2 + \left(1 + C(\varepsilon_+'' + \frac{\tilde{\delta}}{\varepsilon_+})\right) \lambda_k \cdot \|f\|_{L^2(\mu)}^2. \end{aligned}$$

Finally, from Proposition A.5 applied to a $v \in S$ with norm one, we deduce that v 's corresponding f satisfies:

$$\|f\|_{L^2(\mu)}^2 \leq 1 + C(\tilde{\delta}\sqrt{\lambda_k} + \theta + \tilde{\delta}).$$

From this we conclude that

$$\begin{aligned} \lambda_k^{\varepsilon_+, \varepsilon_-} &\leq \frac{C N N_0}{w_{\min}^3 n^2 (\varepsilon_+^{m+2} - \varepsilon_-^{m+2})} \left(1 + C' (\lambda_k^{m/2+2} + \tilde{\delta}\sqrt{\lambda_k} + \theta + \tilde{\delta}) \right) \\ &+ \left(1 + C(\varepsilon_+'' + \tilde{\delta}\sqrt{\lambda_k} + \theta + \frac{\tilde{\delta}}{\varepsilon_+}) \right) \lambda_k. \end{aligned}$$

This establishes the upper bound for $\lambda_k^{\varepsilon_+, \varepsilon_-}$ in terms of λ_k .

For the lower bound, we follow completely analogous arguments as the ones above, relating functions $u \in L^2(\mu^n)$ with $f \in L^2(\mu)$ via the map \mathcal{I} and applying Propositions A.4 and A.5. \square

A.6. Proof of Theorem 2.7.

Proof of Theorem 2.7. We use an energy estimate based on A.4 to find a relationship between eigenvectors of $\mathcal{L}^{\varepsilon_+, \varepsilon_-}$ and eigenfunctions of $\Delta_{\mathcal{M}}$. We follow a similar strategy to the one in [44].

Let λ be an eigenvalue of $\Delta_{\mathcal{M}}$ and let $k \in \mathbb{N}$ be the first integer for which $\lambda = \lambda_k$ (here λ_k is as in (2.5)). Let l be the multiplicity of λ so that $\lambda = \lambda_k = \dots = \lambda_{k+l-1} < \lambda_{k+l}$. The gap γ_{λ} associated to λ is given by:

$$\gamma_{\lambda} := \frac{1}{2} \min\{|\lambda - \lambda_{k-1}|, |\lambda - \lambda_{k+l}|\} \quad (\text{A.21})$$

if $\lambda > 0$, and $\gamma_{\lambda} := \lambda_{l+1} - \lambda_{k+l}$ otherwise.

Now, we can pick $\varepsilon_+, \varepsilon_-, \theta, \tilde{\delta}$ to be small enough so that

$$e + C(\varepsilon_+ + \theta + \tilde{\delta}) \lambda \leq \gamma_{\lambda}$$

Then, for these choices of parameters, we know from Theorem 2.5 that

$$|\lambda^{\varepsilon_+, \varepsilon_-} - \lambda| \leq \gamma_{\lambda} \quad (\text{A.22})$$

Let S be a subspace of $L^2(\mu^n)$ spanned by all eigenvectors of $\mathcal{L}^{\varepsilon_+, \varepsilon_-}$ with eigenvalues

$$\lambda_k^{\varepsilon_+, \varepsilon_-}, \dots, \lambda_{k+l-1}^{\varepsilon_+, \varepsilon_-},$$

and let us denote the orthogonal projection onto S as P_S , the orthogonal projection onto the span of the eigenvectors of \mathcal{L} with eigenvalue strictly smaller than $\lambda_k^{\varepsilon_+, \varepsilon_-}$ as P_{S_-} , and the orthogonal projection onto the span of the eigenvectors of \mathcal{L} with eigenvalue strictly larger than $\lambda_{k+l-1}^{\varepsilon_+, \varepsilon_-}$ as P_{S_+} .

Let f be a normalized (w.r.t $L^2(\mu)$) eigenfunction of $\Delta_{\mathcal{M}}$ with eigenvalue λ and let $u = \tilde{P}f$. Notice that we can assume without the loss of generality that f takes the form in (2.4) for one of the manifolds \mathcal{M}_k (in particular the support of f is \mathcal{M}_k). Based on Proposition A.4 and its proof (specifically the bound (A.20)) we have:

$$\begin{aligned} e + \left[1 + C(\varepsilon_+ + \theta + \tilde{\delta}) \right] \lambda &\geq e + \left[1 + C(\varepsilon_+ + \theta + \tilde{\delta}) \right] D(f) \\ &\geq b^{\varepsilon_+, \varepsilon_-}(u) = \langle \mathcal{L}^{\varepsilon_+, \varepsilon_-} u, u \rangle \\ &\geq \lambda_k^{\varepsilon_+, \varepsilon_-} \|P_S u\|_{L^2(\mu^n)}^2 + \lambda_{k+l}^{\varepsilon_+, \varepsilon_-} \|P_{S_+} u\|_{L^2(\mu^n)}^2 \\ &\geq \lambda_k^{\varepsilon_+, \varepsilon_-} \left(\|u\|_{L^2(\mu^n)}^2 - \|u - P_S u\|_{L^2(\mu^n)}^2 \right) \\ &+ \lambda_{k+l}^{\varepsilon_+, \varepsilon_-} \left(\|u - P_S u\|_{L^2(\mu^n)}^2 - \|P_{S_-} u\|_{L^2(\mu^n)}^2 \right). \end{aligned} \quad (\text{A.23})$$

Using the results about γ_λ we obtained above and Proposition A.5 we deduce

$$|\lambda_2 - \lambda_2^{\varepsilon+, \varepsilon-}| \leq e + C(\varepsilon_+ + \theta + \tilde{\delta}) \lambda \leq \gamma_\lambda; \quad |1 - \|u\|_{L^2(\mu^n)}^2| \leq C(\theta + \tilde{\delta})$$

Here C is some constant may correspond to λ . Combining the above inequalities with A.23, we obtain:

$$\begin{aligned} & e + \left[1 + C(\varepsilon_+ + \theta + \tilde{\delta}) \right] \lambda \\ & \geq \lambda + (\lambda_2^{\varepsilon+, \varepsilon-} - \lambda_2) + \lambda_2^{\varepsilon+, \varepsilon-} (\|u\|_{L^2(\mu^n)}^2 - 1) + (\lambda_{k+2}^{\varepsilon+, \varepsilon-} - \lambda_2^{\varepsilon+, \varepsilon-}) \|u - P_S u\|_{L^2(\mu^n)}^2 \\ & - \lambda_{k+l}^{\varepsilon+, \varepsilon-} \|P_{S-} u\|_{L^2(\mu^n)}^2 \\ & \geq \lambda - e - C(\varepsilon_+ + \theta + \tilde{\delta}) + 2\gamma_\lambda \|u - P_S u\|_{L^2(\mu^n)}^2 - \lambda_{k+l}^{\varepsilon+, \varepsilon-} \|P_{S-} u\|_{L^2(\mu^n)}^2. \end{aligned}$$

From this and the upper bound for $\lambda_{k+l}^{\varepsilon-, \varepsilon+}$ in terms of λ_{k+l} :

$$\|u - P_S u\|_{L^2(\mu^n)} \leq \left[\frac{e}{\gamma_\lambda} + \frac{C}{\gamma_\lambda} (\varepsilon_+ + \theta + \tilde{\delta}) \right]^{1/2} + \sqrt{\lambda_{k+l}} \|P_{S-} u\|_{L^2(\mu^n)}.$$

We now compare the functions u and f at the data points x_i . Notice that for every data point $x_i \in \mathcal{M}_k$ we have:

$$|u(x_i) - f(x_i)| = |\tilde{P}f(x_i) - f(x_i)| \leq n \int_{\tilde{U}_{ik}} |f(x) - f(x_i)| \tilde{\rho}_n(x) d\text{vol}_{\mathcal{M}_k}(x) \leq \|\nabla f\|_{L^\infty(\mu_k)} \tilde{\delta}.$$

Also, due to (A.20) we know that $\|\nabla f\|_{L^\infty(\mu_k)} \leq \sqrt{w_k} C(\mathcal{M}_k, \rho_k) (\lambda^{m/4+1} + 1) \leq C(\mathcal{M}, \rho) (\lambda^{m/4+1} + 1)$. Thus,

$$|u(x_i) - f(x_i)| \leq C(\mathcal{M}, \rho) (\lambda^{m/4+1} + 1) \tilde{\delta}, \quad \forall x_i \in \mathcal{M}_k.$$

Notice that on the other hand, $u(x_i) = f(x_i) = 0$ for $x_i \in \mathcal{M} \setminus \mathcal{M}_k$ by definition of \tilde{P} and the fact that f is zero outside of \mathcal{M}_k . We conclude that:

$$\|u - f\|_{L^2(\mu^n)} \leq C_{\mathcal{M}, \rho} (\lambda^{m/4+1} + 1) \tilde{\delta},$$

and in turn

$$\|f - P_S \tilde{P}f\|_{L^2(\mu^n)} \leq \left[\frac{e}{\gamma_\lambda} + \frac{C}{\gamma_\lambda} (\varepsilon_+ + \theta + \tilde{\delta}) \right]^{1/2} + C_{\mathcal{M}, \rho} (\lambda^{m/4+1} + 1) \tilde{\delta} + \sqrt{\lambda_{k+l}} \|P_{S-} \tilde{P}(f)\|_{L^2(\mu^n)}. \quad (\text{A.24})$$

From this point on the idea is to use an inductive argument. We describe in detail the base case and outline the inductive step. **Base Case:** When $\lambda = 0$ (and $\lambda_1 = \dots = \lambda_N = 0 < \lambda_{N+1}$) we have $\|P_{S-}\|_{L^2(\mu^n)} = 0$ and thus we can drop the last term in (A.24). This means that if f_1, \dots, f_l form an orthonormal basis for the space of eigenfunctions of $\Delta_{\mathcal{M}}$ with eigenvalue λ , then we can find an orthonormal set v_1, \dots, v_l spanning S such that

$$\|f_i - v_i\|_{L^2(\mu^n)} \leq \left[\frac{e}{\gamma_\lambda} + \frac{C}{\gamma_\lambda} (\varepsilon_+ + \theta + \tilde{\delta}) \right]^{1/2} + C(\mathcal{M}, \rho) \tilde{\delta}.$$

In turn, this also implies that if u_1, \dots, u_l form an orthonormal basis of $\mathcal{L}^{\varepsilon+, \varepsilon-}$ with corresponding eigenvalues $\lambda_2^{\varepsilon+, \varepsilon-}, \dots, \lambda_{l+1}^{\varepsilon+, \varepsilon-}$, then there exists an orthonormal set $\tilde{f}_1, \dots, \tilde{f}_l$ for Δ_{ρ_l} with eigenvalue λ satisfying the same inequality above with f_i replaced with \tilde{f}_i and v_i replaced with u_i .

Inductive step: having found the desired relationship for the eigenvectors and eigenfunctions associated to the first portion of the spectrum of $\Delta_{\mathcal{M}}$, we return to (A.24) and notice that by Proposition A.5 we can conclude that the term $\|P_{S-} \tilde{P}f\|_{L^2(\mu^n)}$ is smaller than

$$C(\mathcal{M}, \rho) ((\lambda^{(1/4)} + 1) \sqrt{\tilde{\delta}} + \sqrt{\theta}).$$

We can plug this estimate in (A.24) and then proceed as in the base case to obtain the desired result. \square

A.7. Different dimensions: Proof of Theorem 2.8. We start by writing the discrete Dirichlet form $b^{\varepsilon+, \varepsilon-}$ (A.2) as the sum of three terms:

$$b^{\varepsilon+, \varepsilon-}(u) = b_{max}(u_{max}) + b_S(u_S) + b_O(u),$$

where

$$b_{max}(v) := \frac{1}{n^2(\varepsilon_+^{m+2} - \varepsilon_-^{m+2})} \sum_{x_i, x_j \in \mathcal{X}_n \cap \mathcal{M}_{max}} \omega_{x_i x_j} (v(x_i) - v(x_j))^2, \quad v \in L^2(\mathcal{X}_n \cap \mathcal{M}_{max}),$$

$$b_S(u_S) := \frac{1}{n^2(\varepsilon_+^{m+2} - \varepsilon_-^{m+2})} \sum_{k=N_{max}+1}^N \sum_{x_i, x_j \in \mathcal{X}_n \cap \mathcal{M}_k} \omega_{x_i x_j} (u_k(x_i) - u_k(x_j))^2, \quad u_S = (u_{N_{max}+1}, \dots, u_N),$$

and lastly,

$$b_O(u) := b^{\varepsilon+, \varepsilon-} - b_{max}(u_{max}) - b_S(u_S).$$

Notice that b_{max} captures all interactions between points that belong to the manifolds with the maximum dimension m . For this energy we can use all the results presented in section 2.3 and in particular relate it to the Dirichlet form:

$$D_{max}(f) := \begin{cases} \sum_{i=1}^{N_{max}} w_i^2 \int_{\mathcal{M}_i} |\nabla f_i(x)|^2 \rho_i^2(x) d\text{vol}_{\mathcal{M}_i}(x), & \text{if } f \in H^1(\mathcal{M}_{max}) \\ +\infty, & \text{if } f \in L^2(\mathcal{M}_{max}) \setminus H^1(\mathcal{M}_{max}). \end{cases}$$

The energy b_S , on the other hand, captures the interactions between points that are on the same manifold when this manifold is not one of the ones with the largest dimension m . Using (A.5), we can write b_S as:

$$b_S(u_S) = \sum_{k=N_{max}+1}^N \left(\frac{n_k}{n} \right)^2 \cdot \left(\frac{\varepsilon_+^{m_k+2} - \varepsilon_-^{m_k+2}}{\varepsilon_+^{m+2} - \varepsilon_-^{m+2}} \right) \cdot b_k(u_k).$$

Finally, the term $b_O(u)$ accounts for all interactions between points in two different manifolds when the two manifolds are among the ones with dimension smaller than m , or when one of them has dimension m and the other one does not. In short, b_O accounts for all interactions not accounted for by the terms b_{max} and b_S and is thus a non-negative term.

We let $\tilde{\mathcal{I}}_{max} : L^2(\mathcal{X}_n \cap \mathcal{M}_{max}) \rightarrow L^2(\mathcal{M}_{max})$ and $P_{max} : L^2(\mathcal{M}_{max}) \rightarrow L^2(\mathcal{X}_n \cap \mathcal{M}_{max})$ be the maps constructed in section A.2 applied to the data set $\mathcal{X}_n \cap \mathcal{M}_{max}$ and \mathcal{M}_{max} , i.e. the union of manifolds with the same dimension m . We also consider the following maps:

$$\mathcal{I}' : L^2(\mathcal{X}_n) \rightarrow L^2(\mathcal{X}_n \cap \mathcal{M}_{max})$$

$$\mathcal{I}' : u \mapsto u_{max},$$

$$P' : L^2(\mathcal{X}_n \cap \mathcal{M}_{max}) \rightarrow L^2(\mathcal{X}_n)$$

$$P' : v \mapsto u = (v, 0),$$

where by $u = (v, 0)$ we mean that u coincides with v for data points in \mathcal{M}_{max} and $u = 0$ for data points in $\mathcal{M} \setminus \mathcal{M}_{max}$.

It will be convenient to introduce the norms:

$$\|u_k\|_{L^2(\mathcal{X}_n \cap \mathcal{M}_k)}^2 := \frac{1}{n} \sum_{x_i \in \mathcal{X}_n \cap \mathcal{M}_k} (u_k(x_i))^2, \quad u_k \in L^2(\mathcal{X}_n \cap \mathcal{M}_k),$$

and

$$\|v\|_{L^2(\mathcal{X}_n \cap \mathcal{M}_{max})}^2 := \frac{1}{n} \sum_{x_i \in \mathcal{X}_n \cap \mathcal{M}_{max}} (v(x_i))^2, \quad v \in L^2(\mathcal{X}_n \cap \mathcal{M}_{max}),$$

as well as the discrete Laplacians:

$$\mathcal{L}_k u_k(x) := \frac{1}{n_k(\varepsilon_+^{m_k+2} - \varepsilon_-^{m_k+2})} \sum_{y \in \mathcal{X}_n \cap \mathcal{M}_k} \omega_{xy}(u(x) - u(y)), \quad x \in X \cap \mathcal{M}_k, \quad u : X \rightarrow \mathbb{R}.$$

We use $\lambda_{2,k}^{\varepsilon_+, \varepsilon_-}$ to denote the second eigenvalue of \mathcal{L}_k .

Proof of Theorem 2.8. Following the structure of the proofs of Theorems 2.5 and 2.7 we see that we can obtain our desired estimates if we can obtain similar inequalities to the ones in Propositions A.4 and A.5 where now we use the maps $\mathcal{I}_{max} \circ \mathcal{I}'$ and $P' \circ P_{max}$ as interpolation and discretization maps respectively. There is only one small caveat in the almost isometry property of $\mathcal{I}_{max} \circ \mathcal{I}'$ as we explain below.

We start by noticing that from the above definitions we have:

$$b_{max}(\mathcal{I}'u) \leq b^{\varepsilon_+, \varepsilon_-}(u), \quad \forall u \in L^2(\mathcal{X}_n),$$

and by Proposition A.4

$$D_{max}(\mathcal{I}_{max} \circ \mathcal{I}'u) \leq (1 + C(\varepsilon_+ + \frac{\tilde{\delta}}{\varepsilon_+} + \theta + \tilde{\delta}))b_{max}(\mathcal{I}'u),$$

so that

$$D_{max}(\mathcal{I}_{max} \circ \mathcal{I}'u) \leq (1 + C(\varepsilon_+ + \frac{\tilde{\delta}}{\varepsilon_+} + \theta + \tilde{\delta}))b^{\varepsilon_+, \varepsilon_-}(u), \quad \forall u \in L^2(\mathcal{X}_n). \quad (\text{A.25})$$

The above occurs with probability at least $1 - \sum_{l=1}^N (nw_l + t) \exp\left(-C(nw_l - t)\theta^2\tilde{\delta}^m\right) - 2N \exp\left(\frac{-2t^2}{n}\right) - C_1(n)$.

On the other hand, for arbitrary $f \in L^2(\mathcal{M}_{max})$ we have

$$\begin{aligned} b^{\varepsilon_+, \varepsilon_-}(P' \circ P_{max}f) &= b_{max}(P_{max}f) + b_O(P' \circ P_{max}f) \\ &\leq \left(1 + C(\varepsilon_+ + \frac{\tilde{\delta}}{\varepsilon_+} + \theta + \tilde{\delta})\right) D_{max}(f) + b_O(P' \circ P_{max}f), \end{aligned} \quad (\text{A.26})$$

whereas

$$b_O(P' \circ \tilde{P}_{max}f) \leq \frac{C N N_0}{w_{min}^3 n^2 (\varepsilon_+^{m+2} - \varepsilon_-^{m+2})} \left(1 + \lambda^{m/2+2}\right) \|f\|_{L^2(\mathcal{M}_{max})}^2, \quad (\text{A.27})$$

for f an element in the span of $\Delta_{\mathcal{M}_{max}}$'s eigenfunctions with corresponding eigenvalue less than λ , as it follows from a completely analogous computation to the one in (A.19); this holds in the same event of very high probability where (A.25) holds.

We consider now the norm distortion of the maps $\mathcal{I} \circ \mathcal{I}'$ and $P' \circ P_{max}$. First, notice that by definition, for $v \in L^2(\mathcal{X}_n \cap \mathcal{M}_{max})$ we have

$$\|P'v\|_{L^2(\mathcal{X}_n)}^2 = \|v\|_{L^2(\mathcal{X}_n \cap \mathcal{M}_{max})}^2,$$

and thus combining with 1) in Proposition (A.5) we obtain:

$$\left| \|P' \circ P_{max}f\|_{L^2(\mathcal{X}_n)}^2 - \|f\|_{L^2(\mathcal{M}_{max})}^2 \right| \leq C\tilde{\delta}\|f\|_{L^2(\mathcal{M}_{max})} \sqrt{D_{max}(f)} + C(\theta + \tilde{\delta})\|f\|_{L^2(\mathcal{M}_{max})}^2. \quad (\text{A.28})$$

Now, for a given $u \in L^2(\mathcal{X}_n)$ we have:

$$\left| \|\mathcal{I}'u\|_{L^2(\mathcal{X}_n \cap \mathcal{M}_{max})}^2 - \|u\|_{L^2(\mathcal{X}_n)}^2 \right| = \sum_{k=N_{max}+1}^N \|u_k\|_{L^2(\mathcal{X}_n \cap \mathcal{M}_k)}^2.$$

Also, if we let \bar{u}_k represent the average of u_k in $\mathcal{M}_k \cap \mathcal{X}_n$ we see that

$$\|u_k - \bar{u}_k\|_{L^2(\mathcal{X}_n \cap \mathcal{M}_k)}^2 \leq \frac{1}{\lambda_{2,k}^{\varepsilon_+, \varepsilon_-}} \langle \mathcal{L}_k u_k, u_k \rangle_{L^2(\mathcal{M}_k \cap \mathcal{X}_n)} = \frac{1}{\lambda_{2,k}^{\varepsilon_+, \varepsilon_-}} \frac{n_k^2}{n^2} b_k(u_k) \leq C(\mathcal{M}_k, w_k, \rho_k) \varepsilon_+^{m-m_k} b(u),$$

for all $k = N_{max} + 1, \dots, N$, where the last inequality holds with very high probability. Indeed, notice that by Theorem 2.5 applied to a single manifold \mathcal{M}_k we can find a lower bound for $\lambda_{2,k}^{\varepsilon_+, \varepsilon_-}$ in terms of the first non-trivial eigenvalue for $w_k \Delta_{\mathcal{M}_k}$. We have also used the fact that $b_k(u_k) \leq (n/n_k)^2 \varepsilon_+^{m-m_k} b(u)$. This means that

$$\left| \|\mathcal{I}' u\|_{L^2(\mathcal{X}_n \cap \mathcal{M}_{max})}^2 - \|u\|_{L^2(\mathcal{X}_n)}^2 \right| \leq C(\mathcal{M}, \mu) \varepsilon_+^{m-m_{N_{max}+1}} b^{\varepsilon_+, \varepsilon_-}(u) + \sum_{k=N_{max}+1}^N (\bar{u}_k)^2.$$

Combining with Proposition A.5 and using the triangle inequality we deduce that

$$\begin{aligned} \left| \|\mathcal{I}_{max} \circ \mathcal{I}' u\|_{L^2(\mathcal{M}_{max})}^2 - \|u\|_{L^2(\mathcal{X}_n)}^2 \right| &\leq C \varepsilon_+ \|u\|_{L^2(\mu_n)} \sqrt{b^{\varepsilon_+, \varepsilon_-}(u)} \\ &\quad + C(\theta + \tilde{\delta}) \|u\|_{L^2(\mu_n)}^2 + C(\mathcal{M}, \mu) \sum_{k=N_{max}+1}^n \varepsilon_+^{m-m_k} b^{\varepsilon_+, \varepsilon_-}(u) \\ &\quad + \sum_{k=N_{max}+1}^N (\bar{u}_k)^2. \end{aligned} \tag{A.29}$$

Notice that the right hand side in the above expression is small for a u with low Dirichlet energy only when u is close to the orthogonal complement of $\text{Span}\{\mathbb{1}_{\mathcal{M}_{N_{max}+1}}, \dots, \mathbb{1}_{\mathcal{M}_N}\}$ (i.e. the \bar{u}_k are small). Because of this, we will only be able to proceed as in the proofs of Theorems 2.5 and 2.7 to obtain all our estimates if first we show that the top N eigenvectors of \mathcal{L} are close to the indicator functions of $\mathcal{M}_1 \cap \mathcal{X}_n, \dots, \mathcal{M}_N \cap \mathcal{X}_n$. However, this is straightforward from the following observations:

- i) We can obtain an upper bound for the first N eigenvalues of \mathcal{L} following the representation (A.1) and computing the graph Dirichlet energy of the indicator functions of the sets $\mathcal{M}_k \cap \mathcal{X}_n$. Namely, we have:

$$\lambda_k^{\varepsilon_+, \varepsilon_-} \leq \frac{C N N_0}{w_{min}^3 n^2 (\varepsilon_+^{m+2} - \varepsilon_-^{m+2})}, \quad k = 1, \dots, N.$$

- ii) Using the alternative representation:

$$\lambda_{N+1}^{\varepsilon_+, \varepsilon_-} = \max_{S \in \mathcal{G}_N} \min_{u \in S^\perp \setminus \{0\}} \frac{b^{\varepsilon_+, \varepsilon_-}(u)}{\|u\|_{L^2(\mu^n)}^2}$$

we can obtain the lower bound

$$\lambda_{N+1}^{\varepsilon_+, \varepsilon_-} \geq \frac{1}{2} \lambda_{N+1},$$

with very high probability. Indeed, taking $S = \text{Span}\{\mathbb{1}_{\mathcal{M}_1 \cap \mathcal{X}_n}, \dots, \mathbb{1}_{\mathcal{M}_N \cap \mathcal{X}_n}\}$ and a unit norm $u \in S$ (in particular $\bar{u}_k = 0$ for all $k = N_{max} + 1, \dots, N$) we see from (A.25) and (A.29) that

$$b^{\varepsilon_+, \varepsilon_-}(u) \geq \lambda_{N+1} \left(1 - C(\varepsilon_+ + \varepsilon \sqrt{\lambda_{N+1}} + \varepsilon^{m-m_{N_{max}+1}} \lambda_{N+1} + \theta + \frac{\tilde{\delta}}{\varepsilon_+}) \right) \geq \frac{1}{2} \lambda_{N+1}.$$

iii) Combining the previous steps we get an order one lower bound for the gap between $\lambda_N^{\varepsilon_+, \varepsilon_-}$ and $\lambda_{N+1}^{\varepsilon_+, \varepsilon_-}$. We can then follow the proof of Theorem 2.7 to show that there exists an orthonormal set v^1, \dots, v^N consisting of eigenvectors of \mathcal{L} corresponding to \mathcal{L} 's first N eigenvalues such that

$$\left\| \sqrt{\frac{n}{n_k}} \mathbb{1}_{\mathcal{M}_k \cap \mathcal{X}_n} - v^k \right\|_{L^2(\mathcal{X}_n)}^2 \leq \frac{C(\mathcal{M}, \mu) N_0}{n^2(\varepsilon_+^{m+2} - \varepsilon_-^{m+2})}.$$

We deduce that if u belongs to the orthogonal complement of $\text{Span}\{v^1, \dots, v^N\}$, then

$$(\bar{u}_k)^2 \leq \frac{C(\mathcal{M}, \mu) N_0}{n^2(\varepsilon_+^{m+2} - \varepsilon_-^{m+2})},$$

with very high probability.

As discussed above, with the above estimates in hand we can now proceed as in the proofs of Theorems 2.5 and 2.7. \square

DEPARTMENT OF STATISTICS, UNIVERSITY OF WISCONSIN, MADISON, WISCONSIN, USA
Email address: garciatrillo@wisc.edu

DEPARTMENT OF STATISTICS AND PROBABILITY, MICHIGAN STATE UNIVERSITY, EAST LANSING, MI, USA
Email address: hepengf1@msu.edu

DEPARTMENT OF STATISTICS, UNIVERSITY OF WISCONSIN, MADISON, WISCONSIN, USA
Email address: cli539@wisc.edu